Investigation of Sternal Photoplethysmography – Design of a Vital Sign Patch

Chreiteh, Shadi

Publication date:
2016

Document Version
Publisher's PDF, also known as Version of record

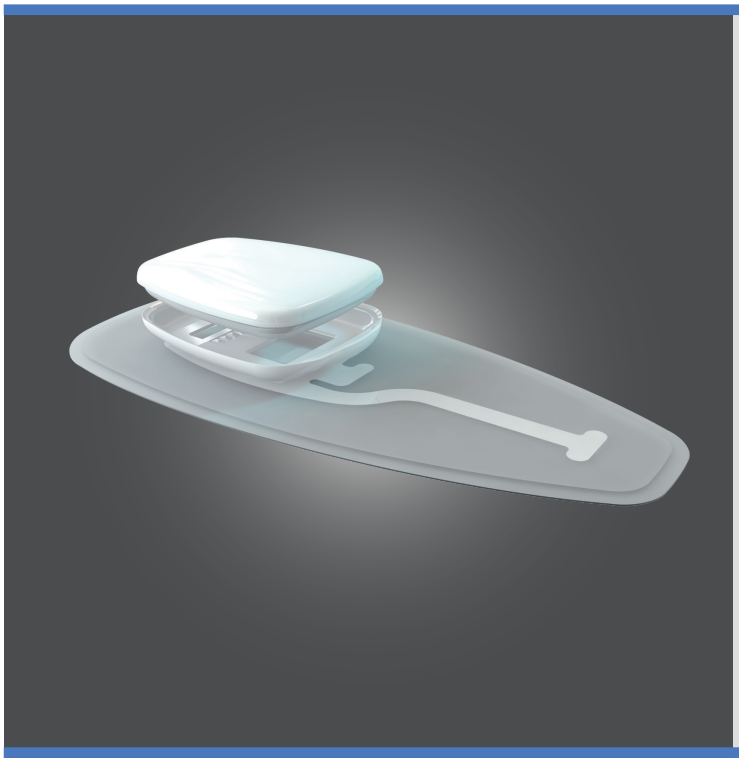

Investigation of Sternal Photoplethysmography

Design of a Vital Sign Patch

Shadi Chreiteh
PhD Thesis March 2016

DTU Nanotech
Department of Micro- and Nanotechnology

Investigation of Sternal Photoplethysmography – Design of a Vital Sign Patch

Shadi Samir Chreiteh

March 21, 2016

Technical University of Denmark
Department of Micro and Nanotechnology
DK-2800 Kgs. Lyngby
Denmark

Submitted in partial fulfillment of the requirements for the degree of Doctor of Philosophy at Technical University of Denmark.

PREFACE

The research provided in this Ph.D. dissertation has been conducted as a partial fulfilment of the requirements for the degree of Doctor of Philosophy in Engineering. The Ph.D. project is an Industrial Ph.D and was carried out in cooperation between the MEMS Applied Sensors group at the Department of Micro- and Nanotechnology, Technical University of Denmark (DTU), the Body Sensors group at the Danish company DELTA, and the Department of Anesthesiology Bispebjerg Hospital, Copenhagen University Hospital. The conducted clinical experiments have been conducted at the Department of Pulmonary Medicine and the Medical Admissions ward in Bispebjerg Hospital, Copenhagen University Hospital.

The research work presented in this dissertation have been carried out over a period of three years together with supervising two master students, participation in international conferences, and engineering work conducted at DELTA.

The project was financially supported by DELTA and the Danish Ministry of Higher Education and Science.

Shadi Samir Chreiteh, March 2016

ACKNOWLEDGEMENT

It would not have been possible for me to accomplish this Ph.D. project without the help and support of great group of people, who were always available whenever it was needed.
I would like to express my deepest appreciation and thanks to my principal supervisor Professor Erik V. Thomsen, for being a tremendous mentor and always encouraging my research. I am truly grateful for his ability of being positive during all the stages of this project. I would like to thank my co-supervisor Dr. Bo Belhage for his endless support, sharing his deepest knowledge and experience within the medical field and for introducing me to the hospital environment. I would also like thank my co-supervisor Research Manager Karsten Hoppe for his valuable support during this journey and for the numerous hours of passionate discussions and for sharing his expertise and useful knowledge with me.
A special thanks to Key Account Manager Jens Branebjerg for believing in me from day one and for the fruitful discussions and guidance. Thank you to Dr. Nassim Nabipour for the clinical support, discussions and scientific contributions. A special thanks to my friend and colleague Dr. Dorthe B. Saadi for her ongoing advice and ability to come up with suggestions when things go dark. I would like to thank all the Ph.D. students in the MEMS Applied Sensors group for the valuable morning discussions. Thanks to my colleagues, at DELTA for always taking the time to help me and a special thanks to research and development engineers Søren Garbos, Lasse Bay and Morten Flintrup for their support in terms of hardware, software and general support. Working in such a great multidisciplinary environment has been an unforgettable experience for me.
I would specially like to thank all the staff at the Department of Pulmonary Medicine, the Department of Anesthesiology and the Medical Admission ward in Bispebjerg Hospital.
A special thanks to my family for their support and having confidence in me. Last but not least, I would like to express my appreciation to my beloved wife and life companion Randa for her patience, ongoing encouragement and proof reading this dissertation. My lovely children Celine and Samir thank you for always making me a happy father.

ABSTRACT

It is important to obtain reliable measures of vital sign parameters, e.g. heart rate, respiratory rate (RR), and the oxygen saturation of the blood (S_pO_2). In current clinical practice the RR is assessed by manual count of the chest movements and pulse oximetry probes have been limited to the fingertip or the earlobe. These methods are documented to be time consuming or inaccurate when monitoring patients with low blood flow or decreased perfusion at the extremities (e.g. patients with obstructive lung diseases, diabetes, or heart failure). Furthermore, they are obtrusive for long-term recordings.

The main focus of this project is to investigate the clinical applicability of photoplethysmography (PPG) measured at the chest bone (sternum). PPG is an optical method from which the RR and the S_pO_2 level can be obtained.

For this purpose we have developed a prototype of a wearable PPG sensor and conducted three clinical studies both on healthy participants and on patients with obstructive lung diseases. The first clinical study was a controlled desaturation study. All 14 subjects were exposed to hypoxia by breathing an air mixture of reduced oxygen concentration in a closed system. We obtained an average root mean squared error (A_{rms}) of 1.75 $\%$ compared to invasive measures of the oxygen saturation in the radial artery (S_aO_2) which is within the clinically and commercially accepted range. Furthermore, this study served as a calibration of the PPG sensor in a clinical relevant range (100 $\%$ - 70 $\%$).

In the second study, sternal PPG recording was conducted from 30 admitted patients with either asthma or Chronic Obstructive Pulmonary Disease (COPD). We compared the S_pO_2 levels simultaneously obtained from the sternal PPG recording and a conventional finger pulse oximeter. The Pearson correlation between the S_pO_2 levels estimated from the two body locations was found to be 0.89 ($p < 0.05$) and the mean system bias was only 0.052 $\%$ with upper and lower limits of agreement of 2.5 $\%$ and -2.4 $\%$, respectively. The RR was also obtained from sternal PPG and compared to conventional capnography. In a range of 11 to 36 breaths/min the Pearson correlation was 0.93

($p < 0.001$) and the system mean bias was 0.6 breaths/min. The upper and lower limits of agreement was found to be -2.8 to 4 breaths/min.

In the last clinical study, the focus was to investigate the clinical reliability of long-term PPG recordings from the sternum. Fifteen admitted patients were included in the study and were monitored with the sternal PPG sensor for approximately 20 hours. On average it was found that clinically reliable S_pO_2 and RR estimates could be calculated for 58 $\%$ of the recording time. Furthermore, the average longest period of time with unreliable data in terms of the S_pO_2 level and the RR was only 23.6 minutes and 20 minutes, respectively.

The results of this project show that it is possible to obtain reliable quasi-continuous recording of the S_pO_2 level and the RR from sternal PPG in many different clinical applications in the future.

DANSK RESUME

For kritisk syge patienter er det af stor vigtighed at opnå pålidelige målinger af de vitale parametre som for eksempel puls, respirationsfrekvens og iltmætningen af blodet. Med den nuværende klinisk praksis måles respirationsfrekvensen ved manuel optælling af brystkassens bevægelser over et minut. Målingen af iltmætningsniveauet udføres med et pulsoximeter, i form af en fingerklips, som placeres på patientens finger eller øreflip. Disse målemetoder er dokumenteret tidsskrævende og unøjagtige for patienter med lav blodgennemstrømning eller nedsat perfusion i ydreekstremiteterne, hvilket eksempelvis ses hos patienter med obstruktiv lungesygdom, diabetes eller hjertesvigt.

Dette ErhvervsPhD-projekt omhandler måling af respirationsfrekvensen og iltmætningen i kroppen ved hjælp af en pulsoximetersensor placeret på brystbenet (sternum). Målemetoden kaldes for fotoplethysmografi (PPG) og er baseret på, at lys med en bestemt bølgelængde sendes ind i huden. Lyset, PPG-signalet, der sendes ind i huden bliver reflekteret i vævet, hvorved blodets iltmætning og pulsen kan bestemmes ud fra karakteristikaene af det reflekterede PPG-signal. Det reflekterede PPG-signal, som kan registreres på sternum, er endvidere overlejret med et signal indeholdende information om vejrtrækningen. Fysiologiske undersøgelser har vist, at denne information om vejrtrækningen er relateret til ændringen i det intrathorakale tryk under vejrtrækning der giver anledning til ændringer i den venøse blodvolumen, samt strækning og udvidelse af huden på sternum.

Hovedfokus i dette projekt er at undersøge den kliniske anvendelighed af PPG målt på sternum. Til dette formål har vi udviklet en prototype af en kropsbåren PPG-sensor. Endvidere er der gennemført tre kliniske studier i samarbejde med Bispebjerg Hospital på både raske forsøgsdeltagere og på patienter med obstruktive lungesygdomme.

Det første kliniske studie omhandlede kontrolleret nedsænkning af iltmætningen i blodet og måling heraf med den udviklede PPG-sensor. I alt 14 raske forsøgspersoner undergik hypoksi ved at trække vejret i et lukket genåndingssystem med atmosfærisk luft, hvor iltindholdet gradvist blev reduceret. Der blev opnået en gennemsnitlig nøjagtighed (average RMS accuracy) på 1,75 % for den

udviklede PPG-sensor sammenlignet med invasive referencemålinger af blodets iltmætning fra arterielle blodprøver. Data fra dette studie er anvendt til kalibreringen af den udviklede PPG-sensor.

I det andet kliniske studie blev sternumbaseret PPG målt på 30 indlagte patienter med enten astma eller kronisk obstruktiv lungesygdom (KOL). Den på sternum målte iltmætning blev sammenlignet med konventionel pulsoximetri målt på fingeren. Pearson-korrelationen mellem iltmætningen estimeret fra de to placeringer, blev givet til at være 0,89 ($p < 0,05$). Bland-Altman analysen viste en lav systematisk forskel på kun 0,052 $\%$. Respirationsfrekvensen blev også fundet ved hjælp af sternumbaseret PPG og blev sammenlignet med respirationsfrekvensen fra den kapnografibaserede reference. I et interval mellem 11 til 36 åndedrag/minut, var Pearson-korrelationen 0,93 ($p < 0,001$) og den gennemsnitlige afvigelse var på 0,6 åndedrag/minut.

I det tredje kliniske studie var fokus at undersøge den kliniske troværdighed af langtidsmålinger med sternumbaseret PPG. 15 indlagte patienter var inkluderet i dette studie og blev overvåget med sternumbaseret PPG i tilnærmelsesvis 20 timer. Det blev vist at den klinisk troværdige iltmætning og respirationsfrekens kunne blive udregnet for 58 $\%$ af målingsperioden. Ydermere, de længste respektive perioder med ikke-troværdig data, angående iltmætning og respirationsfrekvens, var henholdsvis 23,6 minutter og 20 minutter.

Resultatet af dette projekt indikerer et højt potentiale for implementeringen af kvasikontinuerte målinger af iltmætningsniveauer og respirationsfrekens fra sternumbaseret PPG i mange forskellige applikationer i fremtiden. Resultatet åbner samtidigt op for fremtidige muligheder for proaktiv patientmonitorering, hvor patientforværring kan blive identificeret tidligere og behandling kan startes tidligere end muligt i dag.

ABBREVIATIONS

AC	Alternate current
ADC	Analog-to-digital converter
ANS	Autonomic nervous system
A_{rms}	Average root mean square accuracy
BMI	Body Mass Index
BP	Blood pressure
$CoHb$	Carboxyhemoglobin
$COPD$	Chronic Obstructive Pulmonary Disease
C_{xy}	Magnitude squared coherence
DAQ	Data acquisition device
DC	Direct current
DST	Discrete Saturation Transform
ECG	Electrocardiography
$ETCO_2$	Tidal carbon dioxide
fCO_2	fraction of carbon,dioxide
FFT	Fast Fourier Transform
FiO_2	Fractional inspiratory oxygen
GCP	Good Clinical Practice
H_2O	Water
Hb	Deoxyhemoglobin
HbO_2	Oxyhemoglobin
HF	High frequency
HR	Heart rate
HRV	Heart rate variability
IQR	Interquartile range
LED	Light emitting diode
LF	Low frequency
$MetHb$	Methemoglobin
PD	Photo detector
PPG	Photoplethysmography
PRV	Pulse rate variability

PSD	Power spectral density
R	Optical ratio
$RIIV$	Respiratory induced variation
$RMSE$	Root Mean Squared Error
RR	Respiratory rate
SPO_2	Oxygen saturation in the blood
TIA	Trans-impedance amplifier
USB	Universal serial bus

CONTENTS

CHAPTER

ONE

INTRODUCTION

1.1 Motivation

"Would you like to borrow my finger pulse oximeter device? No thanks, the patient's hands are cold so I can't trust the readings anyways. I will try again later."

For the last decade there has been an emergence of wireless healthcare technologies and advancements in on-body embedded sensor technology. These technology developments may enable the opportunity of changing the conventional healthcare systems with wearable devices that focuses on personalized healthcare. For instance, being able to measure the vital signs continuously (long-term) will not only enhance the quality of life for chronic disease patients, but it will also decrease the economical burden on the hospital facilities. Moreover, there is no doubt that the application of long-term measurement of the vital signs is pivotal in terms of early intervention.

A state-of-the-art example of an on-body embedded health monitoring technology is the ePatch® platform manufactured by DELTA. The ePatch® platform is a continuous electrocardiographic (ECG) recorder that is developed on the "wear and forget" principle which enables continuous ECG monitoring without interrupting any normal life activity of a patient in contrast to regular Holter or telemetry equipment. The ePatch® is worn on the chest bone (sternum). A detailed overview about the ePatch® technology is given in [1].

The vital signs are essential parameters to assess a patient's health condition. The vital signs are: body temperature, heart rate, respiratory rate (RR), blood pressure and the oxygen saturation in the blood. The focus in this research project will be on the RR and the oxygen saturation in the blood.

The standard procedure for monitoring the vital signs in the hospital environment (outside the inten-

sive care unit) currently relies on manual techniques and relatively intermittent manual observation of the patients. Fig. 1.1 shows an example of a vital signs monitoring during a normal day at Bispebjerg Hospital in Copenhagen, Denmark. Furthermore, the vital signs are currently being used to calculate an early warning score (EWS) which is used to determine the degree of illness of an admitted patient. The oxygen saturation and the heart rate are measured by a pulse oximeter attached to the finger or the earlobe and the RR is measured by a manual count of the rib cage (thorax) movement. This procedure is done at least once every 12 hours, which is not only time consuming, but also uncomfortable in relation to the patients. Moreover, the oxygen saturation measurement through the conventional finger probe is in many case difficult or even impossible [2–4]. Conditions such as hypothermia, hypotension, or peripheral vasoconstriction may influence the blood flow and thereby the pulse oximeter reading at the extremities. These conditions may lead to centralization, which is a reduction of the perfusion to the extremities to maintain blood circulation at the central organs. It is for example known that in Chronic Obstructive Pulmonary Disease (COPD) patients may have low perfusion in the peripheral circulations [5], that may affect the pulse oximeter readings.

The RR is known to be an early indicator for detecting exacerbations and changes in the severity of COPD [6]. According to the World Health Organization, COPD is currently the third leading cause of death globally. Exacerbation of COPD is not only one of the major causes of morbidity and mortality, but it also puts a high economic burden on the healthcare facilities [7]. In a small country like Denmark, with around 6 million citizens, it is estimated that approximately 23,000 acute COPD-related patients are admitted to the hospital every year and the readmission rate is as high as 24 $\%$ [8]. The mortality rate during admission is furthermore 8 $\%$, which is in line with the mortality in acute myocardial infarction [7]. In spite of this, recent studies have found that the RR and the oxygen saturation of the blood are often not recorded even in cases where the patient's primary problem is a respiratory challenge [9]. The lack of consistent routine vital signs monitoring may be a consequence of shortcomings in today's measuring techniques.

The sternum provides an alternative measurement site due to the local anatomy and the proximal position to the heart. It was recently discovered that the oxygen saturation of the blood and the RR can be estimated from photoplethysmography (PPG) recorded at the sternum [10]. However, the research group was not sure about how reliable the technique is and if it can be used on patients with obstructive lung diseases. Thus, the goal of this project is to explore the potentials of monitoring the oxygen saturation in the blood and the RR using PPG at the sternum, not only for short-term measurement, but also for continuous long-term measurement on patients with obstructive lung diseases.

Figure 1.1: Conventional monitoring procedure of the vital signs. GE Carescape V100 on a roll stand is one of many vital signs monitors used at the hospital. However, the respiratory rate is measured by a manual count of thorax movements over 60 seconds.

Four scientific hypotheses form the basis for this dissertation:

1. *It is possible to make reliable short-term monitoring of reflective pulse oximetry at the sternum.*
2. *It is possible to make reliable short-term monitoring of the respiratory rate derived from sternal PPG.*
3. *It is possible to make reliable long-term monitoring of reflective pulse oximetry at the sternum.*
4. *It is possible to make reliable long-term monitoring of the respiratory rate derived from sternal PPG.*

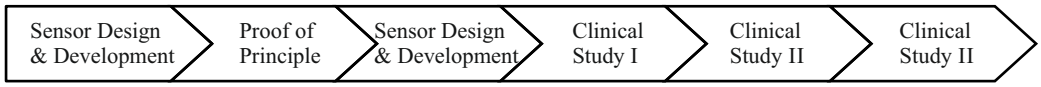

Figure 1.2: Illustration of the progress of the conducted research. First a PPG probe has been developed, then a proof of principle study has been conducted. Afterwards, another version of a prototype PPG sensor was developed and used to investigate the clinical applicability of sternal PPG through three clinical studies.

The process of the conducted research is illustrated in Fig. 1.2. The first step of this project was to develop a prototype PPG probe in order to investigate the feasibility of estimating the RR and the oxygen saturation level in the blood from sternal PPG, which was conducted through a pre-clinical experiment. Then, another improved prototype PPG sensor was developed and used in three clinical studies. The general aim of all three studies is to investigate the clinical applicability of sternal PPG.

1.2 Thesis Outline

The structure of the this thesis is based on the progress of the conducted research. The preliminary chapter introduces the used modalities and the measurement techniques, followed by a chapter describing a proof of principle based on a preliminary study. Then, a description of the design and development of the prototype PPG sensor, three chapters describing the conducted clinical experiments and last a conclusion and future perspective of the research project. The background, methodologies and results described in the papers are reproduced in this dissertation. Some sections may however contain more details and extended work related to what is reported. The following is a brief description of each chapter:

Chapter 1 provides an introduction of the thesis by describing its motivation and major research objectives.

Chapter 2 provides a description of the background information required for the understanding of this project.

Chapter 3 presents the results of a pre-clinical experiment that was conducted to investigate the feasibility of using the sternum as a measurement site for monitoring the RR and the oxygen saturation of the blood. The aim of this study was also to investigate the morphology of the sternal PPG. The findings of this chapter has been published in paper I and II.

Chapter 4 presents the conception and the development of a prototype sternal PPG sensor that can be integrated with current state-of-the-art ePatch® platform. The hardware, the software and the opto-mechanical design is described and evaluated.

Chapter 5 presents the description and the results of a hypoxia/desaturation study conducted on healthy participants. The study is used to calibrate the sternal PPG sensor. This content is also addressed in paper IV.

Chapter 6 demonstrates the description and the results of a clinical study of short-term measurements conducted on COPD and asthma patients. This study is also addressed in paper III and IV.

Chapter 7 demonstrates the description and the results of a clinical study of long-term measurements conducted on healthy participants and on a group of COPD and asthma patients. Parts of this study is addressed in paper V.

Chapter 8 summarizes the main conclusions of the research described in the other chapters.

1.3 List of Papers

The following is a list of scientific contributions in the field of photoplethysmography with the focus on the RR and the oxygen saturation recorded from sternal photoplethysmography:

- S. S. Chreiteh, B. Belhage, K. Hoppe, J. Branebjerg, and E. V. Thomsen, *"Sternal Pulse Rate Variability Compared with Heart Rate Variability on Healthy Subjects"*. Engineering in Medicine and Biology Society (EMBC), 2014 Annual International Conference of the IEEE, pp. 3394-3397. **Status: Published.** (Paper I)
- S. S. Chreiteh, B. Belhage, K. Hoppe, J. Branebjerg, R. Haahr, S. Duun, and E. V. Thomsen, *"Estimation of respiratory rates based on photoplethysmographic measurements at the sternum"*. Engineering in Medicine and Biology Society (EMBC), 2015 Annual International Conference of the IEEE, pp. 6570-6573. **Status: Published.** (Paper II)
- S. S. Chreiteh, B. Belhage, Nassim Nabipour, K. Hoppe, and E. V. Thomsen, *"Monitoring of Respiratory Rate in COPD and Asthma Patients Using Sternal Photoplethysmography"*. Submitted to the European Clinical Respiratory Journal. **Status: In review.** (Paper III)
- S. S. Chreiteh, Dorthe B. Saadi, B. Belhage, Nassim Nabipour, K. Hoppe, and E. V. Thomsen, *"A Clinical Study of Short-Term Sternal Photoplethysmography: Recordings from Patients with Obstructive Airways Diseases"*. Submitted to the Engineering in Medicine and Biology Society (EMBC), 2016 Annual International Conference of the IEEE. **Status: In review.** (Paper IV)

- S. S. Chreiteh, Dorthe B. Saadi, B. Belhage, Nassim Nabipour, K. Hoppe, and E. V. Thomsen, *"Long-Term Quasi-Continuous Oxygen Saturation Levels Obtained from Sternal Photoplethysmography on Patients with Obstructive Lung Diseases"*. Submitted to the Engineering in Medicine and Biology Society (EMBC), 2016 Annual International Conference of the IEEE. **Status: In review.** (Paper V)

CHAPTER

TWO

PRELIMINARIES

Objective *This chapter will provide a short description of the primary modalities used in this project and the fundamental theory behind photoplethysmography will be described in terms of the pulse oximetry.*

2.1 Electrocardiography

The electrocardiogram (ECG) reflects the electrical activity of the heart. The ECG is an extremely important diagnostic tool in current clinical practice, which is primely used to track any myocardial infarction, cardiac rhythm disturbances or changes in the electrical conduction system of the heart. Moreover, the ECG is considered to be the gold-standard in terms of heart rate monitoring [11]. In short, when the cardiac cells depolarize (increasing potential) and repolize (decreasing potential), the electrical current is spread throughout the body and can be measured at the skin for example silver/silver chloride electrodes placed at a specific body positions. The time delay between the depolarization and the repolarization of the atria and the ventricles of the heart produces the ECG waveform [12]. For each heartbeat the ECG constitutes of a P-wave, QRS-complex, and a T-wave as seen in Fig. 2.1. The heart rate is defined as the time delay between two consecutive heartbeats (i.e. QRS complexes). In the context of this project the ECG signal is measured to compare the timing/pulse with sternal PPG and in the signal processing of the PPG signal (more about that in chapter 5). The R-peak in the QRS-complex is the most important wave in regarding to this project. The QRS-complex represents the depolarization of the ventricles. To record the ECG signal with the highest R-peak a lead-II electrode configuration is used. As seen in Fig. 2.2, the positive electrode is on the left side on the upper thigh and the negative electrode is on the right side of the upper chest.

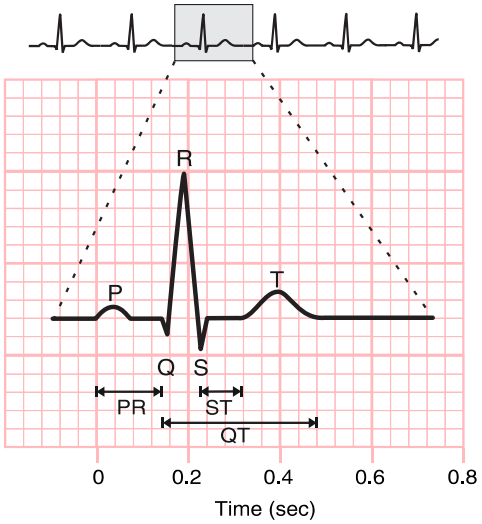

Figure 2.1: An electrocardiogram from a healthy subject. It is a typical ECG that can be acquired through lead-II configuration. The P-wave is related to the contraction of the atria, the QRS-complex to the contraction of the ventricles, and the T-wave is related to the repolarization of the ventricles. Adapted from [12].

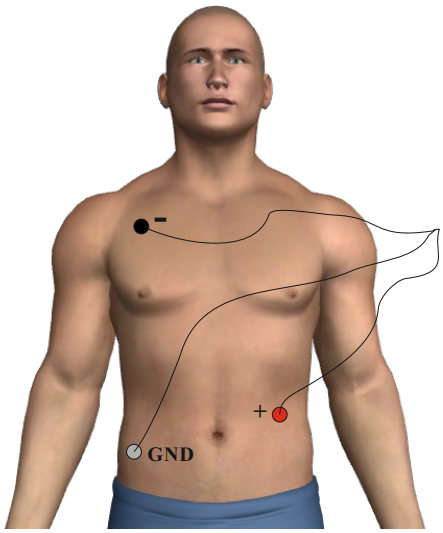

Figure 2.2: Lead-II electrode configuration. This configuration gives the largest R-peak in the ECG recording.

On the right thigh a grounding electrode for recording purposes is attached.

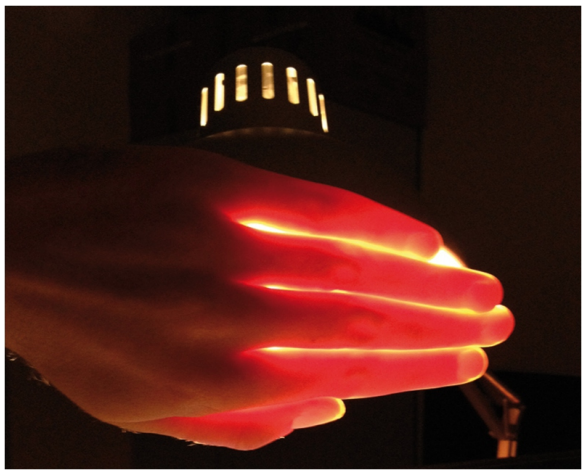

Figure 2.3: When the hand is illuminated by the light, the entire hand glows where the skin color becomes red due to the dominated concentration of the blood.

2.2 Photoplethysmography

From an optical point of view the human skin is considered strongly scattering (opaque). However, most soft tissue will behave as translucent and therefore transmit and absorb both visible and infrared light [13]. For example when illuminating a hand using a lamp in a dark room, it can be seen that some of the light is transmitted through the whole hand. The transmitted light is red because of the dominating concentration of the blood in the hand as seen in Fig. 2.3. In other words, light is emitted into the skin where it undergoes absorption and scattering, which results in reduced transmitted light intensity at the photo detector. This is what the photoplethysmography (PPG) is based on and can be utilized using two different modes; transmission mode and reflectance mode. In transmission mode the tissue is illuminated on one side and the light transmitted through it and detected on the other side. This mode is of course confound to the extremities like fingers or toes but also earlobe. Where in reflectance mode, the light source and the photo detector is placed on the same side. It can be used on body locations like the forehead or at the sternum. The two different PPG modes are shown in Fig. 2.4.

The PPG signal contains two components, a pulsatile (AC component), which fluctuates due to the arterial blood and is superimposed on a ”DC” component that varies with the respiration [15]. Non-pulsatile absorbers such as the venous blood and the bones also contribute to the DC component. The pulsatile AC component oscillates in sync with the cardiac cycle. For every heartbeat, the ventricles of the heart is contracted and blood is ejected (the QRS-complex in the

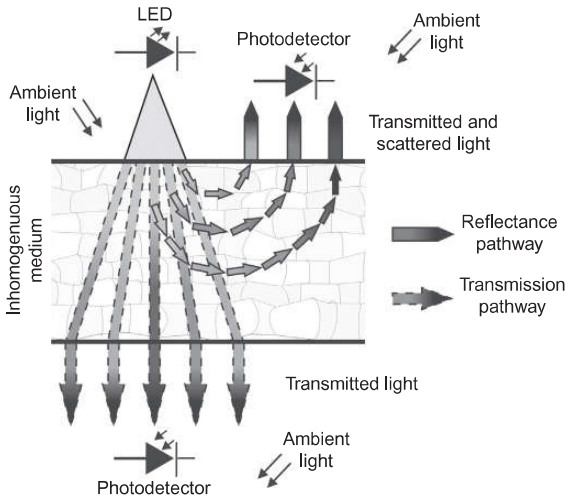

Figure 2.4: Illustration of the transmission and reflectance mode PPG. The region of application for the transmission mode is in the extremities, while the reflectance mode can be used in the proximal regions of the body. Adapted from [14].

ECG) to the cardiovascular bed, which gives a larger blood volume, which means a larger absorption and a lower light intensity is received at the photo detector. Giving the rising edge of the PPG waveform, during the ventricular relaxation and filling (diastole) of the heart is shown in the falling edge of the PPG waveform. So as a result of this volume change during the cardiac cycle, the path length of the light will also periodically change. In compliance to the Beer-Lambert's law, the absorption is proportional to the optical path length and therefore the volume change will be reflected at the photo detector.

The AC component of the PPG waveform is two to three orders of magnitude smaller than the DC component. However, the ratio between the AC and DC components depend on the measuring site, the perfusion and the skin temperature [13, 15]. A typical AC component of the PPG waveform is seen in Fig. 2.5a and b, where Fig. 2.5a is recorded at the sternum and Fig. 2.5b is recorded on the finger. Both signals are synchronized with the ECG signal seen in Fig. 2.5c. The PPG waveforms are inverted, meaning that the rising edge corresponds to higher absorption due to the systolic phase, while the falling edge corresponds to the diastolic phase. Moreover, it is seen that the sternal PPG waveform appears before the finger PPG waveform because of the proximal position of the sternum compared to the finger. These morphological differences are further discussed in chapter 3.

The wavelength of the light source is crucial in the interaction of light and tissue. As mentioned before the tissue is a turbid media and the heterogeneity of the tissue exhibit different absorbers with

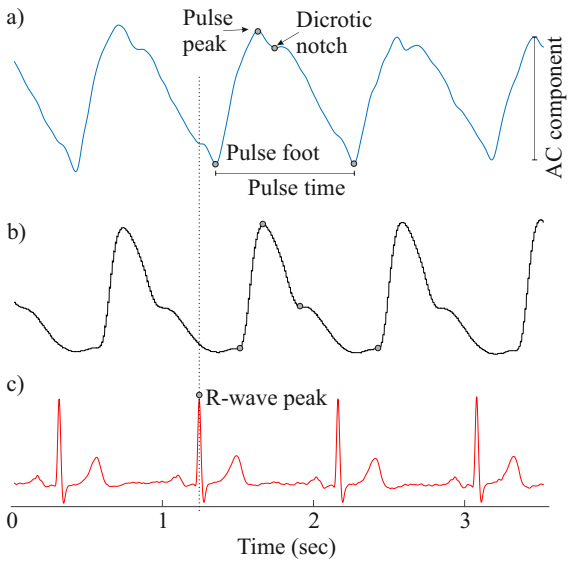

Figure 2.5: Typical AC component of the PPG waveforms recorded on the sternum (a) and on the index finger (b). Both signals are synchronized with the ECG signal (c). Interesting but not surprisingly the rising edge of the sternal PPG signal comes before the one at the finger PPG. The same case with the diacrotic notch. This is due to the proximal location to the heart compared to the finger. The PPG signals are inverted, meaning that the rising edge corresponds to the systole (highest absorption) while the falling edge corresponds to the diastole (lowest absorption).

different absorption coefficients. The main contributors to the absorption in the tissue is Hemoglobin (Hb) which is the main constituent of blood. The absorption coefficient of Hb change with its chemical binding and the wavelength of the emitted light. Oxyhemoglobin (HbO_2) and Deoxyhemoglobin Hb, have different absorption coefficients as a function of wavelength, this is what the pulse oximetry takes advantage of (explained in the next section). Another main contributors to the absorption of light is water (H_2O), Melanin and Collagen as seen in see Fig. 2.6. However in terms of pulse oximetry the "optical tissue window" is the most used wavelength range. In this range (650 nm - 950 nm) the absorption of water is smaller than the absorption of HbO_2 and Hb, cf. Fig. 2.6. Furthermore, the tissue is optically most transparent in this region [13].

PPG has been used to estimate various physiological parameters besides pulse oximetry, such as the estimation of the RR, blood pressure, cardiac output, tissue perfusion, vascular assessment and pulse rate variability. A comprehensive review of the clinical application of the PPG is given by Allen [15] and recently by [17]. In the next section the theory behind pulse oximetry is given.

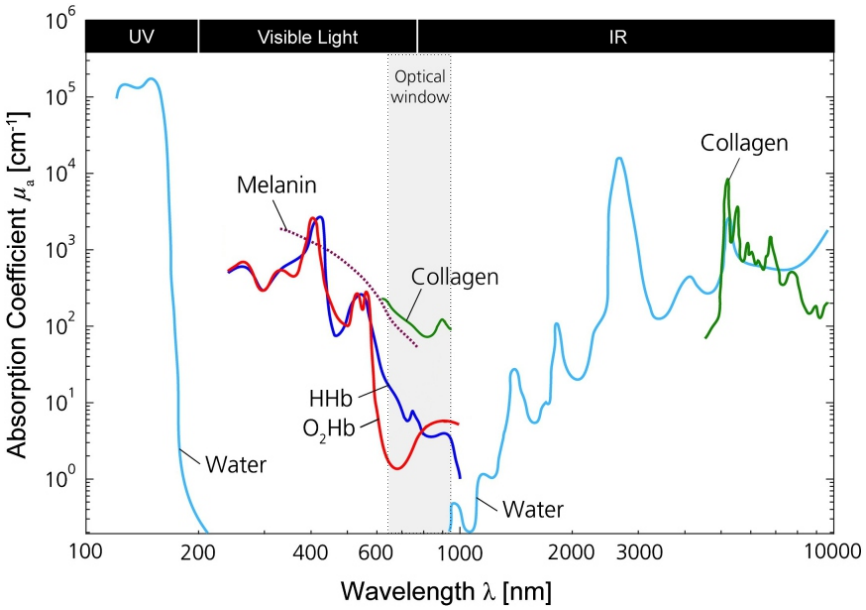

Figure 2.6: Absorption coefficient of main biological tissue content (H_2O, HbO_2, Hb, Collagen and Melanin). Adapted from [16].

2.2.1 Principles of Pulse Oximetry

The blood of an human adult consists of four different types of hemoglobin:

Oxyhemoglobin (HbO_2): Hemoglobin that is fully saturated with oxygen.

Deoxyhemoglobin (Hb): Hemoglobin that is not fully saturated with oxygen.

Methemoglobin ($MetHb$): Oxidized hemoglobin.

Carboxyhemoglobin ($COHb$): Hemoglobin combined with carbon monoxide (CO).

The last two types of hemoglobin is present in small concentrations (proportion of 0-2 $\%$ of the total Hb) in the blood of an healthy adult. The fractional oxygen saturation is therefore defined as:

$$Fractional\ S_aO_2(\%) = \frac{cHbO_2}{cHbO_2 + cHb + cCOHb + cMetHb} \tag{2.1}$$

However because of the small concentrations of $MetHb$ and $COHb$ they are excluded in the definition of functional oxygen saturation that is expressed as:

$$Functional\ S_aO_2(\%) = \frac{cHbO_2}{cHbO_2 + cHb} \tag{2.2}$$

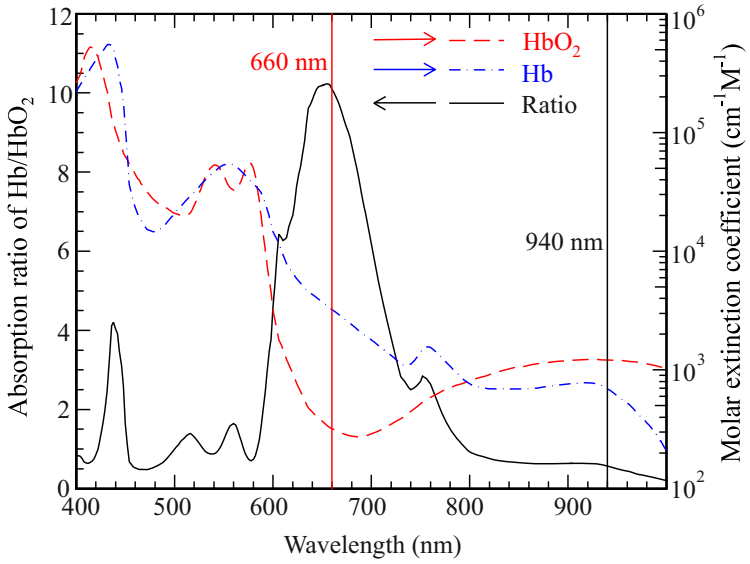

Figure 2.7: Molar extinction coefficients of HbO_2 and Hb. The oxygen saturation is a ratio between the two types of hemoglobins. At least two wavelengths 660 nm and 940 nm with two different Molar extinction coefficients are required to estimate the S_pO_2 level. The largest difference in absorption between HbO_2 and Hb is seen at 660 nm and the smallest and most stable region is in the infrared region (i.e 940 nm which is commonly used). Adapted from [10].

In the application of pulse oximetry, the functional oxygen saturation definition is commonly used and the two wavelengths that are used is red ($\lambda = 660nm$) and infrared ($\lambda = 940nm$). The abbreviation used for this definition when estimated by pulse oximetry is S_pO_2. The S_pO_2 is determined by taking the ratio of two PPG signals recorded using light emitting diode (LED) with red and infrared wavelength. The reason behind the choice of 660 nm and 940 nm is illustrated in Fig. 2.7. The largest difference of extinction coefficient between HbO_2 and Hb is seen at 660 nm, this is a key factor because with this large difference in absorption, small changes in oxygenation will be detected [13]. The choice of 940 nm is not only because the difference is small, but also because the absorption spectra of the HbO_2 and the Hb at this region is stable and a slight variation of peak wavelength will not affect the accuracy of the pulse oximeter [13].

The estimation of pulse oximetry has been applied in a theoretical model based on Beer-Lambert law, that described the absorption of light when it passes through a homogeneous medium containing a variety of light absorbing molecules. The model is based on the assumption that there are no scattering effect and the optical modulation depends only to an increased path length during the systolic phase. The model is fully described in [13] and expressed as:

$$S_pO_2 = \frac{\epsilon Hb(\lambda_{Red}) - \epsilon Hb(\lambda_{IR})R}{\epsilon Hb(\lambda_{Red}) - \epsilon HbO_2(\lambda_{Red}) + (\epsilon HbO_2(\lambda_{IR}) - \epsilon Hb(\lambda_{IR}))R} \tag{2.3}$$

where R is the optical ratio of ratios and the molar extinction coefficients λ for HbO_2 and Hb are 0.08 and 0.81 $mmol^{-1}cm^{-1}$ for 660 nm and 0.29 and 0.18 $mmol^{-1}cm^{-1}$ for 940 nm [13]. Fig. 2.8 illustrates the optical ratio as a function of S_pO_2 based on Beer-Lambert model.

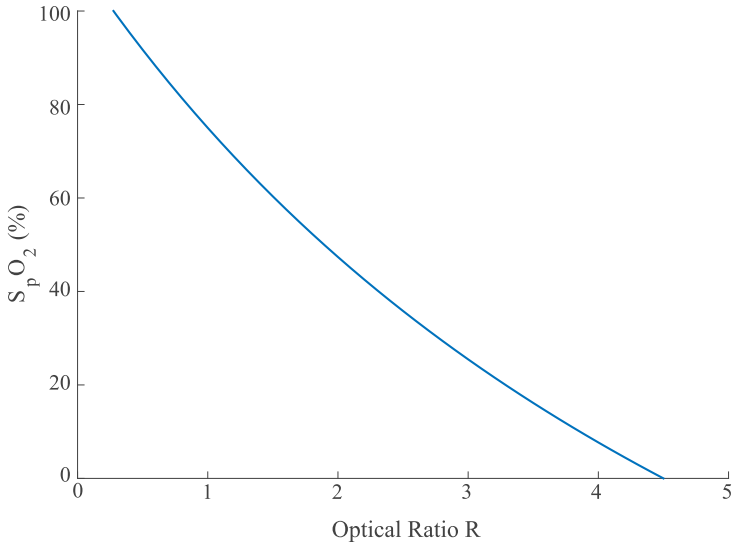

Figure 2.8: Calibration curve for pulse oximeter in compliance with Beer-Lambert model from equation 2.3.

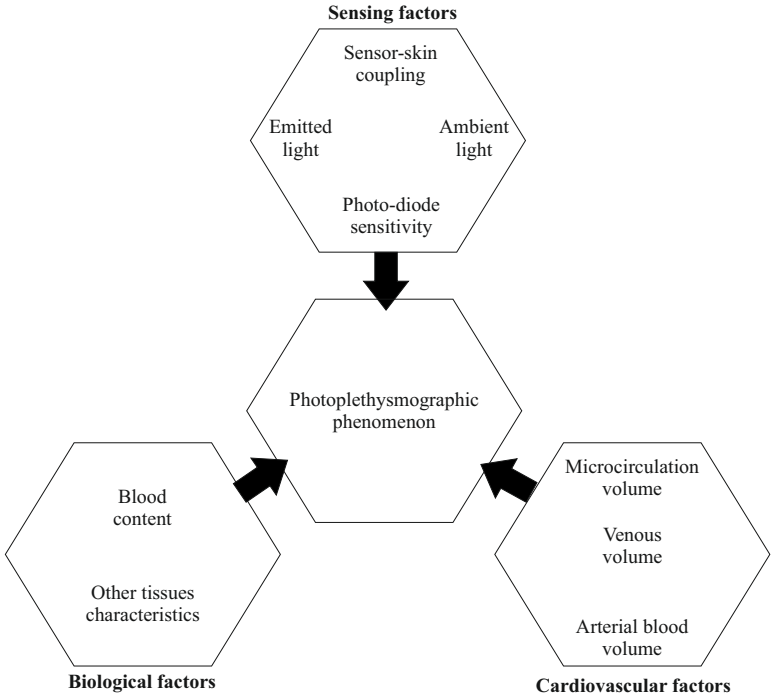

Figure 2.9: Three factors that can affect the PPG; Sensing factors (blue), biological factors (orange) and cardiovascular factors (red). After [14].

In practice the value of R is not calculated as stated in equation 2.3. Instead the amplitude of the PPG signal (AC) and its average level (DC) are commonly used to calculate the ratio of ratios as [13, 18]:

$$R = \frac{\frac{AC_{Red}}{DC_{Red}}}{\frac{AC_{IR}}{DC_{IR}}} \tag{2.4}$$

Unfortunately, the assumptions made in the Beer-Lambert model makes it incomplete in terms of reality, not only the light interaction is complex in the tissue, but also the orientation of the erythrocytes in the blood also affects the optical modulation in addition to the path length [18]. Other limitations are shown in Fig. 2.9, for example the DC component of the PPG signal is not constant, but influenced by the respiration (this influence is discussed in chapter 3). Moreover, the sensor-skin coupling of the corresponding PPG device also affects the PPG signal [14, 17]. As illustrated in Fig. 2.9 three main factors may influence the PPG signal; Biological factors, cardiovascular factors, and sensing factors.

To overcome these factors all commercial pulse oximeters use an empirically generated calibration curve. As in compliance with [13] the calibration curve can be used as a linear approximation in the clinically important range of S_pO_2 level (100 $\%$ to 70 $\%$) with a negative slope:

$$S_pO_2 = -aR + b \tag{2.5}$$

where a and b are constants. This procedure is performed in this project and is further described in chapter 5.

2.3 Summary

Two primary modalities are used in this project: the ECG and the PPG. The former reflects the electrical activity of the heart whereas the latter contains information about the cardiac activity (AC component) and respiratory activity (DC component). By using two PPGs with different wavelengths, it is possible to estimate the oxygen saturation in the blood. However, due to the limitation of Beer-Lambert model and the inhomogeneity of the tissue a calibration scheme is needed in order to estimate the oxygen saturation level. The calibration is usually performed using a linear regression from data recorded on healthy subject during a hypoxia experiment. In the next chapter a proof of principle regarding sternal PPG and its feasibility of extracting the RR, cardiac pulse and the oxygen saturation level is discussed.

CHAPTER

THREE

PROOF OF PRINCIPLE: STERNAL PHOTOPLETHYSMOGRAPHY

Objectives *In the beginning of this project, the knowledge about the sternal PPG was very limited, and it was therefore not well understood whether the sternal PPG could provide satisfactory clinical information in terms of the respiratory rate (RR) and the oxygen saturation level in the blood (S_pO_2). In the previous chapter some fundamental background theory was given to ease the understanding of the scientific work of this project. The following chapter will describe the proof of principle of this project aiming of investigation of the feasibility of RR monitoring at the sternum. The pulse rate is also investigated in terms of pulse rate variability (PRV). This chapter is composed upon the two papers (I and II).*

3.1 Background

The whole idea of this project is to investigate the possibility of measuring the RR and the S_pO_2 level at the sternum. As mentioned previously PPG is primarily performed peripherally in the application of pulse oximetry. The most common measuring sites are the fingertip, earlobe, and forehead. However, a number of other sites have been investigated such as the sternum [19–21] and the shoulder [22]. Monitoring the RR from PPG has previously been studied through analysis of peripheral PPG. Leonard et al. [23] and Clifton et al. [24] have described the derivation of RR from finger PPG and Lindberg et al. [25] have shown the possibility of RR monitoring from reflective PPG signals measured on the forearm. Whereas Shelley et al. [22] have found that the respiratory component is significant in the regions of the head (the ear and the forehead) compared to the component derived from the finger. This indicates that the measuring site has a significant

importance for the magnitude of the respiratory component in the PPG signal. Furthermore, it may also indicate that the smaller the distance to the chest, the less attenuation of the respiratory component by the vasculature. This assessment is supported by Nilsson et al. [26] who found that the respiratory and cardiac induced variations in the PPG were different at different measuring sites (finger, forearm, wrist, forehead, and shoulder). Additionally, they found that the forearm had the most pronounced respiratory component variation and the finger the least. In the literature, it is thus a consensus that the magnitude of the RR component is attenuated in the arms and fingers. The RR obtained from sternal PPG has been claimed in a patent by Kronberg and Leist [27]. However, no studies have been conducted on investigating the clinical applicability of RR obtained from sternal PPG.

In terms of S_pO_2 measurement, it was reported by Nogawa et al. [19] that the relative AC amplitude of sternal PPG was 10 $\%$ compared to the finger PPG, whereas the AC amplitude of the PPG from the forehead was 30 $\%$ relative to the finger PPG. Konig et al. [28] reported that the signal quality on the sternum is comparable to the arterial blood samples. This is also in line with Mendelson et al. [29]. Additionally, Mendelson and McGinn [30] reported that the error on estimating the S_pO_2 from the forearm and calf is slightly larger compared to the forehead and the sternum. Recently, it was reported by Vetter et al. [20] that the S_pO_2 level can be estimated within an absolute error of 3 $\%$.

From the literature it can be concluded that sternal PPG can be used for the estimation of the S_pO_2 level. However, the quality of the signal is lower than those obtained from the forehead and fingertips. Moreover, nothing of the above cited papers reported any results from clinically relevant patients. All the reported experiments have been conducted on healthy subjects.

3.2 PPG at the Sternum

The sternum is expected to be a robust location for acquiring PPG signals, because of the central body location and the proximity to the heart and lungs. The anatomy of the thoracic cage and the blood supply to the subcutaneous vessels at the sternum are very relevant components when measuring the PPG signal at that region. As seen in Fig. 3.1a, the blood flow is ejected from the ventricles of the heart, then into the ascending aorta, where it continues to the left and the right brachiocephalic trunks. The blood is subsequently supplied to the internal thoracic arteries on both sides of the sternum, on the posterior side which then supplies the perforating branches that goes into the micro-musculature of the subcutaneous tissue of the sternum, cf. Fig. 3.1b.

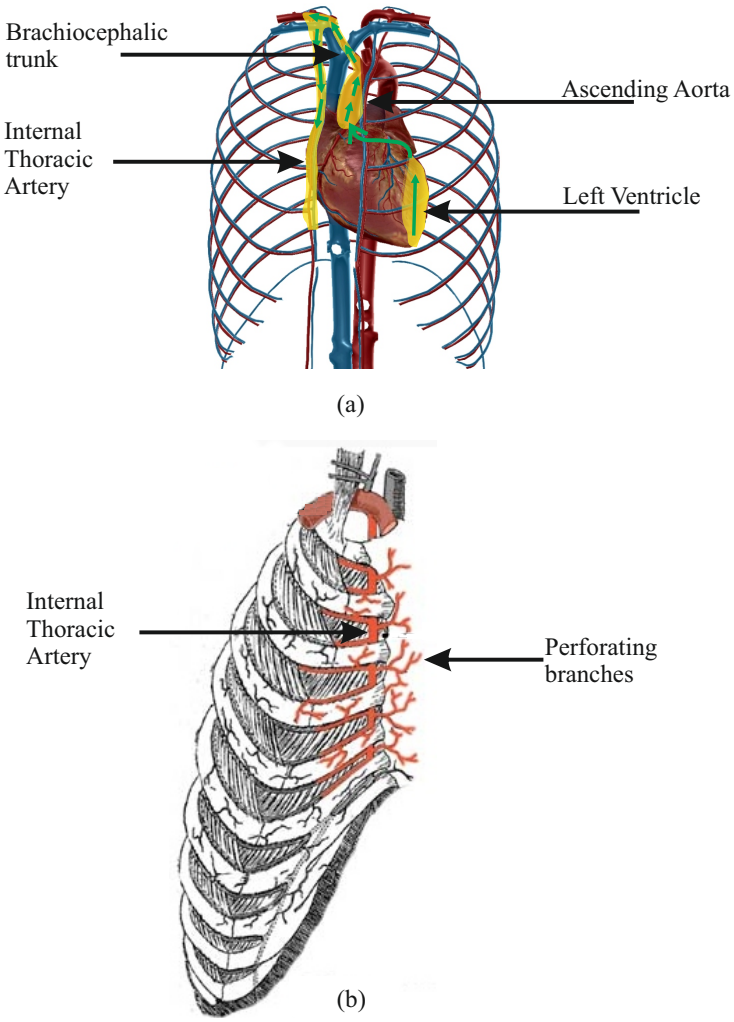

Figure 3.1: The local anatomy of the thoracic cage. (a) The route of arterial blood supply to the sternal region (indicated by the green arrows). Both at the arterial and the venous site the blood is pumped out from the ventricles of the heart and ends at the internal thoracic arteries and veins which supply the sternal tissue through the perforating branches seen in (b).

The respiratory-induced intensity variation (RIIV) in the PPG is well documented in the literature [31–35]. It is the intra-thoracic pressure variations that happens during the exchange of blood between the pulmonary and the systemic circulation that is reflected in the venous and the artery system and causes the baseline variations. However this is the only mechanism that reflects the respiration in the extremities. Where as, at the sternum the local variation is believed to contribute to larger pressure variations during respiration. The pressure variations in the thoracic cavity change and affect the blood volume in the internal thoracic arteries and the anterior perforating branches of in-

tercostal vessels. The PPG signal measured at the sternum would basically be measuring the blood flow through the sternal micro-musculature of the subcutaneous tissue supplied from the perforating branches seen in Fig. 3.1b. To investigate the PPG signal measured at the sternum a PPG probe has been developed and a pre-clinical experiment was conducted. A more comprehensive description of a more advanced version of the PPG probe and the rational behind the proposed design is given in chapter 4.

3.3 Methods and Materials

3.3.1 PPG Probe

For the purpose of this pre-clinical experiment a PPG probe has been designed and developed, shown in Fig. 3.2. Four photo detectors (PD1-PD4) were placed radially around a dual LED, where the LED can manually be switched ”on” and ”off” and emit red (660 nm) or infrared (940 nm) light. The overall sensitivity area for each photo detector is 4.4 mm^2 and the output from the four photo detectors was treated as four independent PPG channels. The reason for choosing four photo detectors is to acquire light intensity from different sternal positions, since the perfusion at the chest is known to be lower than at the periphery [20]. Another configuration could be to parallel connect all four photo detectors and thereby get a summation of the generated current.

The light and photo detector distance was chosen to 7 mm as proposed for less perfused skin areas by [36]. The bottom of the probe is covered with optically transparent polycarbonate. Each of the four photo detectors measure the light intensity and produce a small current, which is amplified and converted to a voltage signal by a high gain-low noise trans-impedance amplifier. The voltage signal is afterwards high-pass filtered to eliminate any offset from the trans-impedance amplifiers. The signal is then amplified and low-pass filtered. The cut-off frequencies for the two filters are 0.05 Hz and 20 Hz respectively to preserve the respiratory information in the PPG signal (6-30 breaths/min) and to maintain the cardiac component (30-240 beats/min). The 20 Hz was chosen to minimize 50 Hz power line interference.

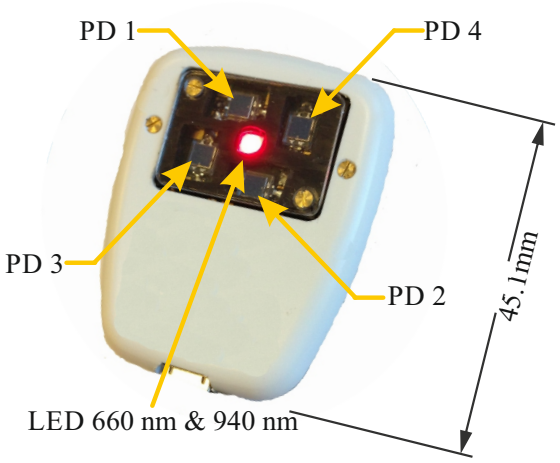

Figure 3.2: An illustration of the developed PPG probe. The photo detectors (PD1-PD4) are radially arranged around the dual LED and separated by an optical shield to prevent direct light from the LED.

3.3.2 Study Design and Data Acquisition

A group of 10 healthy volunteers (9 males, 1 female) with mean age of 39.2±12.6 years and a mean Body Mass Index (BMI) of 24.5±3.2 kg/m^2 were recruited for this pre-clinical study.

The reflective PPG probe was positioned on the skin over the sternum using adhesive tape, a transmission mode PPG was obtained using a conventional finger probe (Datex-Ohmeda AS/3, GE Healthcare, USA) and lead-II ECG was also acquired and used as a cardiac reference signal. As a reference signal to the RR derived from sternal PPG, the inspiratory and expiratory fraction of carbon dioxide (fCO_2) was acquired via a nasal catheter. The reference signals and the sternal PPG signals were collected simultaneously and digitized with a sampling rate of 1000 Hz (Powerlab 8/35, 16 bit ADC, ADInstruments, USA) and stored on a laptop computer using Lab Chart 7 Pro (Lab Chart Version 7.3.7, ADInstruments, USA) data acquisition software. Fig. 3.3 outlines the experimental setup. For each subject being in a supine position data were collected in two stages:

1. Spontaneous respiration: The subjects were instructed to relax and breathe with natural RR for 10 min.
2. Paced respiration: The subjects were instructed to breathe in time with a visual scale. The pace was set to 6, 17, 24, 12, and 27 breaths/min for three minutes each.

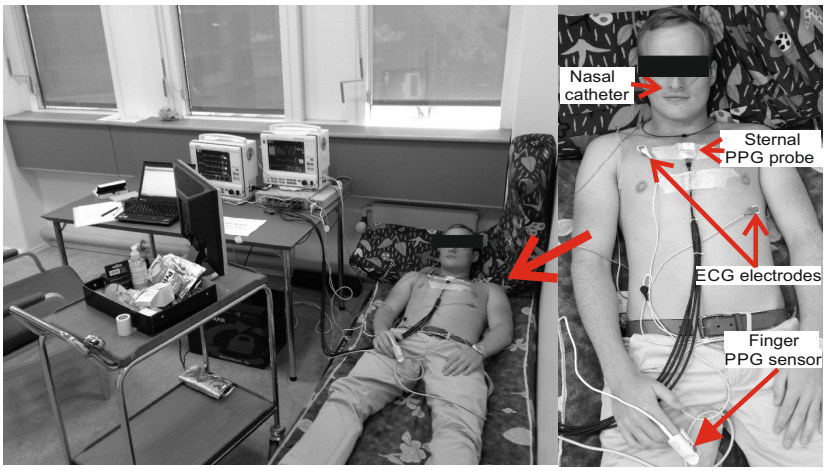

Figure 3.3: A picture of the measurement setup. For each subject, the four channels sternal PPG sensor (PD1-PD4), lead-II ECG, conventional finger PPG, and nasal (fCO_2) were acquired simultaneously. All the equipment is connected to the data acquisition system through BNC cables, and the test subjects were positioned in a supine position.

The subjects were instructed not to make any unnecessarily body movements to avoid motion artifacts. The room temperature was $20 - 22\,^{\circ}\mathrm{C}$.

3.3.3 Respiratory Rate Analysis

In order to quantify the respiratory and cardiac contents of the sternal PPG signals and compare them with the reference signals, we used three methods: (1) Power spectrum analysis, (2) Magnitude squared coherence analysis, and (3) time-domain RR estimation. All three methods have been applied on data acquired during the first stage of the experiments, where, only the last method has been used for the second stage of the experiment.

Power Spectrum Analysis

The power spectral density (PSD via Welch's averaged, modified periodogram- method, 50% overlap, 160-s Hamming window) for the sternal PPG signal was calculated and the power $(\%)$ within the range of 0.1 to 0.45 Hz (6 to 27 breaths/min) was used as a measure of the respiratory component. The same procedure was used to estimate the cardiac content within the range of 0.5 to 2 Hz (30 to 120 beats/min) for the sternal PPG. The same PSD for the reference signals has also been calculated for comparison. Eight minutes recording periods were used in the analysis.

Magnitude Squared Coherence Analysis

The similarity between the fCO_2 reference signal and the sternal PPG signal as well as between the ECG reference signal and the sternal PPG signals is calculated using the magnitude squared coherence analysis [26]. The magnitude squared coherence $C_{xy}(f)$ is given in (3.1)

$$C_{xy}(f) = \frac{|Pxy(f)|^2}{Px(f)Py(f)} \tag{3.1}$$

The result is a normalized measure between 0 and 1 of the correlation between the frequency content of two signals x and y at the frequency f, where $P_{xy}(f)$ is the cross-spectral density between x and y, and $P_x(f)$ and $P_y(f)$ are the power spectra densities of x and y respectively. $C_{xy}(f)$ was calculated at the frequency of the reference RR and heart rate, respectively.

Calculation of the Sternal PPG based RR

The sternal PPG signal was filtered using a zero-phase 3rd order Butterworth band-pass filter with cut-off frequencies at 0.1-0.5 Hz (6 to 30 breaths/min) [37]. These cut-off values are chosen to suppress the cardiac-related variations and the frequencies below the respiratory frequency in the PPG signals. After the filtering process MATLAB's peak detection algorithm has been applied. The same procedure was applied to the capnographic reference fCO_2 signal. The RR was calculated using one-minute, non-overlapping segments.

3.3.4 Pulse Rate Analysis

The hemodynamic and the morphology of the sternal PPG is investigated using the approach of heart rate variability (HRV).

HRV obtained from ECG recordings is a commonly used method that reflects the balance between sympathetic and parasympathetic modulation of the heart rate [38]. HRV parameters are derived by analysis of the temporal relationship between successive heartbeats (R-R intervals) in the ECG signal. From these intervals we can compute time and frequency domain, and nonlinear dynamics analysis to extract features to assess the autonomic nervous system (ANS) modulation of the heart rate. The morphology of the PPG signal is useful for the study of autonomic control of the peripheral vascular tone [15]. The physiological information derived from the R-R intervals can also be derived from the pulse-to-pulse (P-P) intervals of the PPG signal. Studies on pulse rate variability (PRV) have been conducted on the peripheral location of the body, mainly at the fingertip

and the earlobe using a conventional pulse oximetry probes [39]. Prior to the extraction of R-R and P-P intervals, the ECG signals were band-pass filtered using a second order Butterworth filter with cut-off frequencies of 0.05 Hz and 40 Hz. As for the PPG signals the cut-off frequencies were 0.05 Hz and 15 Hz. The R-peak detection was performed using Pan and Tompkins QRS detection algorithm [40]. The R-R intervals were extracted from the located R-peaks. As for the PPG signals, the foot of the sternal PPG were located (using MatLab's peak detection function) and used to produce the P-P intervals. The peak can also be used, but for sternal PPG the foot is more distinct.

To compare the HRV and PRV methods, a commonly used time and frequency domain parameters were computed according to the standard definitions of HRV parameters [38]. As for the time domain parameters, the mean value of the R-R and P-P intervals (mean NN), the standard deviation of N-N intervals (SDNN), the square root of the mean of the squares of differences between successive N-N intervals (RMSSD), and the pNN50, which is the proportion of differences of successive intervals differing more than 50 ms was calculated. Prior to the frequency domain calculations the R-R and P-P intervals were resampled at 4 Hz and cubic spline interpolated [38]. From the power spectrum density the normalized low frequency (LF) power (0.04-0.15 Hz), the normalized high frequency (HF) power (0.15-0.4 Hz), and the LF/HF ratio has been computed. The time domain parameters are related mostly with the overall variability of the heart rate. The LF components represents the sympathetic and parasympathetic tones, while the HF components is more related to parasympathetic modulation.

The Pearson correlation coefficient was used to correlate the calculated parameters derived from the ECG and PPG respectively. In addition, the lower and the upper limits of agreement and the mean system bias between the two methods is compared using the Bland-Altman analysis. Furthermore, the mean squared error is computed between the values of the HRV parameters derived from the R-R and P-P intervals.

3.4 Results

Fig. 3.4 shows a 30 second segment of a typical recording, it is a recording during spontaneous respiration. From (a) to (d) the sternal PPG (PD1-PD4) acquired by the four photo detectors of the PPG probe, the rest are the signals recorded by the patient monitoring system; Finger PPG (e), ECG (f) and in- and exhaled carbon dioxide fraction (g). It is clearly seen that all the sternal PPG contains the cardiac pulses which are beat-by-beat synchronous with the heartbeats in the ECG signal and the pulses in the finger PPG. At the same time, it is seen how the cardiac pulses are superimposed on the respiratory baseline. These variation are in all four sternal PPG signals in sync with the nasal

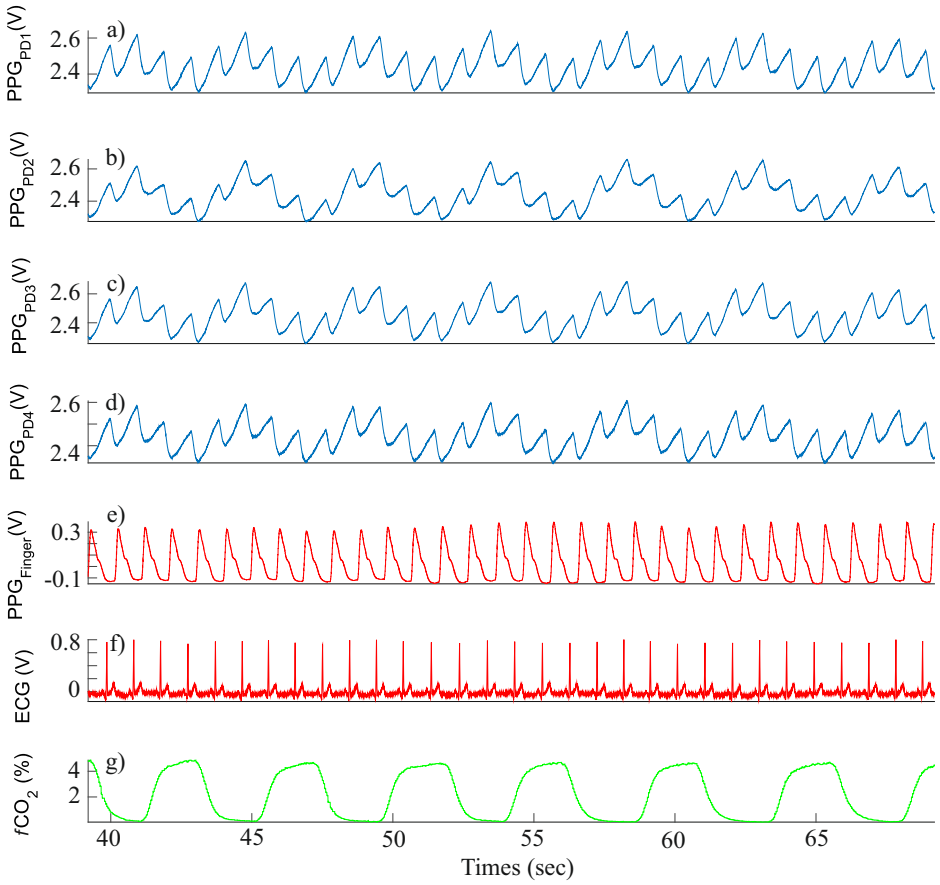

Figure 3.4: All the recorded modalities from the experiments. From (a) to (d) sternal PPG from the corresponding photo detectors (PD1-PD4). The rest of the signals are recorded through the patient monitoring system; (e) Finger PPG, (f) ECG and (g) in- and exhaled carbon dioxide fraction. All the signals in the figure are unfiltered data.

(fCO_2) signal. Fig. 3.5 shows a typical result of the power spectral analysis for all three acquired signals. The figure shows that the sternal PPG signal contains both a respiratory and a cardiac component. However, the power spectral content of the respiratory variations in the sternal PPG is larger than the power spectral content of the cardiac variations, which is the case for all the recorded signals.

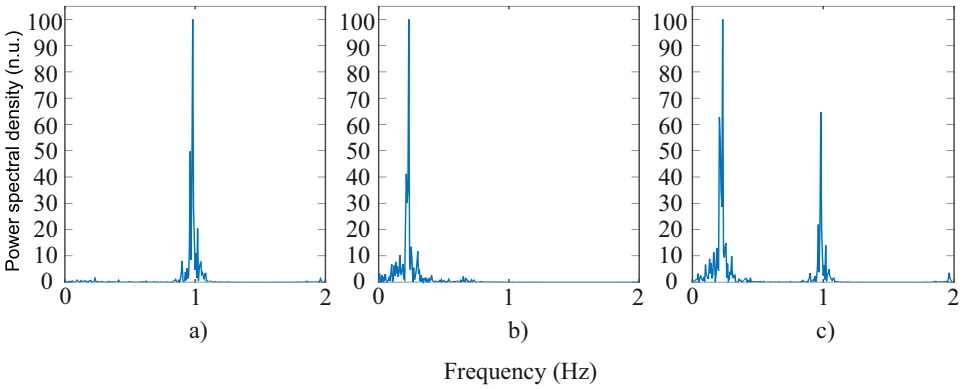

Figure 3.5: Power spectrum analysis of one of the recordings. (a) The ECG signal, (b) The respiratory reference signal, and (c) The sternal PPG signal. Generally, the sternal PPG signal contains both a respiratory and a cardiac component.

3.4.1 Respiratory and Cardiac Variations

During spontaneous respiration the median and interquartile range of the RR was calculated to 10.99 (3.68) breaths/min and 11.41 (3.32) breaths/min from sternal PPG and the reference signal respectively. As seen in Fig. 3.5 the sternal PPG signal contains both a respiratory and a cardiac component. The power spectral content of the respiratory variations in the sternal PPG is larger than the power spectral content of the cardiac variations. The median and interquartile range of the respiratory power spectral content in the PPG signal acquired for each photo detector (PD1-PD4) is 73.43 (25.37) %, 79.67 (23.91) %, 79.12 (29.55) %, and 70.1 (26.82) %. The pulse spectral power at the sternum is 23.76 (18.79) %, 18.19 (21.13) %, 18.81 (15.53) %, and 26.76 (19.11) % for all four sternal PPG signals respectively. The distribution of the spectral power content for all the participants from the recorded PPG signals is shown in Fig. 3.6. The result from the squared coherence calculation is shown in Table 3.1. The values are calculated for the respiration and for the pulse. As seen in the table the sternal PPG signal shows strong coherence with both the respiratory reference signal and the ECG reference signal, respectively. The results for the paced respirations are summarized in Table 3.2. RRs derived from sternal PPG are significantly correlated with reference RRs.

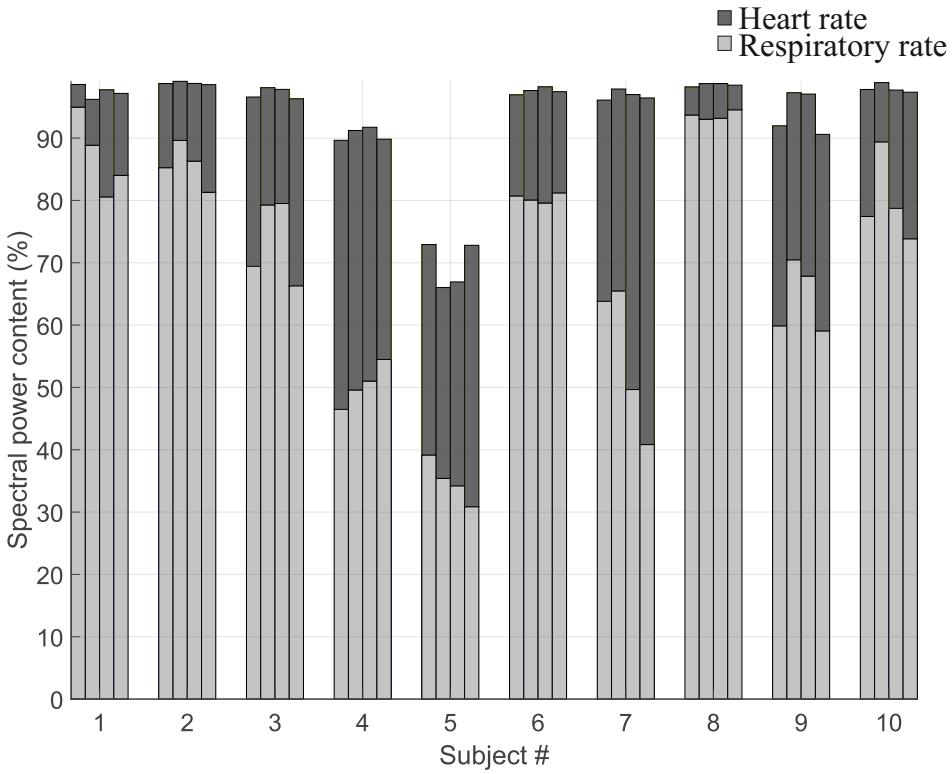

Figure 3.6: The respiration and cardiac spectral power content derived from each of the four sternal PPGs for each subject.

Table 3.1: Result of the squared coherence values when comparing sternal PPG from each photo detector with the respiration (resp) reference signal and pulse rate reference (pulse) ECG signal, respectively. IQR is the interquartile range.

Subject #	PD1		PD2		PD3		PD4	
	Resp	Pulse	Resp	Pulse	Resp	Pulse	Resp	Pulse
1	0.98	0.98	0.98	0.99	0.97	0.99	0.94	0.99
2	0.94	0.99	0.96	0.99	0.96	0.99	0.94	0.99
3	0.96	0.99	0.96	0.99	0.95	0.99	0.94	0.99
4	0.99	0.99	0.99	0.99	0.99	0.99	0.99	0.99
5	0.96	0.95	0.96	0.96	0.95	0.96	0.96	0.99
6	0.99	0.99	0.99	0.99	0.99	0.99	0.99	0.99
7	0.98	0.99	0.98	0.99	0.98	0.99	0.98	0.99
8	0.99	0.99	0.99	0.99	0.99	0.99	0.99	0.99
9	0.92	0.99	0.95	0.99	0.96	0.99	0.97	0.99
10	0.98	0.99	0.98	0.99	0.98	0.99	0.98	0.99
Median (IQR)	0.98 (0.03)	0.99 (0.01)	0.98 (0.03)	0.99 (0.00)	0.98 (0.03)	0.99 (0.00)	0.97 (0.05)	0.99 (0.00)

Table 3.2: Summary of the RRs during paced respiration. The results are expressed in median (interquartile range).

Visual scale RR (breaths/min)	fCO_2 RR (breaths/min)	Sternal PPG RR (breaths/min)
6	6.10 (0.14)	6.03 (0.15)
12	12 (0.14)	11.95 (0.12)
17	17.01 (0.55)	16.97 (0.12)
24	23.99 (0.15)	23.86 (0.24)
27	26.98 (0.01)	26.98 (0.13)
Correlation Coefficient		0.99 (p <0.001)

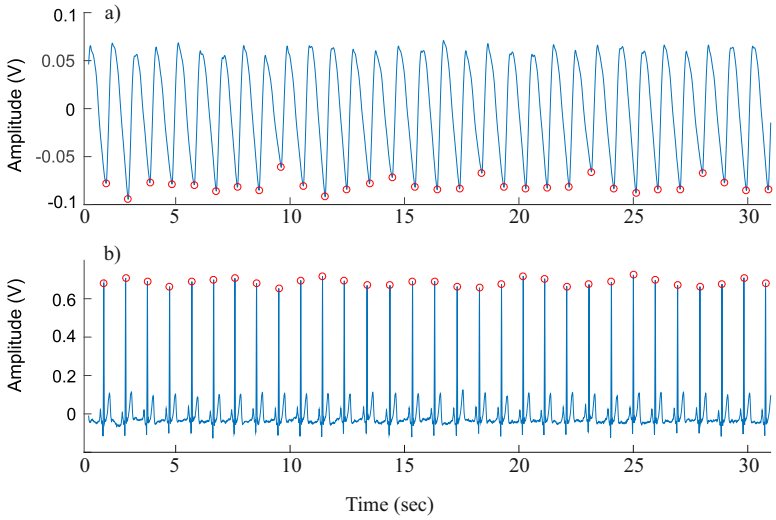

Figure 3.7: (a) A band-pass filtered PPG signal (PD2) with the detected foot (red markers) that are used to form the P-P interval. (b) A filtered ECG signal and the detected R peaks (red markers) are used to form the R-R intervals from which the HRV analysis is performed.

3.4.2 Pulse Rate Analysis

A band-pass filtered signal of sternal PPG is shown in Fig. 3.7 together with the corresponding detected foot. From the detected indicies the P-P interval time series is derived and shown in Fig. 3.8a. The same procedure is done with the ECG signal and the R-R interval time series is derived as shown in Fig. 3.8b. All detected peaks were visually inspected and manually corrected. For all the subjects the derived parameters obtained from PRV and HRV are presented in Table 3.3. All the computed parameters derived from the PRV had correlation coefficients of > 0.95 (p <0.001) when compared to HRV. The error analysis showed insignificant differences between the parameters derived from the two methods (p <0.05). The Bland-Altmann analysis showed close agreement between the parameters derived from ECG and PPG. During spontaneous respiration the average system bias for the mean NN interval was -0.03 ms and the lower and upper limits of agreement was -0.561 ms and 0.501 ms respectively, cf. Fig. 3.9a. As for the LF/HF ratio, the average system bias was -0.0064 ms and the lower and upper LOA was -0.27 ms and 0.25 ms respectively as seen in Fig. 3.9b. Similarly, high degree of agreement was found for the rest of the parameters under spontaneous respiration. During paced respiration the average system bias increased in the same direction for all parameters. It is also seen in Table 3.3, that the LF/HF ratio increased from 1.045 to 2.99 for HRV and from 1.05 to 2.76 for PRV.

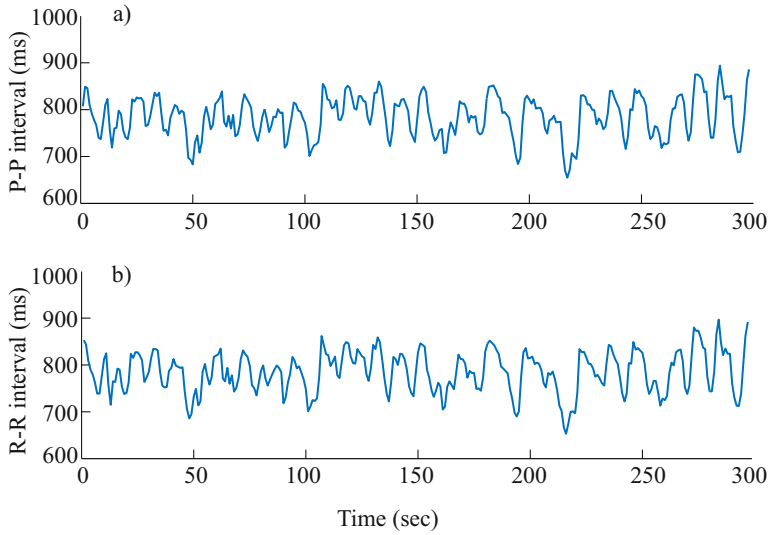

Figure 3.8: Comparison of the (a) P-P interval derived from the sternal PPG signal and (b) R-R interval derived from the ECG signal.

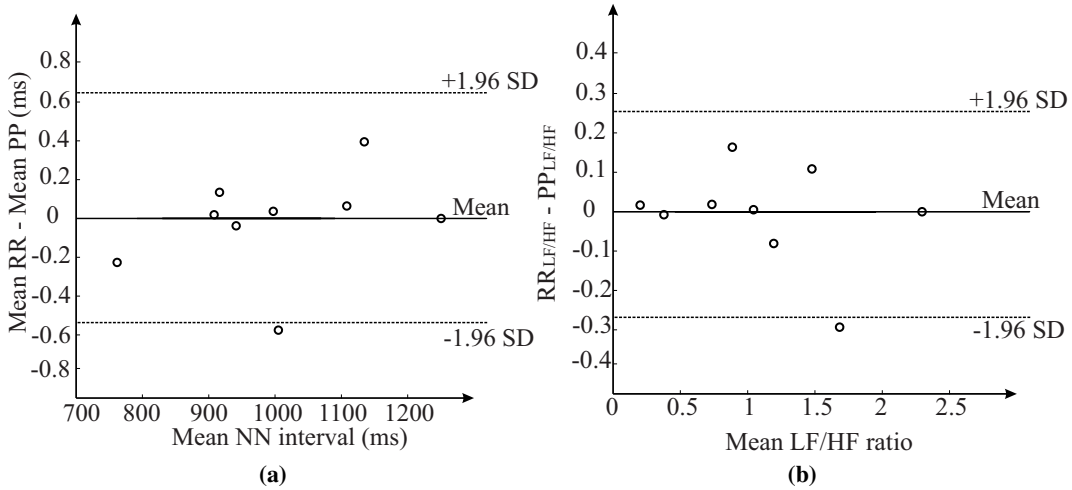

Figure 3.9: (a) Bland-Altman plot of the Mean NN derived from the sternal PPG signal and the Mean NN derived from the ECG signal.(b) Bland-Altman plot of the LF/HF ratio derived from the sternal PPG signal and the LF/HF ratio derived from the ECG signal.

Table 3.3: The time and frequency domain parameters, correlation coefficients and Bland-Altmann analysis derived from P-P and R-R intervals respectively. LOA corresponds to the limits of agreement lines.

	Parameters	HRV (Mean±SD)	PRV (Mean±SD)	Bias	Lower LOA	Upper LOA	Correlation coef.	Abs. error
Spontenous resp.	*Time domain:*							
	Mean NN (ms)	1012±134	1012±134	-0.03	-0.56	0.5	0.99	0
	SDNN (ms)	63±34	63±34.6	-0.2	-2.5	2.15	0.99	0
	RMSSD (ms)	50.5±41.2	50.64±41.6	-0.1	-5.8	5.53	0.99	0
	pNN50 (%)	21.01±23.7	20.9±23.3	0.04	-5.9	5.9	0.99	0
	Freq. domain:							
	LF/HF	1.045±0.6	1.05±0.7	0	-0.3	0.3	0.98	0
Paced resp.	*Time domain:*							
	Mean NN (ms)	953±112	954±112	-0.1	-1.3	1.1	0.99	0
	SDNN (ms)	52±24	55±23	-3.1	-9.1	3	0.99	0.1
	RMSSD (ms)	45.1±32.9	53.8±35.7	-8.7	-23.2	6	0.98	0.2
	pNN50 (%)	22.5±21.7	29.5±24.6	-6.9	8.8	-22.7	0.95	0.2
	Freq. domain:							
	LF/HF	2.9±1.9	2.8±1.7	0.2	-0.9	1.4	0.95	0.1

3.5 Discussion

The key findings of this pre-clinical study are that sternal PPG shows very strong coherence with the respiratory fCO_2 reference signal and the ECG signal, respectively. Furthermore, the power spectral analysis showed that the sternal PPG contains larger power spectral content of the respiratory variations than the cardiac variations. This is a key result, which illustrates that the RR can be derived at the sternum with high accuracy within a clinical relevant range (6-27 breaths/min). Additionally, the results showed a high correlation 0.99 ($p > 0.001$) between the capnography based RR and the PPG based RR. The power spectral density and magnitude squared coherence analysis are widely used in the literature in order to quantify the respiratory content in the PPG signal. In this study we used similar approach as reported by Nilsson et al. [26]. These authors reported that the best site for measuring the RR is at the forearm, but they did not investigate the PPG at the sternum. In this study the sternal PPG had a relatively large respiratory component compared to what is reported in [26]. A direct comparison to peripheral PPG is described in chapter 6. Furthermore, the magnitude squared coherence analysis showed a strong similarity (0.98) between the sternal PPG signal and the ECG reference signal. In terms of the pulse rate variations, the study showed a close agreement between the HRV parameters derived from the PPG signals and the ECG signals on a healthy group of subjects at rest and under paced respiration.

Although, the average system bias increased between the parameters derived from PRV and HRV, the absolute values changed in the same direction as seen in Table 3.3. The LF/HF ratio derived from PRV increased during paced respiration, confirming that the change in the autonomic tone was also reflected in the PRV as it did in the HRV. The sternal PPG sensor is reliable for recording a PPG signal from, which HRV parameters can be derived, at least in healthy subjects at rest. The morphology of the PPG signal acquired at the sternum has also a clear systolic and end-diastolic peak, as seen in Fig. 3.7. This might be useful for different types of pulse wave analysis since other clinically relevant features may be extracted. Recent studies have reported that the use of PPG recordings might be a more convenient method for the measurement of HRV in clinical environments and for ambulatory recordings than ECG. However, there has been a difference in the accuracy between the PRV derived from finger PPG and HRV both at rest and during physical and mental tasks [41]. Furthermore, there is a clear uncertainty regarding the measuring site [41].

The vascular properties of the skin differ between various locations on the body. The tissue at the sternum is less perfused when compared with the peripheral locations such as the fingertip [20]. Nevertheless, acquiring the RR from sternal PPG has several advantages that makes the sternum an appropriate sensor position. First of all, a probe placed at the sternum is less obtrusive than earlobe or finger probes. Secondly, the sternum can be used to monitor other clinically relevant parameter such as pulse oximetry [20]. Respiratory pressure variations in the thoracic cavity affects the blood volume on the venous side and on the arterial side. We propose that the center location at the sternum and the anatomical structure of the thoracic cage is the main contributor to a pronounced respiratory effect. The perforating veins and arteries that surround the chest bone affect the PPG signal at the sternum. In addition to this mechanism, we propose that the mechanical tension over the sternum during inhalation/exhalation causes the skin to stretch. This affects the underlying vasculature of the skin and due to the thin wall of the veins, this mechanical effect is believed to be more prominent in the veins than in the arteries and therefore contributes to the respiratory component in the sternal PPG signal.

3.6 Conclusive Remarks

This proof of principle study has shown through different kind of signal analysis that the RR and the pulse rate can be calculated from the sternal PPG. We propose that the local anatomy of the skin at the sternum and the physiology of the thoracic cage create three mechanisms that dynamically affect the blood volume and makes sternum superior in terms of monitoring the RR from PPG compared to other measurement sites mentioned in the literature. For the thoracic cage, the three mechanisms that affect the sternal PPG are:

The mechanical stretching over the sternum in relation to expansion of the thoracic cage and stretch of the skin produces a compression pressure to the underlying blood vessels. This is most noticeable for the veins because their thinner vessel walls make them more pressure sensitive when compared to the arteries.

Respiratory induced variations arises from the venous return to the heart, caused by the alterations in intrathoracic pressure. This mechanism is well documented [31–35].

The arterial effect is seen as cardiac pulsations with similar frequency as in the ECG. The cardiac pulse is from the pulsating nature of the arterial blood volume, which is taken advantage of in ordinary pulse-oximetry using the relation between PPG signals at two different wavelengths (mainly 660 nm and 940 nm). The cardiac pulse variations was seen in the raw PPG signal of the sternum, although roughly $75\ \%$ of the total blood volume is present in the venous compartment (Fig. 3.4a-d).

Another important finding is that there was no significant difference between the four PPG signals acquired from each photo detector. This finding is important for the future design of a PPG sensor. Based on this, four photo detectors is found to be redundant in the developed PPG probe. However, connecting the photo detectors in parallel and thereby sum the total currents might be a useful approach. It is a trade-of between signal quality and sensor design constraints. During the experiment it was observed that the signal quality got enhanced when a pressure is applied on the skin where the sensor is placed. The effect of probe pressure and coupling media is discussed in the next chapter. Additionally, a description of a developed PPG sensor is given.

CHAPTER

FOUR

DEVELOPMENT OF A VITAL SIGN PATCH

Objectives *Central to the PPG sensor design is the ability of long-term monitoring and reliable sensor attachment to the sternum. In the previous chapter the PPG probe with four photo detectors was briefly introduced and used in a proof-of-principle study. This chapter will focus on the conception, development and evaluation of a fully functional prototype pulse oximeter sensor (PPG-patch). Prior to this, a short review of previous reflective pulse oximeter designs is given. Some information regarding the design and the fabrication of the PPG-patch is not included in this dissertation due to confidentiality reasons.*

4.1 Background

Sternum as a measurement site challenges the design of the device and demands a new paradigm in designing the reflectance sensor. As mentioned in chapter 3, the sternal PPG contains both a cardiac and a respiratory component and with a proper sensor-skin coupling it was possible to obtain a reliable PPG signal at the sternum as shown in the proof of principle study, cf. Chapter 3.

The work of designing reflection mode pulse oximeter sensors is well documented in the scientific literature and in the patents. Interestingly was the beginning of Nellcors progression in the medical device market using their first reflection mode probes [42]. Moreover, other attempts in developing reflection mode pulse oximeter sensors was done in the late 80's and in the 90's [19, 36, 43–45]. The focus was on developing sensors with multiple wavelength or photo detectors, sensors with improved handling of motion artifacts and better accuracy during low saturations

levels. An early design made by Dassel et al. [46] shows a sensor design with an array of three photo detectors and one single light source as seen in Fig. 4.1a. A similar design approach has been used by Mendelson et al. [47, 48]. Their aim was to lower the pulse oximeter's power consumption using low LED drive current but large photo detector area. Another design approach by Takani et al. [49] used 16 LEDs radially placed around one single photo detector as seen in Fig. 4.1b. A combination of this sensor design and the sensor designed by Mendelson's group was recently adapted by Sola et al. [50] and is shown in Fig. 4.1c. This PPG probe has eight photo detectors and 16 dual LEDs. The sensor is designed to be placed at the sternal area using an elastic band that surrounds the whole upper thorax [20]. The elastic band is used to obtain a contact pressure between the skin and the PPG probe. Similar principle is used by [51] on the forehead using a commercially available headband (OxiMax MAX-FAST headband; Nellcor Healthcare, Pleasanton CA). However, the headband is not only used to enhance the contact interface, but to compress the superficial veins so the blood oxygen saturation readings are not affected by the venous pooling.

In the attempt of making a sensor design with large photo detector area radially oriented around a light source embedded in a an electronic patch has recently been designed by Duun et al. [10]. All these designs have two functionalities in common; firstly large photo detector area (one large or multiple photo detectors) and secondly many LEDs. The first case gives a large detecting area with low power consumption and the latter gives a better PPG signal quality, but larger power consumption.

Another important design aspect that needs to be taken into account is the separation distance between the photo detector and the light source. The light backscattered from the tissue contains the same information in all scattering directions. This gives the reason to design the sensor so that the photo detectors are distributed from an area concentric with the light source. It is well known that this distance is significant for the quality of the recorded PPG signal [15]. If the distance is very small the AC/DC ratio of the PPG signal will be low and therefore it will contain very small pulsatile information. If the distance is very large the light penetration depth will increase and the overall signal-to-noise level will be low. Moreover, it will affect the power consumption of the device because more light is needed when the light and photo detectors are distant. The intensity of the backscattered light decreases in direct proportion to the square of the separation distance between the photo detector and the light source [36, 52]. Hicky and Kyriacou [53] found that the optimal separation distance was in the range of 3-6 mm when testing on the finger, while Takatani et al. [49] and Mendelson et al. [47] are suggesting between 4 mm and 10 mm based on experiments conducted on the forearm. Furthermore, it was suggested that the separation distance of 7 mm is the most optimal. In a later study conducted by Mendelson and Pujary [54] separation distances between 6 mm and 10 mm were used. Thus, the ideal separation distance between the photo detector and the light source involves a trade-of between signal quality and power consumption.

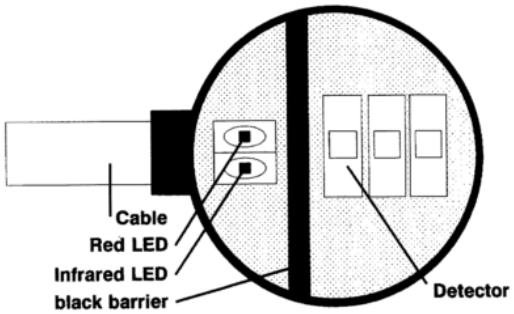

(a) Sensor design by Dassel et al. [46]. The sensor design constitute of one dual wavelength LED and an array of three photo detectors.

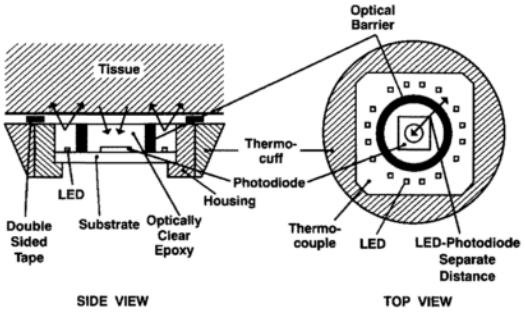

(b) Sensor design by Takatani et al. [49] The sensor has 16 LEDs radially oriented around one photo detector.

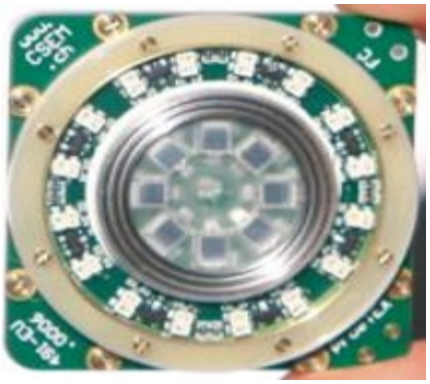

(c) Sensor design by Sola et al. [50]. The sensor contains eight photo detectors and 16 dual LEDs.

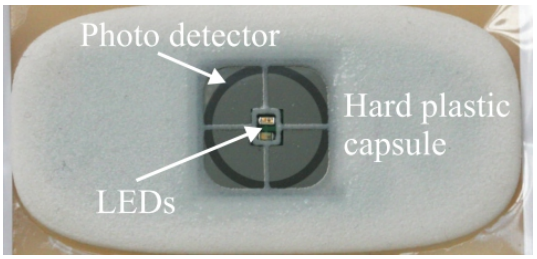

(d) Sensor design by Duun et al. [10]. This sensor has an annular photo detector that surrounds one dual wavelength LED.

Figure 4.1: Four different reflection mode pulse oximeter designs.

Thus, in the context of this work it is important to lower the power consumption by choosing only one light source and separation distance between the optical elements in the range of 4 mm to 10 mm. In regarding the photo detector area it was shown in the proof-of-principle study, that the use of four separately connected photo detectors (each having 4 mm^2 sensitivity area) gave no significant difference. Therefore, it is assessed that four photo detectors may be redundant and the amount of photo detectors can easily be reduced.

Another important aspect is the contact force between the sensor and the skin. When a pressure is exerted on the skin by the sensor, the geometry of the superficial layers of the skin changes and the arterial and venous vessel diameters is affected. The quality of the PPG signal is significantly affected when pressure is applied. This claim is reported by numerous research groups [55–58]. There is a consensus in the literature that the optimal pressure varies and depends on the measurement site. However, no optimum or accepted standardization have been implemented for clinical or experimental PPG measurements.

In the context of this work a contact force between the sensor and the skin was applied by designing the optical window such that it is higher than the rest of the sensor body.

4.2 Sensor Design Specifications

It is important that the PPG-patch can operate in two modes; A mode for short-term measurement and a mode for long-term measurement. The technical setup for the first mode is sketched in Fig. 4.2a. The output pins from the PPG-patch are connected through BNC cables to a data acquisition system. The PPG-patch can be configured and controlled through a microcontroller that is connected to a computer via USB. With this setup, it is possible to connect other hospital devices (i.e. capnography, conventional pulse oximeters and ECG recorder) to the same data acquisition system and thereby simultaneously acquire all the connected signals. In the second operation mode the PPG-patch electronics is connected to the ePatch® electric front-end. All the data acquisition is done through the ePatch® electronics and modified firmware. This configuration mode does not require any external wires. However, it limits the design of the PPG-patch because of the geometry and the limited space inside the ePatch® mechanical body, cf. Fig. 4.2b. On the other hand, it will be possible to acquire PPG, ECG and accelerometer signals synchronously from the same device. Moreover, it can be attached to the body through DELTA's ePatch® electrode. A sketch of the ePatch® electrode is seen in Fig. 4.2b.

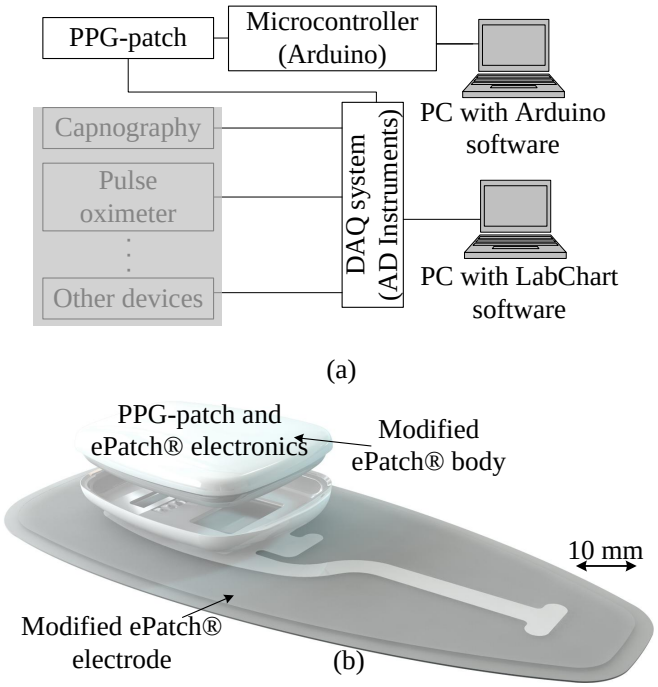

Figure 4.2: (a) The technical setup where PPG-patch can function independently of the ePatch® framework. The faded blocks can be any device from the hospital that has a digital or analog output. (b) The PPG-patch sensor configuration. It was necessary to modify both the ePatch® and the corresponding electrode.

The primary design constraint of the PPG-patch was that it must fit in the ePatch®electrode socket manufactured by DELTA. Therefore, the front-end architecture and the opto-mechanics should fit into the mechanical body of the ePatch®. The secondary constrain was that the PPG-patch can work independent of the ePatch®platform. Meaning that by connecting it to a data acquisition system while it is attached to the skin one should be able to record the PPG signal.

Therefore it was decided that the PPG-patch must have the following properties:

- The printed circuit board (PCB) of the PPG-patch must fit in the area where the ePatch battery is located, hence the PCB must only have a dimension of 32 x 20 mm.
- The PPG-patch must have two photo detectors and one dual LED; red and infrared ($\lambda = 940$ nm and $\lambda = 660$ nm). The photo detectors must have relatively high spectral sensitivity in the red and infrared region.
- The LED and photo detector separation distance must be between 4 mm and 10 mm.

- The LED and photo detectors must be separated such that no direct light can be registered by the photo detectors.
- The PPG-patch electronics can be connected with the ePatch® electric front-end. So in addition to the PPG signals, one channel ECG and three accelerometer channels (X, Y, Z) can be acquired in the internal flash memory of the ePatch® .

All the electronics components must be surface-mount devices (SMDs) and operate with 3.7 V power supply.

4.3 Opto-Mechanical Construction

As mentioned previously the mechanical body of the ePatch® was used to integrate the whole PPG-patch solution. It was chosen to use silicone photo detectors (VBP104SR, Vishay Semiconductors) with an active sensing area of 4.4 mm^2, cf. Appendix B. A dual LED component (SML12R3KIR941T-TR, Ledtronics, INC.) with peak emission wavelength of 660 nm and 940 nm was chosen as a light source. The seperation distance between the optical elements was chosen to be 7 mm. To minimize the amount of light transmission and reflection between the LEDs and the photo detectors an optical opaque shield of black polyoxymethylen was placed such that it surrounds the optical element. The LEDs and photo detectors was encapsulated with an optically transparent and biocompatible epoxy (EPO-TEK 302-3M, Epoxy Technology, Inc.), cf. Appendix B. The chosen epoxy has a refractive index of 1.56 which is close to the refractive index of the epidermal layer of the human skin, which is approximately 1.43 at 660 nm and 1.42 at 940 nm [59]. The final result after this coating process can be seen in Fig. 4.3.

4.4 PPG-patch Front-end Architecture

The electronics of the PPG-patch has been made to support the purpose of embedding the solution into the ePatch® platform utilizing the recording of two PPG channels in addition to ECG and triaxial accelerometer at the sternum. Moreover, the PPG-patch front-end was also designed to work independently of the ePatch® platform utilizing the ability of short-term measurement. In this section a description of the PPG-patch electronics together with its functionality independently of the ePatch® platform will be given. In the next section it is described how the PPG-patch sensor has been embedded with the existing state of the art ePatch® platform. A diagram of the front-end architecture of the PPG-patch is shown in Fig. 4.4 and the corresponding circuit schematic is shown in Fig. 4.5. Going from the optical domain to the electrical and then to the digital requires

three fundamental blocks; a signal conditioning block, a LED intensity regulation block, and a data acquisition and processing block. The three blocks are marked with red dashed squares in Fig. 4.4.

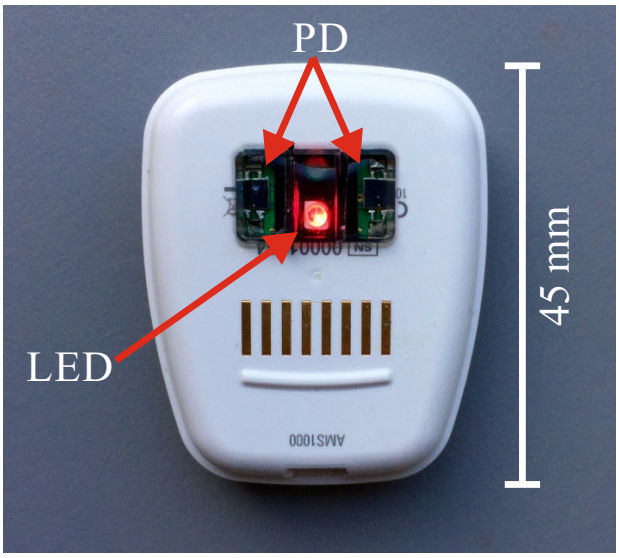

Figure 4.3: The final result of the PPG-patch. It is seen how optically transparent the optical window is.

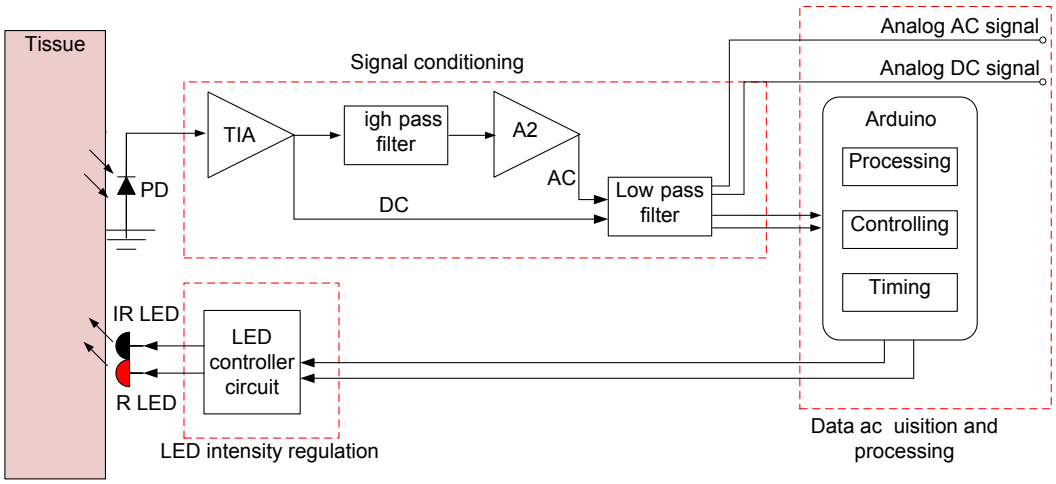

Figure 4.4: Diagram of the PPG-patch electronic front-end architecture. It contains three main blocks (surrounded by red dashed lines); Signal conditioning, LED intensity regulation Data acquisition and processing.

4.4.1 Signal Conditioning

The photo current detected by the photo detectors (PD) is passed through a trans-impedance amplifier (TIA) each. The signal conditioning is the same for both photo detectors so only the signal from one photo detector is described. Going from the TIA the signal is subsequently passed through different stages carrying out the following functions:

- Filtering.
- Dividing the signal into AC and DC components.
- Providing further amplification for the AC component of the signal, and adjusting the DC level to better take advantage of the input dynamic range of the A/D converter.

Current-to-voltage Conversion

The photo detector detects the light signals coming from the tissue and produces a current proportional to the intensity of the received light. By earlier experimental tests, the current reaching the photo detector was found to be $< 1\mu$A. To convert the current signal to a useful voltage signal the TIA was used. The schematic diagram of the TIA is shown in Fig. 4.6.

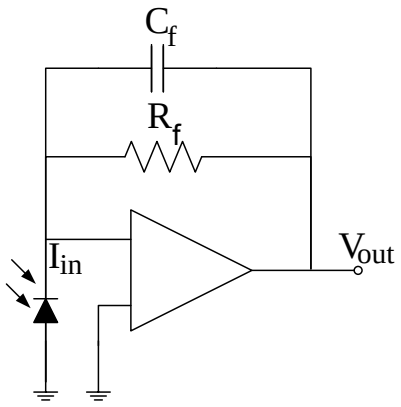

Figure 4.6: Electric diagram of the trans-impedance amplifier (TIA) that converts the photo detector current I_{in} into the voltage output V_{out}. The gain is given by the feedback resistor R_f and the bandwidth limitation is employed by the feedback capacitor C_f across R_f.

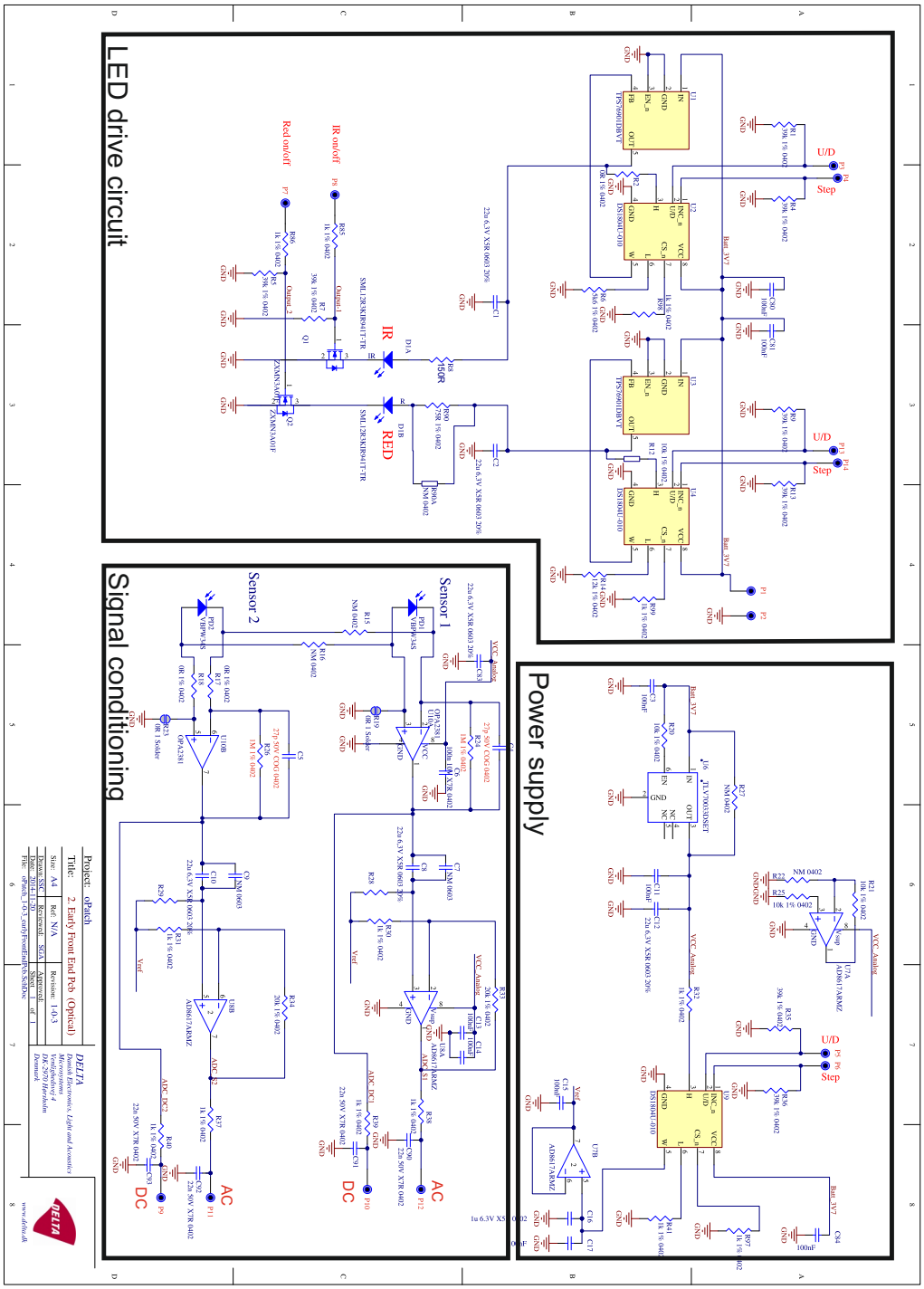

Figure 4.5: Schematic of the PPG-patch electronic front-end architecture.

The current through the feedback resistor R_f creates a voltage at the output that is proportional to the current coming from the photo detector I_{in}. The output voltage can be calculated using Ohm's law across R_f;

$$V_{out} = I_{in} R_f \tag{4.1}$$

and thus the desired amplification is determined via R_f. The noise spectral density produced by R_f increases with the square-root of R_f, whereas the output signal increases linearly, therefor the signal-to-noise ratio is improved when all the required gain is placed at this amplification stage [13]. To accomplish this, the feedback resistor was chosen to be $1M\Omega$. The total noise increases with an increased bandwidth. Thus, the bandwidth of the TIA has been limited using a feedback capacitor C_f across R_f. This approach serves as a low-pass filtering and also stabilize the TIA and prevents oscillations in the required bandwidth range. Although, the PPG signal bandwidth is 0.1-5 Hz, it is important to take into account the switching rate of the LEDs as this will determine the bandwidth of the TIA. The PPG for a given wavelength is acquired when the LED corresponding to that wavelength, is turned on. It was chosen to apply a switching rate of 500 Hz. However, it is possible to change this rate in the firmware of the PPG-patch as described in section 4.4.3. It was decided to have 6 kHz as a cut-off of the TIA bandwidth to make it possible to increase the switching frequency if this was desired. The feedback capacitor value C_f can therefor be calculated as follows:

$$\begin{aligned} C_f &= \frac{1}{2\pi R_f f_{-3dB}} \\ &= 26.5pF \end{aligned} \tag{4.2}$$

where R_f and f_{-3dB} is $1M\Omega$ and $6kHz$ respectively. The employed feedback capacitor value was 27 pF. The TIA chosen for this application is a low noise OPA2381, which operates with a single low voltage supply (2.7-5.5V), cf. Appendix B.

The output from the TIA contains a PPG signal including the AC and a DC components.

Filtering and Amplification

The next step is to split the DC part of the signal from the relatively smaller AC. Both signals are processed independently as seen in Fig. 4.4. The DC signal is low-pass filtered using a passive low-pass filter with cut-off frequency of 7 kHz. This filter is applied to filter out very high frequencies. The AC part is high-pass filtered using a passive high-pass filter with cut-off frequency of 0.05 Hz. This is applied to filter out any DC offset. The AC part is further amplified through a second stage amplifier, A2. The amplification is applied such that the total dynamic range of the A/D converter is used. The gain at this stage is 20 and can be changed manually by changing a corresponding resistor. Usually this amplification is made changeable through software. But, this is not the case with the

PPG-patch. The final part of the analog processing of the AC signal is a low-pass filter with cut-off frequency of 7 kHz to suppress high frequencies. The DC signal is fed to a custom build Arduino box and is used to regulate the intensity of the LEDs by determining the signal level of DC signal, this regulation is explained in section 4.4.3. The AC signal is also fed to the Arduino board but is only used for visualization purpose.

Both the AC and the DC signals contains a multiplexed PPG signal. The demultiplexing of the signal into a DC and an AC of the red PPG and a DC and an AC of the infrared PPG is done in the post processing stages.

4.4.2 LED Intensity Regulation

The photo detector does not discriminate between received wavelengths. Therefore, the LEDs are switching on and off alternately. The switching frequency is 500 Hz and the LEDs are on each for 2 ms giving a duty cycle of 50 $\%$. The intensity of the LEDs is controlled using two digital potentiometers, which can be modified through digital output pins in the Arduino microcontroller board. The range of the digital potentiometers is from 0-100 Ω. At 0 Ω the maximum current is 17 mA when the red LED is on and 15 mA when the infrared is on. The minimum current is when the potentiometer is at 100 Ω giving 1.6 mA and 1 mA for the red and infrared LEDs respectively. The current for each LED is kept constant through a low-dropout regulator. The on and off switching is controlled through the digital output pins of the Arduino microcontroller board. The timing diagram for each LED is shown in Fig 4.7.

The way the AC and the DC signals are demultiplexed is by having a squared trigger signal generated by the Arduino microprocessor as seen in Fig. 4.7. At the rising edge the red LED is on and at the falling edge the infrared LED is on. Detecting of the rising and falling edges is done in the post processing of the signals.

Prior to PPG recording the LED intensities are regulated based on the level of the DC signals. It is important that the DC levels are equal both when the red and infrared LED are on. Otherwise the second stage amplifier will make the AC signal get out of range. All the terminals from P1-P14 (seen in Fig. 4.5) are connected to a socket from which a cable can be attached to and communicate with the Arduino board. The terminals P9-P12 belong to the AC and DC output signals from each photo detector. A photograph of the PPG-patch with the customized Arduino board (in the black box) is shown in Fig. 4.8. The PPG-patch is powered through the Arduino board which is powered through the USB.

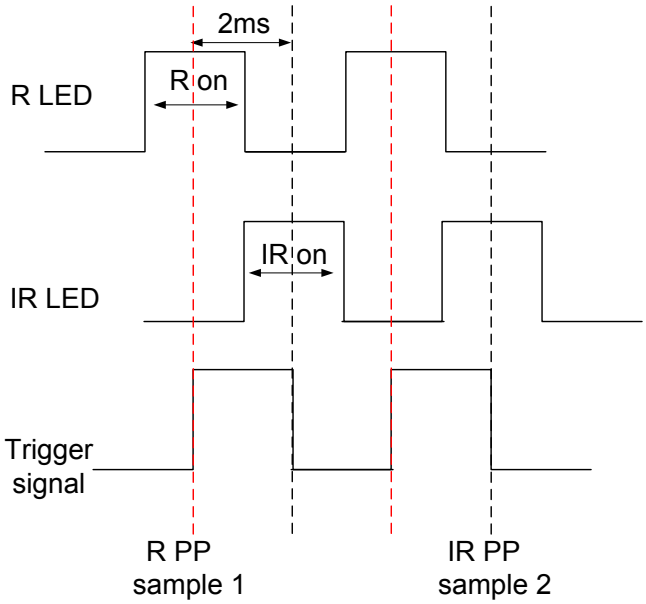

Figure 4.7: Timing diagram of the red (R) and infrared (IR) LEDs on and off. The trigger signal is created by the Arduino microcontroller. On the rising edge the sample belongs to the red PPG signal and on the falling edge the sample belongs to the infrared PPG signal.

4.4.3 Data Acquisition and Processing

To drive the LEDs a firmware was programmed and flashed into the Arduino microprocessor. The firmware can be modified and programmed on a computer. The purpose of the firmware is to control the LED intensities and the switching rates of the LED. The recording of the PPG signal is not done through the Arduino board but via a data acquisition device from AD instruments (Powerlab 8/35, 16 bit ADC, ADInstruments, USA). When the PPG-patch is attached to the sternum either via the modified ePatch® electrode or just via adhesive tape, the firmware loads an algorithm that starts and regulate the intensities of the LEDs such that the DC levels are equal for both wavelengths. A flowchart of this calibration process is shown in Fig. 4.9. First the red LED is turned on and the DC level is read and saved, then it is turned off. Subsequently the infrared LED is turned on and a DC level is detected and saved, and then it is turned off. The next step is now to compare both DC levels. If the DC levels are different then the intensity of the red LED is changed. When a successful calibration is made, the LEDs start switching and the trigger signal does also start. The algorithm is made such that the DC level corresponding to the infrared signal always tries to be equal to the one belonging to the DC level of the red PPG. During a recording, the calibration sequence can be initiated by reseting the Arduino board.

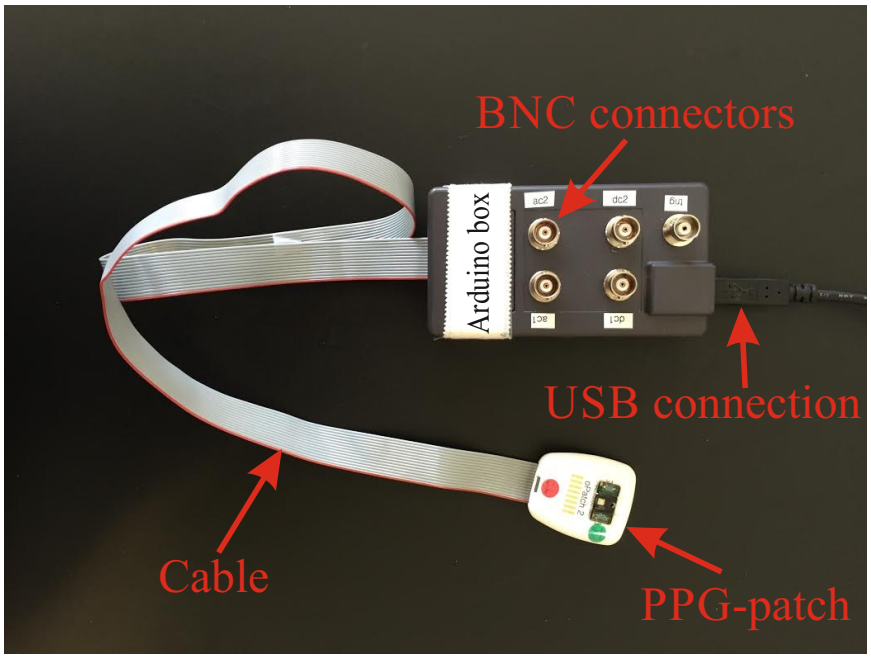

Figure 4.8: A picture of the PPG-patch and the customized Arduino box. With this "toolkit" it is possible to make PPG measurements when the Arduino box is connected to a PC through USB communication. Connecting the BNC connectors with a data acquisition system the PPG signals from both photo detectors can be acquired.

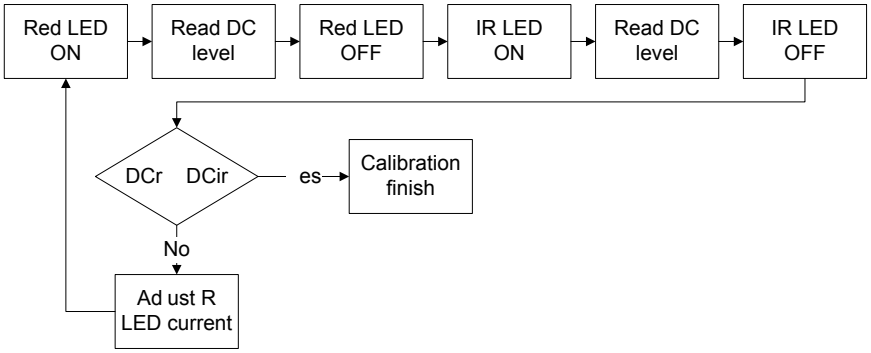

Figure 4.9: A flowchart of the initial calibration process. This sequence continues as long the DC levels of the RED (DCr) and the infrared (DCir) signals are not equal.

The performance of the PPG-patch and data processing system was tested in the laboratory. Red and infrared PPG signals were obtained both on the index finger and on the sternum. The laboratory lights were switched off to eliminate any ambient light interference. Good quality PPG signals with large amplitudes were acquired from all seven devices. A typical PPG signal recorded at the sternum for both wavelengths is shown in Fig. 4.10. As seen the PPG signals are multiplexed. In the post processing the PPG signal is demultiplexed into an AC and a DC signal for each wavelength. Fig. 4.11 shows the timing between the recorded PPG signals and the trigger signal. It is clearly seen how important it is that the samples are taking when the LED current is stable because some times there is an overshoot when the LEDs turns on. The result after the demultiplexing is seen in Fig. 4.12. The result giving is four PPG channels for each photo detector; AC and DC for each wavelengths with a sampling frequency of 256 Hz. The signal contains everything needed in order to calculate the respiratory rate and the oxygen saturation in the blood.

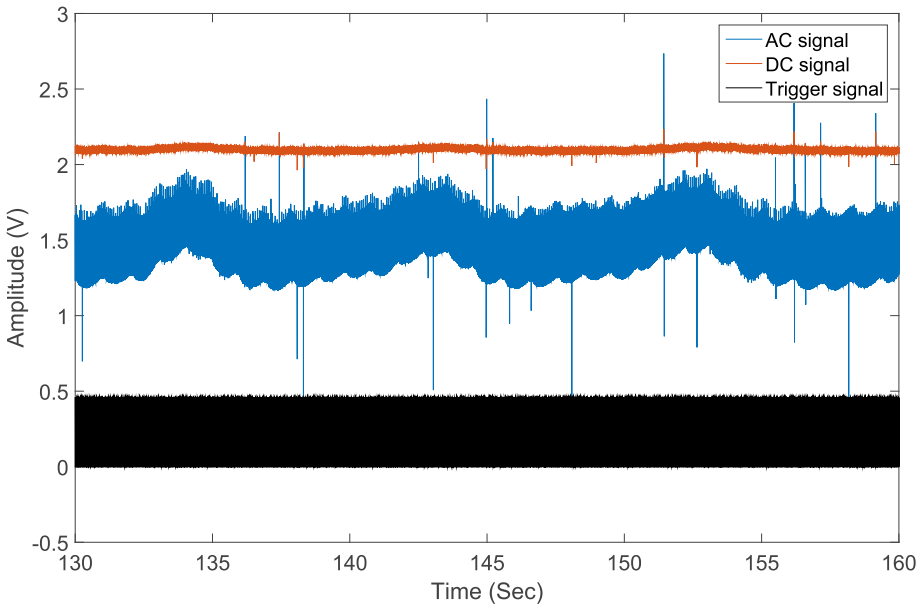

Figure 4.10: PPG signals acquired at the sternum. The AC and DC signals are multiplexed. The trigger signal (bottom) is used to separate the PPG signals into DC and AC for each wavelength.

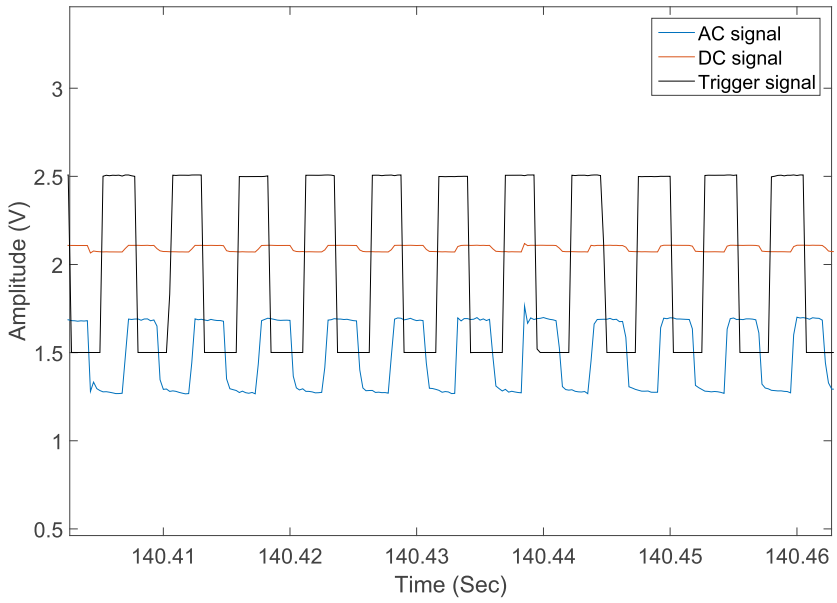

Figure 4.11: The timing between the PPG signals and the trigger signal.

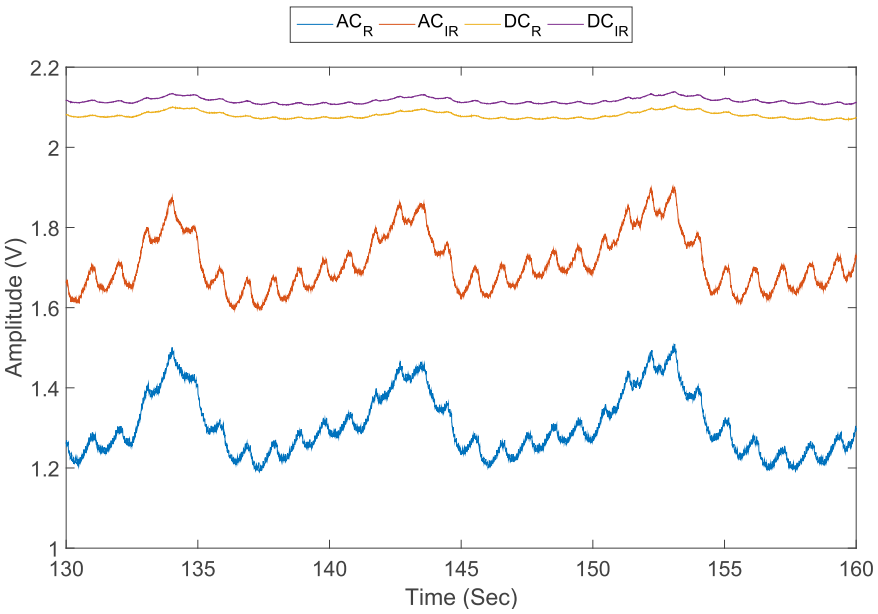

Figure 4.12: Demultiplexed PPG signals. Raw Red and infrared AC and DC signals obtained at the sternum. It is clearly seen how the cardiac pulses are superimposed on the respiratory component. The segment is obtained during a controlled low paced respiration (6 breaths/min) in the laboratory.

4.5 PPG-patch for Long-term Monitoring

As written in section 4.2 the main requirement was that the PPG-patch can be used for long-term monitoring. For this reason the PPG-patch had to have a separate microcontroller and flash memory in order to process and store the acquired PPG signal. For this purpose the ePatch® electronic front-end was connected together with the PPG-patch electronic front-end. The challenge here was that the PPG-patch electronics was designed to work with an earlier version of the ePatch® electronic front-end and the new version came after the fabrication of PPG-patch. However, at the end it was possible to embed the PPG-patch with the recently changed ePatch® electronics. One of the ECG channels that is usually used during a regular ECG measurement with the ePatch® has been disconnected and the DC output from the PPG-patch PCB has been wired to that terminal. It is only possible to use one output from the PPG-patch because of limited analog input and the chosen one was the DC signal after the trans-impedance amplifier. The PPG-patch pin terminals P1-P14 was connected to the ePatch® PCB except P9, P11 and P12.

The input to the ePatch® front-end is a differential input with a voltage range of $\pm$400 mV. This challenges the PPG-patch because the output is single-ended. This issue was solved by connecting a 1.5 V reference value from the circuit together with the PPG-patch output and adjust the LED intensities for the PPG-patch so the output DC level becomes as close as possible to 1.5 V. A test setup was constructed for this purpose and is shown in Fig. 4.13a. This configuration resulted in a small PPG output because it is only the DC signal that is recorded. In the cage shown in Fig. 4.13a the background noise was tested for all the developed devices. Fig. 4.13b shows another test setup that was used to test recording duration and signal quality for all the devices at the same time. A known ECG signal is fed to the input of the devices and recorded until shutdown.

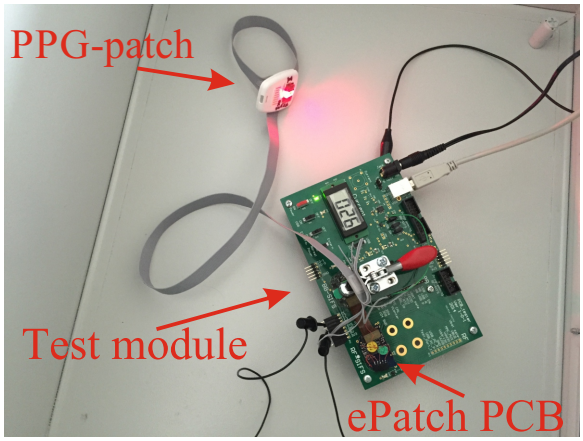

(a)

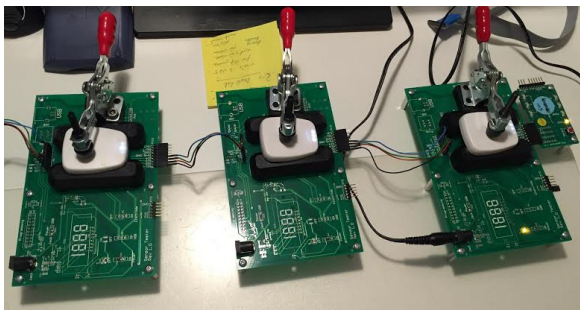

(b)

Figure 4.13: Test setup of the PPG-patch connectivity with the ePatch®. (a) The setup is placed in a Faraday cage to avoid any electrical interference. (b) Shows three PPG-patches being tested. A known ECG signal is fed into the devices and recorded. The LEDs are turned on to the maximum.

As for the PPG-patch firmware it was adapted to the existing firmware of the ePatch® platform. This part was very challenging because the ePatch firmware was not trivial to reprogram. However, it was possible to modify it so that the PPG signal is splitted and saved into two signals red PPG signal and infrared PPG signal. The samplings frequency is 64 Hz and the A/D converter resolution is 24 bit which is very good because the PPG signal amplitude is relatively small. In addition to the PPG signals, it is now possible to acquire ECG and triaxial accelerometer signals. The PPG-patch electronic front-end is powered by the 3.7 V lithium battery with capacity of 375 mAh and the power consumption can last for minimum 20 hours recording and if the LED intensity is at the minimum it can last for 31 hours. The final version of the PPG-patch attached at the sternum and the modified ePatch® electrode is shown in Fig. 4.14. A representative plot of acquired signals in the laboratory is shown in Fig. 4.15.

Figure 4.14: PPG-patch at the sternum (the red light illuminating the skin is also seen.

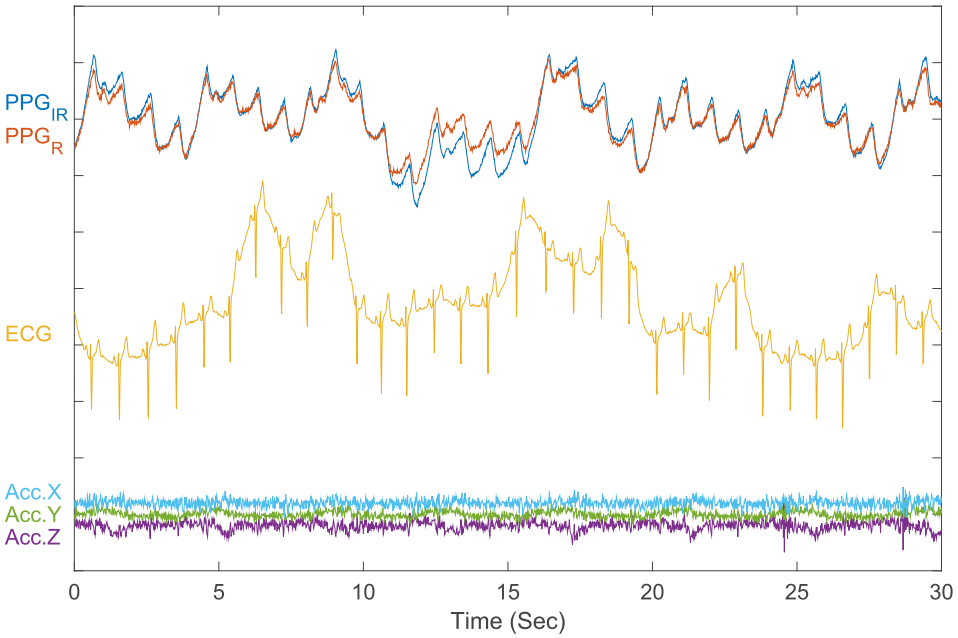

Figure 4.15: Signals recorded with the wireless configuration of the PPG-patch. The viewed snippet is from a recording at the sternum in the laboratory. All the signals in the plot are unfiltered.

4.6 Summary

This chapter described the design and development of a reflectance mode PPG sensor, the PPG-patch. The PPG-patch was successfully developed to operate in two modes; the first mode is for short-term recording where it is possible to record PPG signals through a data acquisition device and a second mode where it can record two PPG channels (red and infrared), one channel ECG and triaxial accelerometer synchronously for 20 hours. All seven sensors were electrically identical and passed all the tests in the laboratory. The functionalities of both mode of operations are summed in Table 4.1.

Table 4.1: Summery of the functionalities of the PPG-patch in the two operation modes.

Properties	PPG-patch mode 1	PPG-patch mode 2
Samplings frequency (Hz)	256	64
ADC resolution	16	24
3-axis Accelerometer	NA	Yes
ECG	NA	Yes
Wireless	NA	Yes
Synchronization with hospital equipment	Yes	NA
Operate without the modified ePatch® electrode	Yes	NA
Real time visualization of a recording	Yes	NA

In an attempt of comparing the sternal signal quality when recording PPG with and without the modified ePatch® electrode we observed an 80 % increase in signal quality when the modified ePatch® electrode is not used [60]. It was decided that the PPG signal quality is sufficient to be used in a clinical environment. Moreover, it is possible to conduct the recording without using the modified electrode.

In order to be able to estimate the oxygen saturation in the blood using the PPG-patch, a sensor calibration must be done. In this project the pulse oximeter calibration method is carried on through a hypoxia in vivo study and is done in accordance with the ISO 80601-2-61:2011 guideline. The protocol and method of this sensor calibration is explained in the next chapter.

CHAPTER

FIVE

CLINICAL STUDY I: INVASIVE CONTROLLED DESATURATION STUDY

Objectives *In the previous chapter a description of the PPG-patch was given. Seven prototype PPG sensors were developed successfully and used in three clinical trials. All three studies took place at two different departments; the department of pulmonary medicine and the medical admissions ward on Bispebjerg Hospital, Copenhagen University Hospital, Copenhagen Denmark. The studies were approved by the Danish regional ethical community (H-6-2014-013), the Danish Health and Medicines Authority (CIV-15-01-013029), the Danish Data Protection Agency, and was monitored by the regional good clinical practice (GCP) unit. In this chapter a description of the first clinical study is given. The work of this chapter is also described in Paper IV.*

5.1 Background

The ability to measure the S_pO_2 level from the sternum was investigated through an invasive controlled desaturation study on healthy volunteers. The goal of this study is twofold. First, to investigate the ability of measuring the S_pO_2 level in the blood at the sternum with the PPG-patch, and second to calibrate the sensor so it can be used in the second and third clinical studies. The accuracy of the PPG-patch is investigated by comparing the calculated S_pO_2 values with the ”gold-standard” measurements of blood S_aO_2. This study was made in accordance with the ISO 80601-2-61:2011 guidelines.

5.2 Method and Materials

5.2.1 Study Design

A total number of 14 healthy Caucasians (nine males and five females), nonsmokers participated in this study. A written informed consent was obtained from the participants prior to the study. The demographics of the subjects are provided in Table 5.1.

As mentioned previously, it is a desaturation study, which means that the level of oxygen saturation in the blood is gradually reduced within the region of clinical interest (100 % to 70 %). The desaturation process was controlled with a closed-loop breathing system. The subjects were breathing in a mask with a manually controlled mixture of oxygen and nitrogen air from a 50 L container (a Douglas bag). The subjects were lying in a supine position and, to avoid the influence of motion artifacts, they were instructed to move as little as possible. The experimental setup is shown in Fig. 5.1. The subjects were monitored using a Datex-Ohmeda AS/3 Compact Patient Monitor, recording the pulse oximetry, the invasive blood pressure, the ECG and the fraction of carbon dioxide in the breathing air from the closed system. Between the breathing mask and the air container there was a CO_2 absorber made of calcium hydroxide, Soda Lime. The experiment protocol procedure took place as follow for each subject:

1. A medical doctor performed an Allen's test on the hand before the subject was included. This test ensures that both the radial and the ulnar arteries are able to individually supply the hand with sufficient amount of blood during the experiment.
2. If the Allen's test was passed, the medical doctor places a catheter in the radial artery under local anesthesia. This catheter is used for collection of arterial blood samples during the experiment.
3. The ECG electrodes are placed on the chest, the invasive blood pressure transducer is connected through the catheter and the conventional finger pulse oximeter is attached to the index finger of the opposite hand.
4. The PPG-patch was mounted at the sternum (using adhesive tape) and another one on the thumb.
5. Finally, the breathing circuit was fitted to the subject and the gas mixture was tuned accordingly.

Table 5.1: Subject demographics.

Gender	9 males, 5 females
Age (years)	Mean: 30.3, SD: 11, Range: 20-56
BMI (Kg/m^2)	Mean: 22,2, SD: 3, Range: 16-25.7

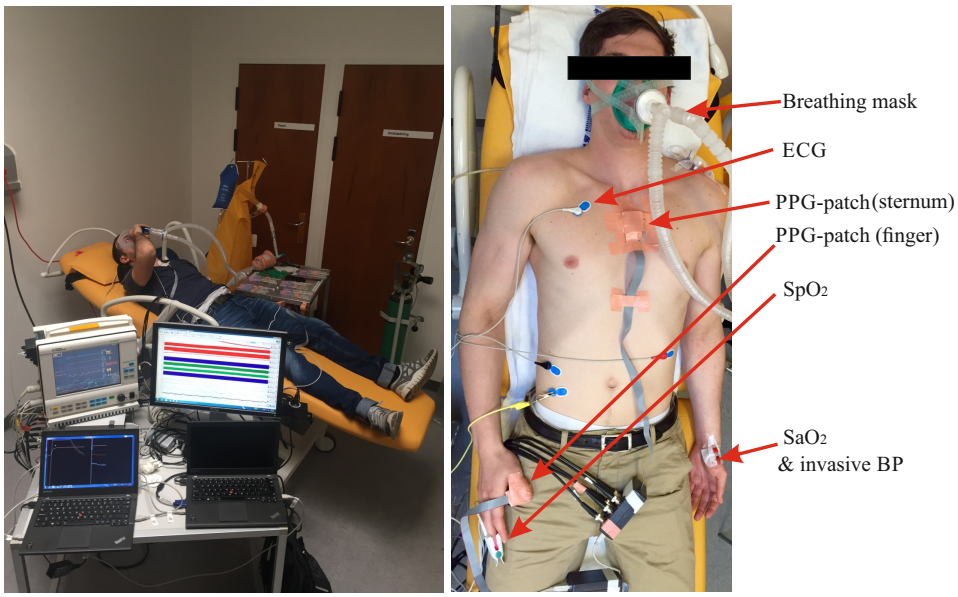

a) b)

Figure 5.1: The participants breathes a manually regulated composition of oxygen and nitrogen in a closed breathing system. (a) The experimental setup. (b) A participant with attached sensors. The PPG-patch is attached at the sternum. Arterial blood sample is taken from the radial artery and the oxygen saturation in the blood (S_aO_2) is used as reference.

All equipments were connected to the data acquisition device (Powerlab 8/35, 16 bit ADC, ADInstruments, USA) and simultaneously acquired on a laptop. Another laptop was used to visualize the PPG signals from the PPG-patch in real-time during the experiment. The room light was switched off to minimize any ambient light interference.

During the recordings, up to 25 blood samples of 2 ml each were taken from each subject. The first five blood samples were taken while the subject was breathing outside the closed system. Each time a blood sample was taken a marker is placed in the data acquisition software, as seen in Fig. 5.2. This ensures synchronization between the time instance for the blood samples and the recorded signals. The oxygen saturation level decreased when the breathing mask was on and the air mixture was regulated in the closed system. The air regulation is done by the medical doctor while monitoring

the fraction of inspiratory oxygen (FiO_2) and the tidal carbon dioxide ($ETCO_2$) on the patient monitor. The pulse oximeter from the patient monitor was used to check the actual level of oxygen saturation. The blood samples were analyzed using Radiometer blood gas analyzer (ABL 800 Flex, Radiometer Co.). The blood gas analyzer was calibrated prior to the experiment. The experiment was stopped when 25 blood samples were obtained and are distributed in the range of 100 % to 70 %, when the subject reached an oxygen saturation of 70 % or when the medical doctor decided to stop (whichever came first). The duration of the hypoxia inducement was different from subject to subject. However, the average lasting time was 25 min. A representative 30 second segment of all the recorded modalities of one subject is shown in Fig. 5.2.

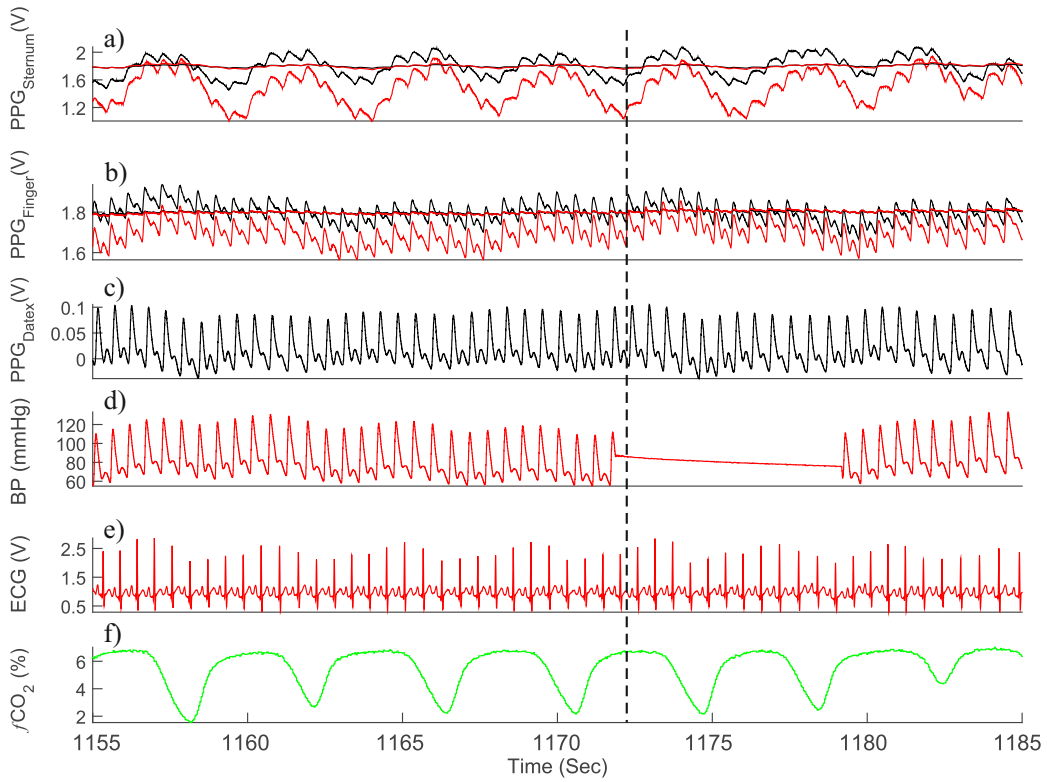

Figure 5.2: All the recorded modalities from the experiments. (a) Contains AC and DC PPG signals for each wavelength recorded from the PPG-patch placed at the sternum and (b) another PPG-patch attached to the first index finger. The signals are inverted so they become similar to the rest of the arterial PPGs, meaning that the peak symbolize the systolic cycle and the minimum end-diastolic. The rest of the signals are recorded through the patient monitoring system; (c) Finger PPG,(d) blood pressure plethysmogram, (e) ECG signal and (f) in- and exhaled carbon dioxide fraction. The dashed line is a marker placed when a blood sample was taken.

5.2.2 Normalization and Filtering

The preprocessing of the PPG data consists of two steps; normalization and filtering. In terms of normalization it was shown in Eq. 2.4 in chapter 2 that the optical ratio R is derived by dividing the value of the systolic peak by the value of the diastolic peak to cancel out any influence by the non-pulsating tissue. However, if the signal contains any motion artifact the approach of finding the systolic and diastolic peak for every cardiac cycle can be challenging and may lead to biased results. To overcome this, and because the DC-level in the PPG signal is relatively larger than the AC component the average of the DC-level can be used [13]. So the normalized signal $y_n(t)$ is calculated as follows;

$$y_n(t) = \frac{x(t) - mean(x(t))}{mean(x(t))} \tag{5.1}$$

where x(t) is the PPG signal. For each 20 second window centered on the time marker for each of the blood samples (corresponding to the window size of the finger pulse oximeter) the normalization has been applied. The next step is band-pass filtering of the normalized signals. The most common type of noise in pulse oximetry is the noise induced by motion artifacts [15]. Different types of motions that affects the PPG signals have been investigated and characterized by Tobin et al. [61]. The study included 350 patients from different hospital wards and it was reported that almost all kind of motions including patient transportations affected the PPG signal because of the overlapping in the arterial pulsation frequency bands. Motion artifacts at the sternum is to our knowledge not yet investigated. However, our observations showed that any movement of the hands do not influence the sternal PPG signal as it does with PPG recorded from the fingertip. On the other hand any movement involving the upper torso affects the signal. In addition, extreme cough does also affect the sternal PPG signal. In order to reduce the motion impact on the PPG signal numerous research groups have investigated different methods involving adaptive noise cancellation using active sensors such as accelerometers [62–65]. Passive motion cancellation was proposed by Wang and Yang [66], their approach were building on the assumption that when the LEDs are off the readings from the photo detectors were only dominated by motion. The algorithm showed promising results during rest and moderate exercise. A similar attempt is claimed in a patent by Nellcor [67], claiming that it is possible to detect motion with PPG recorded with a wavelength above 940 nm where water has a strong absorption. By subtracting the motion signal from the regular PPG signal they were able to reduce the error on the S_pO_2 estimation to below 3 $\%$. None of these methods is used in the PPG-patch, but it could be useful features to add to such a device in the future.

To reduce the motion artifact a 4th order band-pass Butterworth filter was chosen, which is also suggested by [65]. However, we added a modification to the filter design by replacing the fixed cut-off frequency with adaptive cut-offs depending on the patients heart rate. We calculated the heart rate (HR) as the frequency bin with the largest amplitude in the power spectral density of the 20-seconds

ECG segment. Similar work is proposed by [68]:

$$Y(f) = \int_{-\infty}^{\infty} y(t)e^{-2j\pi fT}dt, \tag{5.2}$$

$$HR = max(Y(f)), \tag{5.3}$$

Consider only frequencies from 0.5 Hz to 4 Hz (corresponding to a HR of 30 to 240 beats per minutes). The low cut-off frequency for each window (corresponding to one blood sample) was found by subtracting 0.2 Hz from the detected HR and the high cut-off frequency was found by adding 2 Hz to the detected HR for this specific window.

5.2.3 Estimation of the Optical Ratio R

The next step after the normalization and the band-pass filtering is to estimate the optical ratio R. In recent years, various signal processing methods have been investigated for estimating the optical ratio. Promising results were demonstrated using Fourier transform [68], Hilbert transform [69] and independent component analysis [10, 70–72]. Another state of the art and commercially available algorithm is the Discrete Saturation Transform (DST) algorithm by Masimo Corporation [73]. Another method of calculating the optical ratio is by calculating the root mean square of the normalized and filtered PPG signals, $y_r(t)$ and $y_{ir}(t)$:

$$R = \frac{\sqrt{\frac{1}{N}\sum_{t=1}^{N} y_r^2(t)}}{\sqrt{\frac{1}{N}\sum_{t=1}^{N} y_{ir}^2(t)}} \tag{5.4}$$

where N is the number of samples (20 sec x 256 Hz). This calculation is an averaging of the amplitude size for each PPG signal. It requires a high signal to noise ratio and low level of motion artifacts. As mentioned previously, not all the motion artifacts can be reduced with the band-pass filtering because the motion can happen at the same frequency as the heart rate. The only way this calculation can handle the noise from motion artifacts is by averaging and this may not be optimal. However, by inspection of all the recorded signals, it was seen that the motion artifacts are relatively low in the recordings in this study.

5.2.4 Calibration Curve

The last step is now to mathematically link the calculated R values to the measured S_aO_2 reference values. This provides a formula for future estimation of the oxygen saturation based on the PPG signals directly.

A second-order polynomial was proposed by Fine and Weinreb [74], but the polynomial is not based on any physical interpretation rather than the result of on empirical approach of best prediction of the coefficients. Webster [13] proposed a linear regression given as

$$S_pO_2 = -aR + b \tag{5.5}$$

this linear regression is only valid in the range from 100% to 70% and it is known from the derivation of Beer-Lambert's law that the slope of the linear approximations should have a negative slope, cf. chapter 2. We decided to use the linear regression defined in 5.5, where a and b are the regression coefficients. To ensure a high generalization performance of our calibration curve and to gain knowledge about the performance of the regression on new subjects, we used a leave-one-out scheme to fit the calibration curve. This implies that all blood samples from one subject were left out, while the calibration was conducted on all the blood samples from the remaining 13 subjects. This procedure was repeated with all 14 subjects as the test subject. For each of the 14 iterations, the values of a and b were found and the performance of the obtained calibration curve was evaluated as the root mean squared error (RMSE) between the measured S_aO_2 reference values and the levels estimated based on the calibration curve for the test subject. The final calibration curve was fitted as an average of the regression coefficients obtained in the 14 iterations.

In accordance with the ISO 80601-2-61:2011 guidelines, the accuracy of the sternal PPG sensor was then estimated according to:

$$A_{rms} = \sqrt{\frac{\sum_{i=1}^{n}(S_pO_{2i} - S_aO_{2i})^2}{n}} \tag{5.6}$$

where n is the number of blood samples (n = 324). Furthermore a Bland-Altman analysis is done to compare the calculated S_pO_2 values with the reference S_aO_2 values. The results is given in the following section.

5.3 Results

A total of 324 S_aO_2 values for all the subjects were used for the calibration. The S_aO_2 range was from 99 $\%$ to 59 $\%$. Fig. 5.3 shows two 20 seconds segments of the recorded PPG signals of one subject measured in the beginning of the experiment, where the oxygen saturation level was high (98 $\%$) and at the end where it was low (71 $\%$). When the oxygen saturation level was decreased, larger respiratory fluctuations was shown due to deeper breaths. However, these fluctuations were removed by filtering. The result of the normalization and the band-pass filtering is shown in Fig. 5.4. What is also seen in the figure is an increase in the heart rate, which is a normal physiological response to hypoxia together with the deeper breathing. Additionally, it is seen how the amplitude ratio between the red and infrared signals (i.e., the optical ratio) is less than 1 at high S_aO_2 values and increased to larger than 1 at low S_aO_2 values.

Table 5.2 shows the coefficients of the linear curves functions according to Eq. 5.5. It is seen how the coefficients are almost equal. The RMSE and coefficient of determination (r^2) for each subject is also given. The average RMSE and r^2 for all fits are 1.73 $\%$ and 0.975 $\%$, which indicates validity to apply the linear regression to fit the data. The final calibration line together with the 324 S_aO_2 reference values are shown in Fig. 5.5. The calibration coefficients are -25.89 and 116.48 for a and b respectively. Now for the validation, the calibration curve was used to calculate the S_pO_2 values from the estimated optical ratios. The accuracy of the PPG-patch becomes in accordance to Eq. 5.6 1.75 $\%$. In Fig. 5.6a the S_pO_2 values are plotted against the corresponding reference S_aO_2 values, showing a strong correlation (Pearson correlation coefficient of 0.97). Fig. 5.6b shows the result from the Bland-Altman analysis. The mean system bias is -0.21 $\%$ and the upper and lower limits of agreements are 3.5 $\%$ and -3.9 $\%$ respectively over the whole S_aO_2 range.

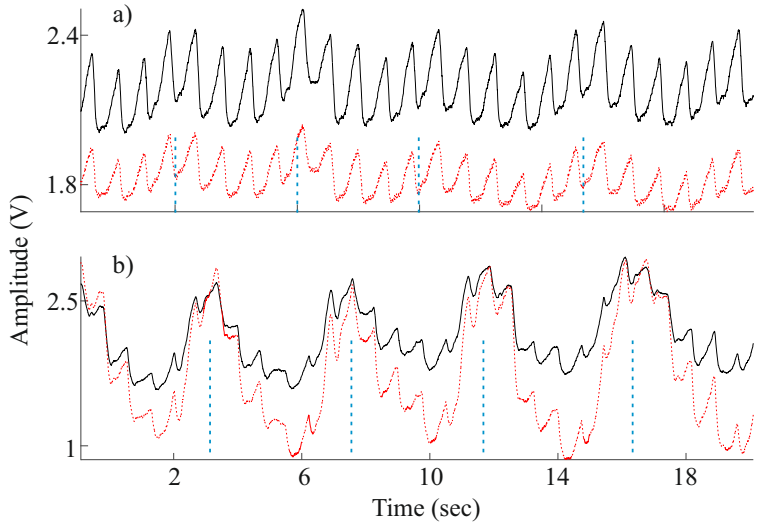

Figure 5.3: Examples of red (red dotted line) and infrared (black solid line) PPG signals recorded with the custom build PPG sensor placed on the sternum with an oxygen saturation of 98 % (a) and 71 % (b), respectively. Both the respiratory component (slow baseline changes indicated with vertical dashed blue lines) and the cardiac component (high frequency fluctuations) are clearly observed in both examples. Finally, it is observed how both the heart rate (HR) and the depth of the breathing are increased during low oxygen saturation.

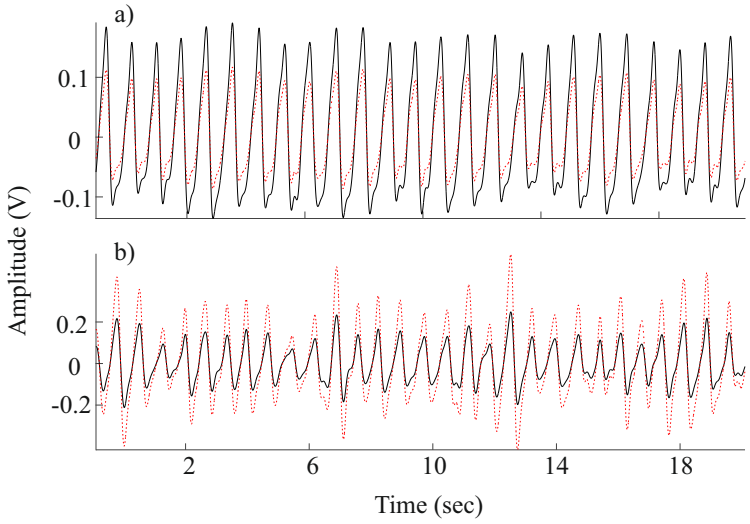

Figure 5.4: Illustration of the effect of normalization and filtering. For comparison, the raw unprocessed signals are provided in Fig. 5.3. It is observed how the relation between the amplitude of the red (dotted red line) and the infrared PPG (solid black line) signals shift for different oxygen saturation levels.

Table 5.2: Coefficients belonging to each calibration lines. a and b are coefficients of the Eq. 5.5, r^2 is the determination coefficient of fit, and RMSE is the root mean square error.

Subject #	a	b	r^2	RMSE
1	-25.8711	116.5141	0.965	0.583
2	-25.5058	116.1815	0.972	1.534
3	-25.8647	116.4556	0.979	0.874
4	-25.8634	116.4871	0.987	1.013
5	-25.4138	115.9021	0.977	2.175
6	-26.0423	116.7752	0.983	2.283
7	-25.7014	116.1643	0.987	0.821
8	-25.989	116.5954	0.937	2.980
9	-26.1708	116.6567	0.982	1.716
10	-25.9946	116.4586	0.974	2.109
11	-26.2852	116.7518	0.974	2.558
12	-25.8889	116.4552	0.970	1.273
13	-25.9276	116.6542	0.970	2.351
14	-25.9203	116.6051	0.986	1.977
Mean	-25.8885	116.4755	0.975	1.732

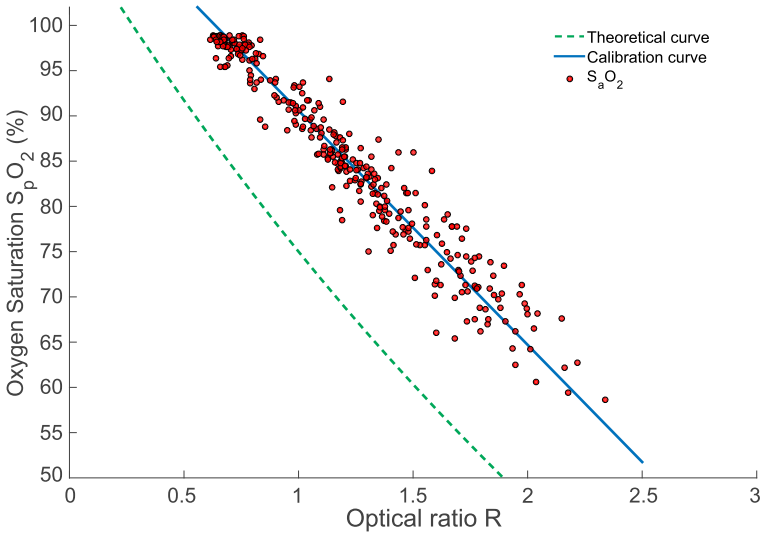

Figure 5.5: Relation between the calculated R values and the measured S_aO_2 reference values (red dots) and the final calibration curve (blue line). The final calibration coefficients were $a = -25.89$ and $b = 116.48$. The average RMSE for the 14 calibration iterations was 1.73 %. The green dashed curve is the theoretical curve from Eq. 2.3 from chapter 2.

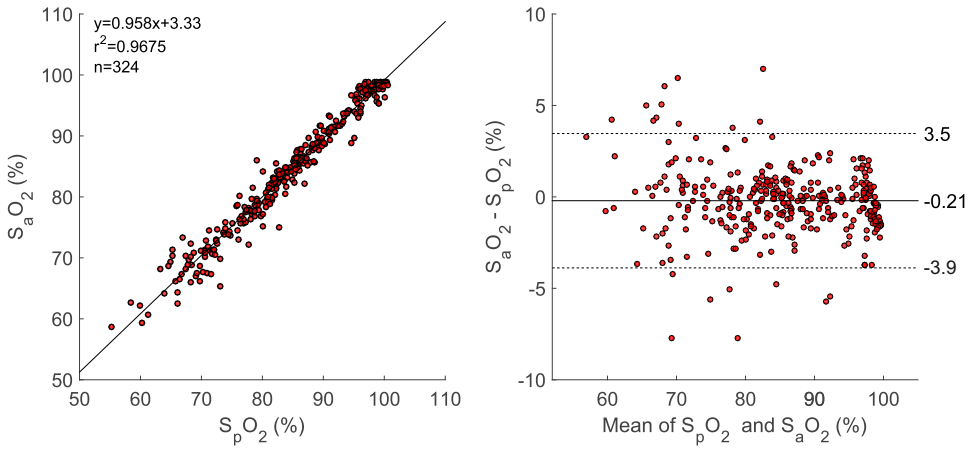

Figure 5.6: (a) The correlation and regression line of S_aO_2 with S_aO_2 in the calibration experiment. (b) Blandt-Altman plot of the comparison between S_aO_2 and S_pO_2. The middle solid line represents the mean system bias, while the upper and lower dashed lines represent limits of agreements $\pm 1.96SD$.

5.4 Discussion

In this experiment the PPG-patch device was calibrated during a controlled desaturation clinical study on 14 healthy volunteers. This step is important in order to use the sensor in study two and three for calculating the S_pO_2 levels. In this section different remarks and uncertainties regarding the experiment will be pointed out.

PPG-patch at the Sternum

Due to different sternal anatomy between the subjects it was challenging to attach the PPG-patch to the sternum via the modified electrode. The optical window does not make good contact with the skin. For each subject the electrode was tried out and the PPG signal was evaluated just before the actual recording. On all the subjects, the amplitude of the PPG signal was significantly larger by placing the PPG-patch using adhesive tape on the sternum without the electrode. In addition, on one of the subjects the PPG-patch was placed adjacent to the sternum on the chest muscle, because of the lack of space at the sternum. Nevertheless, it did not affect the quality of the PPG signal. The PPG-patch device that was attached to the finger did not always show a good signal, because it was difficult to tape it to the index finger and because the subjects move their hands regularly. In general the quality of the PPG signal at the sternum was excellent on all the subjects and it was observed that

during the hypoxia the signal quality got better. This might be because of the rise in blood perfusion at the sternum. The temperature under the PPG-patch was not measured, but the skin on the chest felt warmer compared to the fingers. Additionally, sweating and thermal insulation under the sensor may also enhance the skin and tissue interface.

Experimental Remarks

Different size of breathing masks were used in the experiment, not only to enhance the comfort for the subjects, but to avoid any leakage of air from the closed system. This was the case from one of the subjects, where the experiment duration was above 50 min. Additionally, there was an air flow resistance which made the subject feel uncomfortable during in- and exhalation. For the future shorter tubes with larger diameter is highly suggested. Furthermore, these tube and leakage problems made it difficult to control the breathing air and the oxygen concentration level, which is why saturations level under 70 $\%$ was recorded on some of the participants.

Oxygen saturation plateaus were difficult to obtain throughout the whole hypoxia duration. Although, it is suggested by the ISO 80601-2-61:2011 guidelines. So in our case we barely got 30 seconds between the blood samples during hypoxia. All the taken blood samples were placed in a container with crushed ice. For the first five subjects no blood gas analyzer was available during the experiment, so the analysis were performed after the experiment (at least after 30 min). The guidelines for arterial puncture suggested by Radiometer reports that a blood sample should be analyzed within 30 min. If the blood sample analysis will be delayed for more than 30 min, glass syringes stored in ice slurry water should be used to avoid any effect on the sample values. Unfortunately, for the first five subjects some of the blood samples may have been affected by the time delay.

The S_pO_2 values displayed on the Datex-Ohmeda patient monitor system were delayed and the values did not always correlate well with the values of the blood samples when the actual oxygen saturation levels were below 80 $\%$. The patient monitor has a standard deviation in S_pO_2 of 3 $\%$ points in the range 80 $\%$ to 50 $\%$. Meaning that 99.7 $\%$ of the S_pO_2 values fall within $\pm$9 $\%$ points. Besides, during hypoxia the patient monitor was displaying ”low perfusion”, which implies low signal strength.

5.5 Conclusive Remarks

The result shows that there is an excellent agreement between the S_pO_2 values estimated from the sternal PPG signals and the S_aO_2 reference values (n = 324 blood samples) in the clinical region

of interest (100 $\%$ to 70 $\%$). All the patients were at rest in supine position, which minimized any sort of motion artifacts during the recording. The use of the ECG signal to determine the heart rate and thereby choose the cut-off frequencies for the band-pass filter for the PPG signal based on that seems to be a promising approach. Specially because DELTA's ePatch® records the ECG already.

The accuracy of the PPG-patch was calculated to 1.75 $\%$ which is acceptable according to the ISO 80601-2-61:2011 standards ($< 4\%$). Commercially available pulse oximeters such as Masimo R25-L and NellCore Oximax N-65 reports accuracy of 1.79 $\%$ 1.3 $\%$ respectively. Furthermore, another recent desaturation study conducted with a sternal PPG sensor has obtained an accuracy of 1.7 $\%$ [20]. The calibration thus indicates an accuracy that is well within both the state of the art performance and the clinically acceptable range. We consider the calibration to be successful and we therefore find it reasonable to apply the estimated calibration curve to investigate the clinical performance of the sternal PPG signals on the patient population (study II and III).

Now with this controlled desaturation study the PPG-patch device has been calibrated and validated. So, it is now possible to estimate the oxygen saturation using the developed device. But, the validation was on healthy volunteers. In the next chapter the second clinical study is described. The aim of the study is to investigate whether the sternal PPG can be clinically useful for calculating the RR and the S_pO_2 level on patients with obstructive lung diseases.

CHAPTER

SIX

CLINICAL STUDY II: SHORT-TERM PPG MEASUREMENT ON COPD AND ASTHMA PATIENTS

Objectives *The PPG-patch has been designed tested and calibrated as described in the previous chapters. However, the PPG measurement has only been conducted on healthy participants. The current chapter will consist of an assessment of short-term sternal PPG monitoring and an estimation of the RRs and the oxygen saturation levels on patients with Chronic Obstructive Pulmonary Disease (COPD) and asthma. The chapter is based on Paper III and IV.*

6.1 Background

As mentioned in chapter 3, the application of PPG has previously been studied and is well documented in terms of measuring the RR. The RR derived from PPG was shown to be clinically applicable in terms of age, gender, anesthesia, and mode of ventilation [37, 75]. It was also shown in the pre-clinical study (chapter 3) that the sternal PPG signal has an extremely clear respiratory oscillations in healthy subjects. Therefore, the aim of the current clinical study is to assess the RR from a clinical relevant patient group using sternal PPG. Moreover, the calculation of the S_pO_2 level from the sternal PPG is also validated on the patient group.

Table 6.1: Subject demographics.

	All	COPD	Asthma
Gender (male/female)	11/18	9/15	1/4
Age (years)	Mean: 64.3, SD:14.4	Mean: 64.4, SD:14.2	Mean: 62.4, SD:15
BMI (Kg/m^2)	Mean: 25.8, SD:8.8	Mean: 25.8, SD:8.7	Mean: 25.7, SD:9.1
Recording length (min)	Range: 10-54		

6.2 Method and Materials

6.2.1 Study Design

The data was collected from 30 patients with obstructive lung disease, either COPD or asthma. One of the COPD patients was excluded due to missing data in the recording. The patients provided written informed consent for study participation. The inclusion criteria required that the patients were diagnosed with COPD or asthma and were admitted to the hospital due to an exacerbation of their condition for at least 24 hours prior to their inclusion in the study. The patien't demographics are listed in Table 6.1.

The patients were monitored using the Datex-Ohmeda AS/3 Compact Patient Monitor, recording the fraction of carbon dioxide (fCO_2) via nasal catheter and the lead II ECG. The PPG-patch was positioned on the skin at the sternum using adhesive tape. A second PPG-patch was positioned on the first index finger and a conventional finger pulse oximeter was positioned on the second index finger. All signals were collected synchronously on the Powerlab data acquisition system. During the experiment the patients were at rest in a semi-supine position and the patients were instructed not to make any unnecessary movements during the measurements, though, physiological artifacts, e.g. coughing, was unavoidable. The recording duration was intended to be between 10 and 60 minutes. However, the maximum recording length was 54 minutes, cf. Table 6.1. A photograph of the experimental setup is shown in Fig. 6.1.

Figure 6.1: A photograph of a typical recording situation during the clinical study at Bispebjerg Hospital.

6.2.2 Data Analysis

Regarding the calculation of the RR, the infrared PPG signal was used. But both wavelengths were of course used for the estimation of the S_pO_2.

Calculation of the RR

Automatic extraction of the RR from the PPG signal is emerging and has been reported by numerous authors. The most common method is based on the Fast Fourier Transform (FFT) [25, 76, 77]. Digital filtering such as applying 3rd order Butterworth band-pass filter with cut-off frequencies at 0.1 and 0.3 Hz, corresponding to 6 and 18 breaths/min followed by a peak detection algorithm that marks the events of respiration was reported by Nilsson et al. [37, 75]. They reported an average error of 0.5 breaths/min, where addison et al. [78] developed an algorithm based on the wavelet transform and reported an average error of 1 breaths/min. In an attempt of using autoregressive modeling method to extract the RR from PPG, Fleming and Tarassenko [79] reported an average error of 0.04 breaths/min. Most of the mentioned algorithms requires a long-time period of processing or high computational power, which is not suitable for the future perspective of the

PPG-patch. It is assessed to use the digital filtering method proposed by Nilsson et al. [37], but instead of using a peak detection algorithm after the digital filtering, we used a manual annotation of the peaks conducted by a medical doctor.

The sternal PPG signal was filtered to suppress the cardiac related AC component and increase the respiratory related DC component (using a 3rd order Butterworth band-pass filter with cut-off frequencies at 0.1-0.7 Hz which corresponds to 6 - 42 breaths/min). After the filtering, both the sternal PPG and the capnographic signal were divided into one-minute non-overlapping segments. This yields a total of 1250 segments (half from the PPG and half from the capnographic signals). The 1250 segments were randomized and a medical doctor was asked to visually go through all 1250 segments and manually detect the RR in each one-minute segment. After the manual detection of the RR in each segment, the segments were paired to allow a direct comparison of the RRs obtained with synchronous measurements from the two recording systems. The Bland-Altman assessment for agreement was used to compare the RRs estimated from the two methods. The correlation between the two measurement techniques was calculated using Pearson's correlation coefficient. A p-value less than 0.05 was considered statistically significant. Additionally, the power spectral content analysis that was applied in the pre-clinical study (3) is also done in this study, but because we are able to compare the power spectral content of the finger PPG with the sternal PPG, the work is further extended.

Calculation of the S_pO_2

The calculation of the S_pO_2 is achieved using the calibration curve calculated during the first study, cf. chapter 5. For this purpose the PPG signals are divided into 20-second non-overlapping segments. This yields a total of 1784 segments. Each of them is normalized, band-pass filtered, and the optical ratio R is estimated and fed into the calculated linear calibration curve. Then the S_pO_2 values calculated from the sternal PPG is compared to S_pO_2 values given by the Datex-Ohmeda AS/3 patient monitor.

6.3 Results

Figure 6.2 illustrates three filtered segments from sternal PPG (black) and the corresponding flow signal from capnography (blue) at different RRs. The distribution of all the RRs derived from the capnographic signals and the sternal PPG signals are shown in Fig. 6.3. The RRs are ranged from 11.3 to 35.5 breaths/min. The mean rate was 20.4 breaths/min with a standard deviation of 4.7 breaths/min. Figure 6.4 contains the distribution of the differences between the sternal PPG derived

RRs and the RRs derived from simultaneous measurements obtained with the capnographic signals. The mean bias between the rates was 0.6 breaths/min with a standard deviation of 1.7 breaths/min. The accuracy of the measurement defined as the root mean squared (Arms) difference between measured values of sternal PPG and the reference values from capnography was 1.9 breaths/min. A more detailed view of the differences is further provided in Fig. 6.5. The Bland-Altman analysis demonstrated a mean system bias of 0.6 breaths/min and the 95 $\%$ limits of agreement to be -2.8 to 4 breaths/min. Additionally, Pearson's correlation coefficient between the two techniques showed a significant correlation $(r = 0.93, p < 0.001)$.

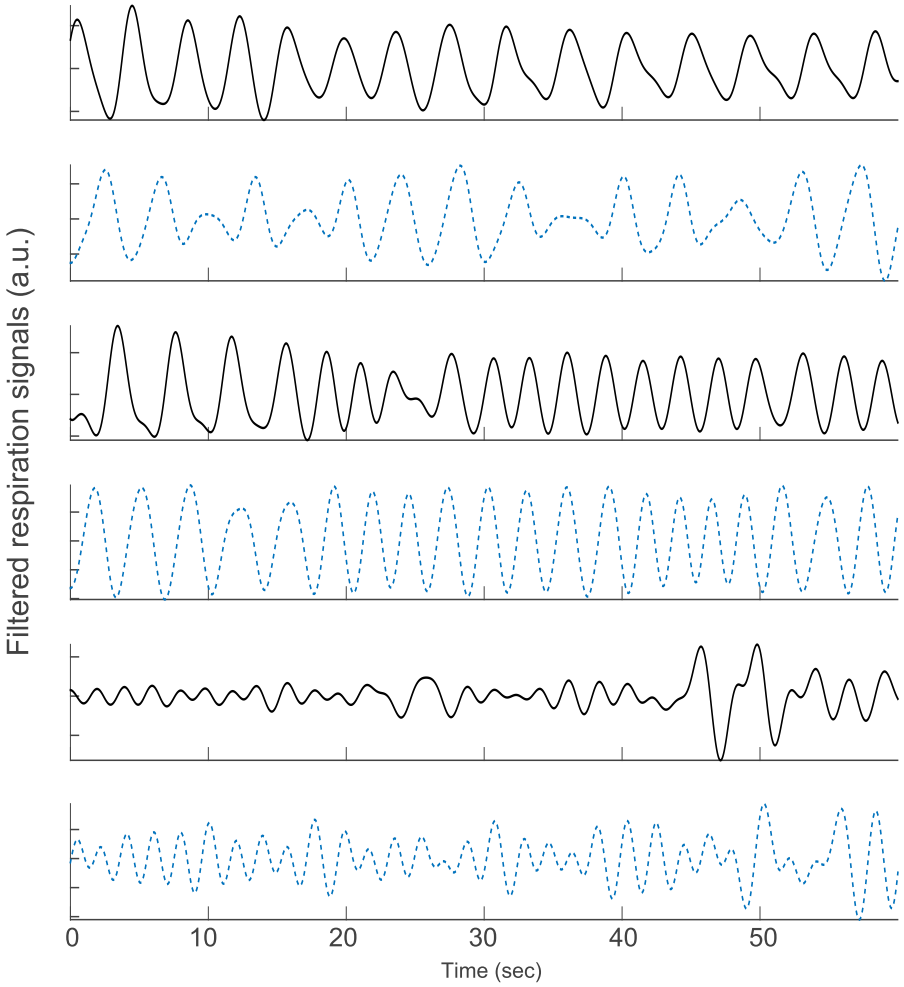

Figure 6.2: Filtered respiration signals from sternal PPG (solid) and the reference flow signal from capnography (blue dashed) respectively. These segments are six of the 1250 segments that the medical doctor annotated.

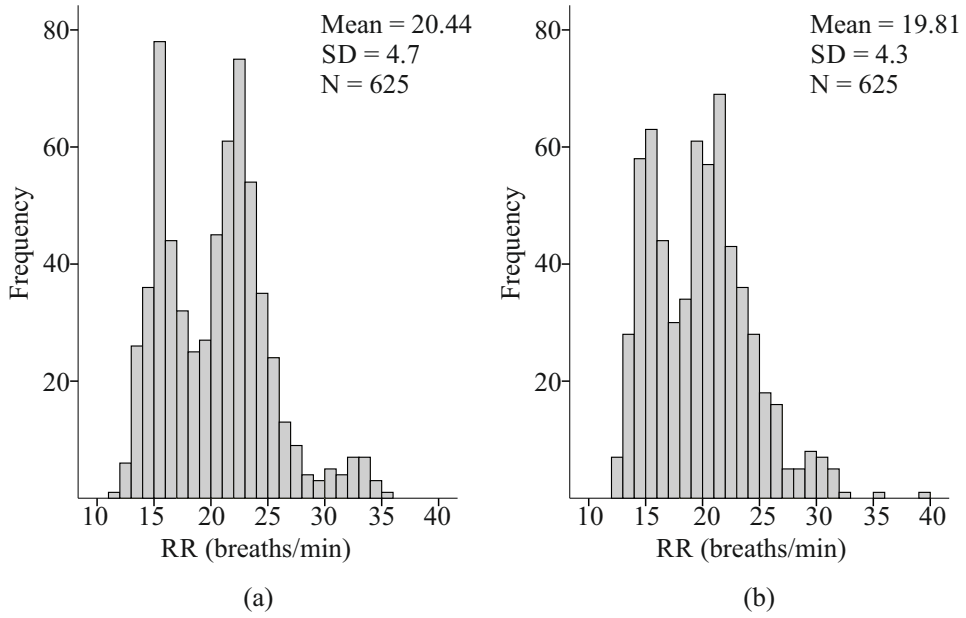

Figure 6.3: Distribution of all the RR of the patients included in this study. (a) The RR are calculated from the capnographic signal (b) and derived from sternal PPG.

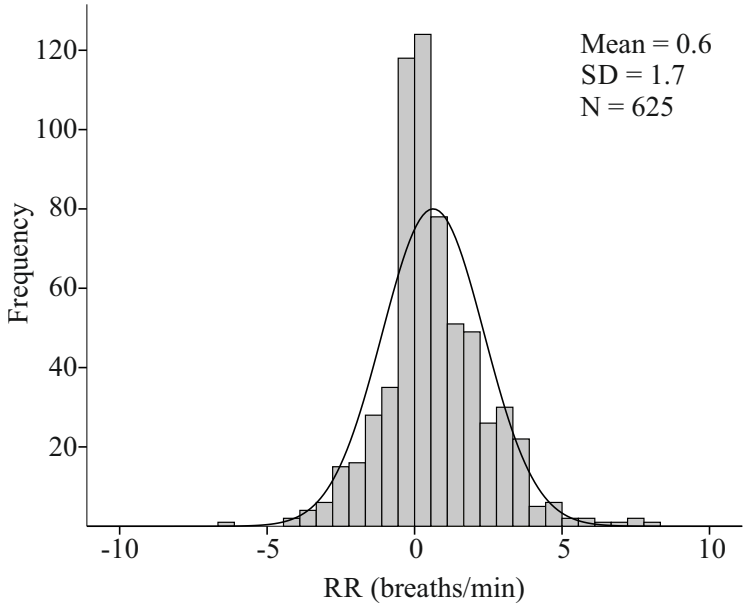

Figure 6.4: The distribution of all the differences between the sternal PPG derived RRs and the RRs estimated from the capnographic signal. The solid curve shows a normal distribution curve of the differences.

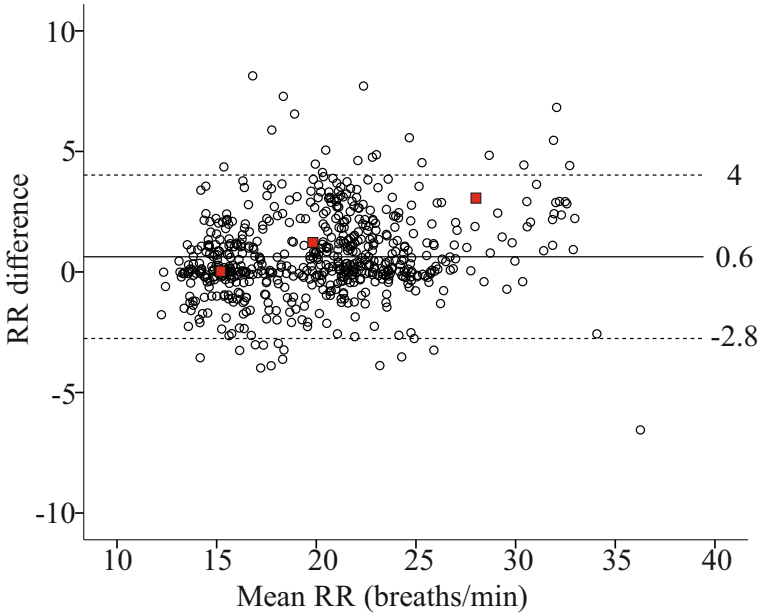

Figure 6.5: The Blandt-Altman plot of the data. The three red squared markers represent the mean and differences for signals shown in Fig. 6.2.

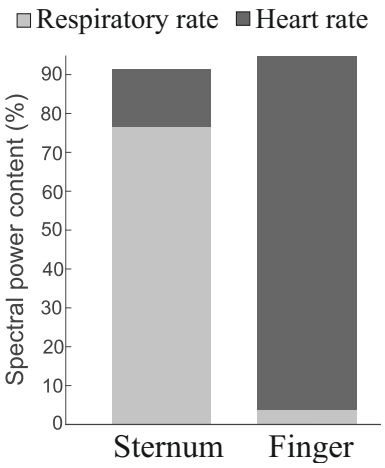

Figure 6.6: The respiration and cardiac spectral power from sternal PPG and reflective finger PPG.

As shown in chapter 3, Fig. 3.6 the respiration and cardiac spectral power content was derived from the sternal PPGs for each subject. For the current clinical study the same method was used on the group of patients. The result is shown in Fig. 6.6. The respiration and cardiac power spectral content (median and interquartile range) for sternal PPG is 76.5 (16.3) % and 14.9 (11.7) % respectively. For the reflective finger PPG it is 3.8 (3.1) % and 91 (4.9) % respectively.

As for the S_pO_2 levels from sternal PPGs compared to the values from the finger PPGs is shown in Fig. 6.7. The Pearson correlation was found to be 0.89 ($p < 0.05$). A representative example of the calculated S_pO_2 levels from one patient is illustrated in Fig. 6.8 together with the S_pO_2 values simultaneously obtained from the finger pulse oximetry. For this patient, it is seen (at the 5th minute) how the S_pO_2 levels for both devices increased as a result of oxygen therapy.

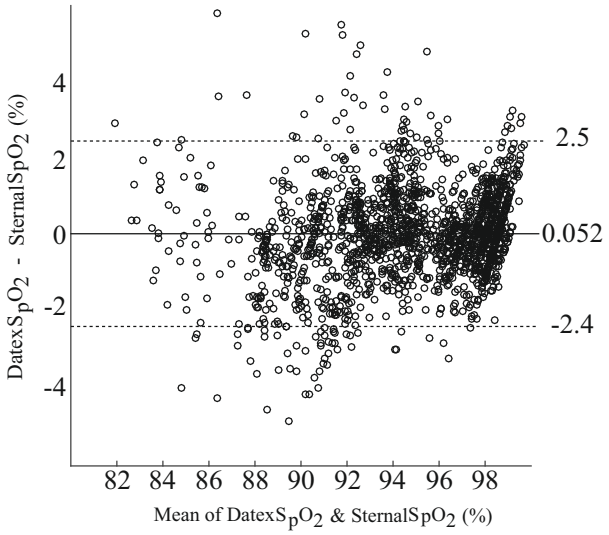

Figure 6.7: The Blandt-Altman plot of the comparison between the two measurement systems. Each dot corresponds to the difference between the obtained S_pO_2 in one of the 20 second analysis windows. The study included a total of 1784 non-overlapping 20 second analysis windows.

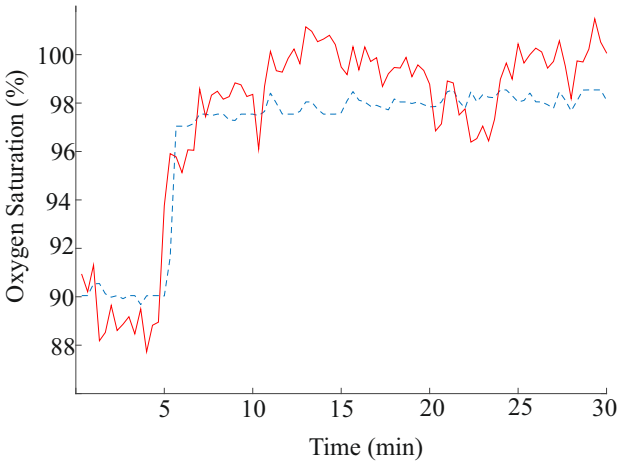

Figure 6.8: Time course of the S_pO_2 measured on the finger (blue dashed line) and estimated from the sternal PPGs (red solid line) for one of the patients. Just before the increase of S_pO_2 values, the patient received oxygen therapy.

6.4 Discussion

The purpose of this study was to examine whether the RRs derived from sternal PPGs can be used for reliable monitoring of patients with obstructive lung disease like COPD or asthma. Besides the importance of monitoring the RR on these patients, it was also important to evaluate how well sternal PPG derived RR could be correctly identified in a clinical setting over a broad range of RRs. Furthermore, the study extends the previous work regarding the respiratory and cardiac content of sternal PPG that was conducted in the pre-clinical study (chapter 3). In addition, the calibration curve for the S_pO_2 calculation that was derived in the first study was validated on the included patients.

The RR for a healthy adult at rest is between 9-16 breaths/min. Also it is known that COPD and asthma patients may have higher RRs [6]. This is reflected in the distribution plots provided in Fig. 6.3. In addition, it is reflected in the figures that there are two main epochs in the distributions, one around 16 breaths/min and one around 24 breaths/min. By further inspection of the recorded data, it was clear that the reason behind the two epochs is because the fact that the study took place at two different hospital wards having the majority of the patients with higher RRs at the department of pulmonary medicine. One of the inclusion criteria of this study was that patients should be hospitalized for at least 24 hours prior to the measurement and when COPD or asthma patients are admitted to the medical admission ward, they receive the needed treatment and some will be

dismissed, while others may need more medical attention. This means that we may have monitored a more stable group of COPD and asthma patients at the medical admission ward than the patients at the pulmonary medicine. Usually when patients require more medical treatment, they will be transferred to the pulmonary medicine ward. The majority of the segments (90 $\%$) with RRs above 28 breaths/min belong to the asthma patients. In conclusion, the patient population in this study seem to provide a realistic clinical basis for investigating the performance of sternal PPG obtained RRs.

The standard procedure of measuring the RR at the pulmonary ward and the medical admission ward at Bispebjerg Hospital in Denmark is by physical assessment, either by direct observation of the chest movement or via breath sounds with a stethoscope. This procedure is done at least once a day. Though, in some rare cases the conventional capnography is used for continuous monitoring of the patients. In this study we compared RRs derived from the sternum with capnography measurements. Good agreement was found between the two measurement methods. The documented accuracy of the used capnograph (Datex Ohmeda AS/3 Compact Patient Monitor) is $\pm$ 5 breaths/min and the result from the Blandt-Altmann analysis showed that the upper 95 $\%$ limits of agreement was 4 breaths/min and the lower limit was -2.8 breaths/min. Even though the two methods are significantly correlated the mean bias in the Blandt-Altmann plot is slightly RR dependent, which may indicate some sources of error in the two methods. Capnography readings is known to have sources of error [80], but still it is a common used system for monitoring the RR at the hospital. We achieved an average root mean squared of the differences of 1.9 breaths/min, which indicates precise estimate by sternal PPG compared with capnography based RR. Comparing the result with the performance of manual respiration counting reported in [81]. They found that the repeatability coefficient for the RR monitoring made consecutively by the same observer is 4.9 breaths/min and a repeatability coefficient of 5.7 breaths/min for RR monitored consecutively by a different observer, and finally a repeatability coefficient of 4.2 breaths/min when simultaneous observers were investigated. Based on this reporting and compared to the results of this study we can say that the RR monitoring using PPG at the sternum is well within the currently clinically accepted tolerance. Importantly, the distribution of the differences seems to follow a normal distribution with a small bias as seen in Fig. 6.4.

As discussed in chapter 3, the respiratory induced variations are also seen in PPG signals from more peripheral located body sites, for example the finger and forearm as shown by Nilsson et al. [26] and that the strength of the respiration component in the PPG signal depended on the measuring site. It was also reported that the largest respiratory induced variations seem to be more prominent proximal to the chest (the largest component was found on the forearm). As seen in the Bland-Altman analysis, there was a good agreement in the whole range of RRs from 11 to 35 breaths/min. The respiratory and cardiac content in sternal PPG for the patient groups was in the same range of the one showed in the pre-clinical study; For the respiratory content the median and (interquartile) is 76.5 (16.3) $\%$ for

the patients (n=29) and 78.8 (38) % for the healthy group (n=10). As for the cardiac content, it was 14.9 (11.7) % for the patients and 19 (18.4) % for the healthy subjects. Additionally, it should be noted that the studies were conducted with two different PPG probes, but same wavelength (λ = 940 nm) and the analysis was done on the same segment length of 8 minutes. The spectral content of the PPG signal at the finger showed significantly lower respiratory content and higher cardiac content compared to sternal PPG as seen in Fig. 6.6. The cardiac content of the sternal PPG is assessed to be sufficient in terms of S_pO_2 calculation which is also confirmed by the result of the Blandt-Altman analysis. As seen in the plot in Fig. 6.7 there is a good agreement with the result from the conventional pulse oximeter, especially when the accuracy of the pulse oximeter is considered. The accuracy is reported as a standard deviation in S_pO_2 of 2 % points in the range 100 % to 80 % and 3 % points in the range 80 % to 50 %.

One of the limitations of this study is that the recording length for each patient is not equal. This means that one recording potentially may bias the results in a negative or a positive direction. Furthermore, lung function data are missing, which would give a picture about the severity of obstructive lung disease of the included patients. According to the measurements, some patients contributed to a normal range of the RR and others to higher rates. If patients were screened using for example spirometry it would be possible to divide the COPD patients into subgroups during the analysis. In regarding the S_pO_2 values, only four subjects did not receive oxygen therapy, the rest did and therefore 89 % of all data points (n=1784) are above 90 % S_pO_2 level. In spite of this high level of S_pO_2 level it is considered accepted for the validation of the sternal PPG, because it will always be the case at least at Bispebjerg hospital, that if a patient has S_pO_2 level below 90 % when it is in bed, it will receive oxygen therapy.

PPG-patch at the Sternum

As in the first study the PPG-patch was positioned at the sternum via adhesive tape. However, this was not the case for all the patients. On ten patients, the modified ePatch® electrode was used to attach the PPG-patch to the chest. All the ten patients had a prominent sternal bone similar to what is seen in Fig. 6.9a, which made the placement almost impossible without the electrode because the skin site was too thin. Figure 6.9b shows the ePatch® electrode attached at the sternum. The PPG-patch is embedded into the electrode just before the recording as seen in Fig. 6.9c. A picture of the sternum after the recording is seen in Fig. 6.9d. Marks of the location of the optical window is clearly seen.

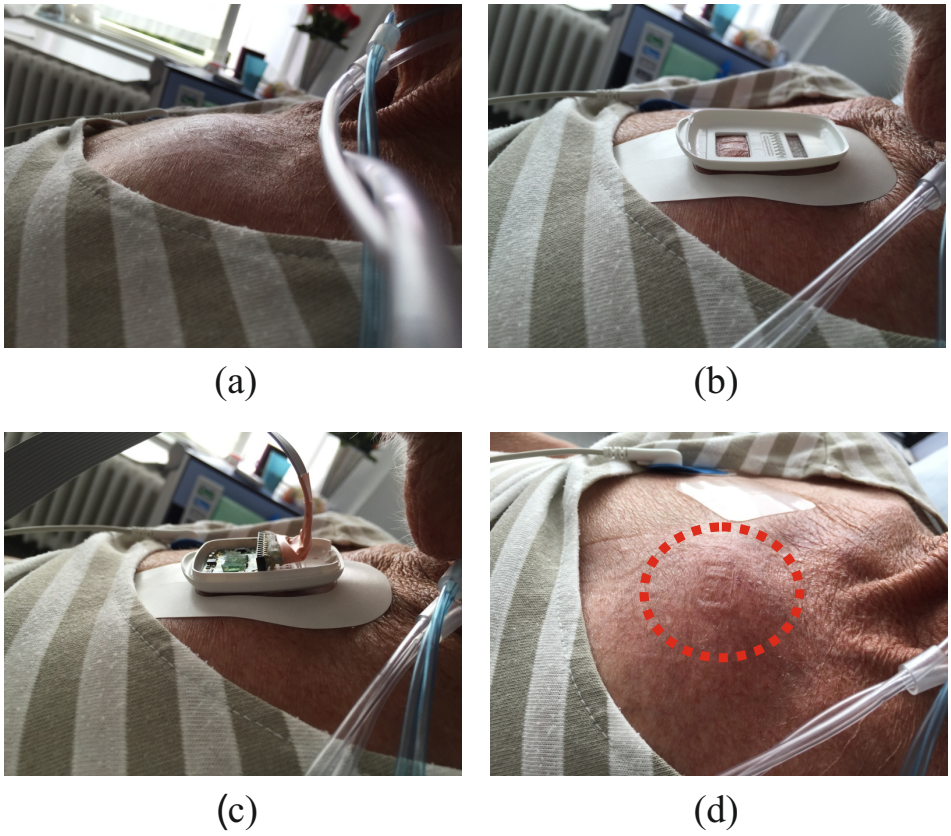

Figure 6.9: Pictures of the sternum of one patient. a) Before recording, shows the different anatomy of the sternal bone. Fortunately suitable for the PPG-patch and corresponding electrode. b) The modified ePatch® electrode is attached at the sternum. c) The PPG-patch is embedded into the electrode. d) Shows clear marks from the optical window that is sticking out from the PPG-patch.

6.5 Conclusive Remarks

To our knowledge, no study has previously reported results regarding the possibility of deriving the RR and the S_pO_2 level from sternal PPG on COPD and asthma patients. In this clinical study we have demonstrated that the RR and the S_pO_2 level can be calculated from sternal PPG on COPD and asthma patients. The results showed good agreement with capnography. Moreover, this may provide a useful clinical relevant improvement over manually obtained RRs in terms of time and early detection of exacerbations. In this clinical study the patients were instructed to move as little as possible. In the next and last study the patients are being monitored without any wires and therefore they were asked to follow their daily routine during the hospitalization. This will lead to an investigation of the ability to conduct and analyze long-term PPG recordings at the sternum. The whole optical window / electrode problem will be a key factor, because the PPG-patch can only work for long-term recording, if it is attached to the modified electrode. However, this utilizes PPG recordings, triaxial accelerometer signals and ECG signal, simultaneously.

CHAPTER

SEVEN

CLINICAL STUDY III: LONG-TERM PPG MEASUREMENT ON COPD AND ASTHMA PATIENTS

Objectives *The current chapter will consist of an investigation of the reliability of long-term continuous sternal PPG monitoring and the estimation of the S_pO_2 levels and the RRs on patients with COPD and asthma and on a group of healthy participants. Some of the outcomes of this chapter is based on Paper V.*

7.1 Background

We have in the previous chapters shown that the S_pO_2 levels and the RRs can be obtained from short-term sternal PPGs recorded on admitted patients with COPD or asthma. These findings show that sternal PPGs are highly applicable for reliable calculation of clinically relevant S_pO_2 levels and RRs in controlled conditions with a minimum influence of artifacts. However, in real-life applications, the recorded PPGs will be influenced by varying amounts of unavoidable artifacts. This includes for instance artifact from motions, changes in the amounts of ambient light, and poor contact between the skin and the sensor. When the PPG signals are affected by these artifacts, the calculation of the S_pO_2 levels and the RRs might be unreliable. From a clinical point of view, it is acceptable to estimate the S_pO_2 level and the RR in quasi-continuous periods with sufficient signal quality, e.g. provide a reliable calculation six times per hour or provide a reliable trend curve for each vital sign. This implies that periods of poor data quality are clinically acceptable as long as they alternate with periods of data that permits a reliable calculation of the S_pO_2 level and the RR.

Table 7.1: Demographics for the patient group and the group of healthy participants.

	COPD & Asthma	Healthy
Gender (male/female)	3/12	11/2
Age (years)	Mean: 67.4, SD:19	Mean: 45, SD: 14
BMI (Kg/m^2)	Mean: 25, SD:4.5	Mean: 24.7, SD:3

7.2 Method and Materials

7.2.1 Study Design

The population of this study is divided into two groups; a group of 15 patients with obstructive airway diseases (2 asthma patients and 13 COPD patients). The second group constitutes of 13 healthy participants. The enrollment of the patients has be conducted using the per protocol approach. Meaning that out of a total of 28 patients, only the patients who completed a full recording and the recorded data are assessed to be analyzable are included in this clinical study. All the patients were admitted at the Department of Pulmonary Medicine at Bispebjerg University Hospital, Denmark. Furthermore, all 15 patients received oxygen therapy when they were included. As for the group of healthy subjects, 15 were enrolled but two subjects were excluded due to sensor shut down error. Both patients and the healthy subjects were instructed to follow their daily routine (except showering). This ensures a realistic impression of the amount and type of artifacts present in long-term recordings obtained from hospitalized patients and from the healthy subjects outside the hospital environment. The demographics for both groups are shown in Table 7.1.

The developed PPG-patch is attached to the sternum via the modified ePatch® electrode. This is illustrated in Fig. 7.1. In the beginning of each recording, the S_pO_2 level was measured using a conventional finger pulse oximeter (Nellcor OxiMax N-65). The PPG-patch is programmed to have a maximum recording length of 20 hours. An example of a full recording of all the modalities is shown in Fig. 7.2 and a more detailed one-minute segment is shown in Fig. 7.3. The figure shows how movement may impact the PPG signal and how the respiration component dissapear when the patient stops breathing for few seconds.

Figure 7.1: (a) A photograph of the chest of a patient before application of the PPG-patch. (b) A photograph showing the the prototype PPG sensor attached to the sternum of the patient using the modified ePatch® electrode. The three dimensional axes defines the coordinate system of the triaxial accelerometer.

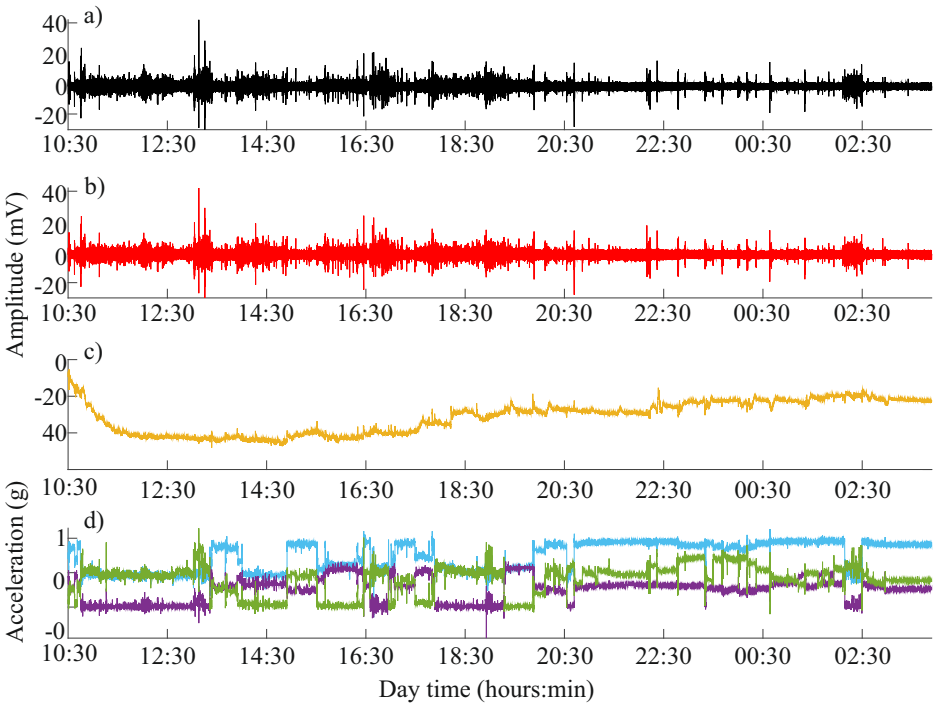

Figure 7.2: Plots showing the raw signals of the recorded modalities at the sternum with the PPG-patch. (a) Infrared PPG signal (b) Red PPG signal. (c) ECG signal. (d) Triaxial accelerometer signals. The blue, green and purple corresponds to x, y and z axes.

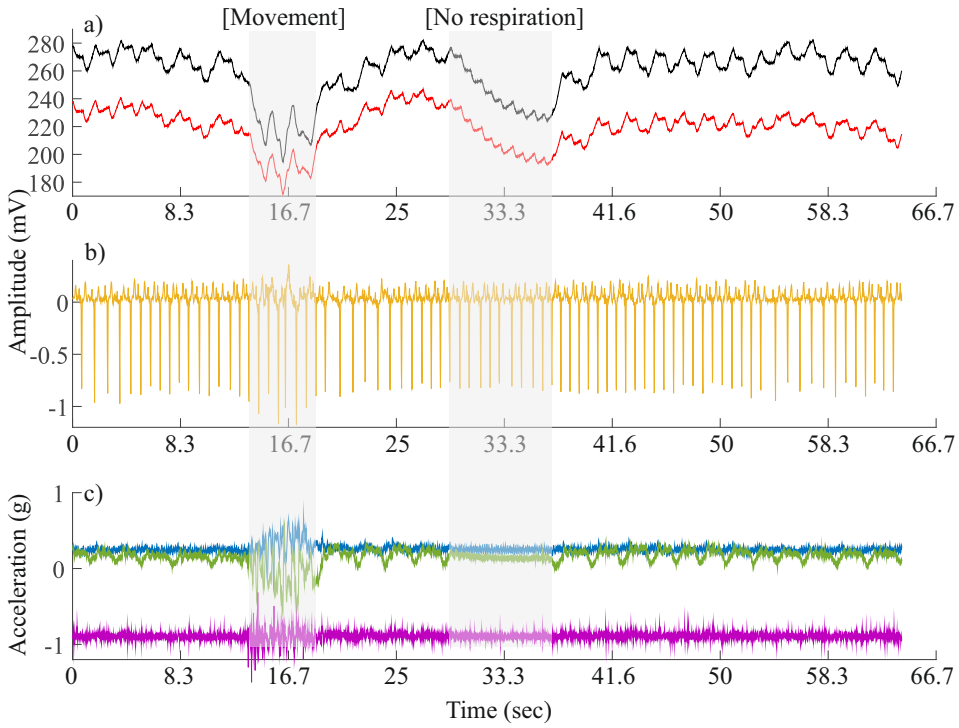

Figure 7.3: Plots showing a one-minute segment of the raw signals of the recorded modalities at the sternum with the PPG-patch. (a) Red and infrared PPG signal (b) ECG signal. (d) Triaxial accelerometer signals. Where the blue, green and purple corresponds to x, y and z axes. Interestingly, this current segment shows spontaneous respiration, movement and stop of respiration. The small spikes corresponds to the cardiac pulses in the PPG signals, while the larger corresponds to respiration.

7.2.2 Data Analysis

The data analysis is separated into two sections; reliability investigation in terms of the S_pO_2 level and in terms of the RR.

Reliability of Sternal PPG in terms of the S_pO_2 level

The recorded signals are divided into non-overlapping windows of 20 seconds and the S_pO_2 level is calculated in each of these windows in the same way as described in chapter 5. The S_pO_2 level was calculated as follow:

$$S_pO_2 = -25.89 * R + 116.48 \tag{7.1}$$

where R represents the relation between the red and infrared PPG signals after normalization and filtering. The window length is chosen to represent enough physiological information to provide a reliable calculation of the changes in the S_pO_2 levels over time. In order to investigate the reliability of the calculated S_pO_2 values, we implemented four criteria to classify the calculated S_pO_2 values into reliable (indicated as binary one) and unreliable (indicated as binary zero) values. An overview of the analysis is provided in Fig. 7.4. The classification is made based on the following criteria:

Cross-correlation: From the basic theory of pulse oximetry, it is known that the red and infrared PPG signals should be highly correlated [13]. However, no specific value is given. But looking at one of the most powerful state of the art algorithms patented by Masimo Inc. it is reported that if the cross-correlation between the red and infrared PPG signals is less than 75 $\%$ the signal segments does not qualify for the calculation of the S_pO_2 levels [82]. The same cross-correlation "limit" is used in the current analysis.

Rate of ΔS_pO_2: From the inherent physiological regulation of the S_pO_2 levels it is expected that the S_pO_2 change observed within one minute may vary very little in healthy subjects with normal lung function [83]. In COPD patients, it is well known that the S_pO_2 levels may fall rapidly when making a relatively small effort [84]. A study conducted on 60 COPD patients who participated in a six minute walk test, it was reported that all the patients desaturated and in 46 $\%$ of the patients had $\Delta S_pO_2 \geqslant 3$ $\%$ within the first 1.2 min and during low endurance cycling exercise 57 $\%$ of the patients had $\Delta S_pO_2 \geqslant 3$ $\%$ after 4.6 min [85]. So the desaturation rate also depends on the type of movement because different group of muscle groups is used to compensate for the demand of ventilation in the different daily situations. The COPD patients in our study have severe COPD and they all received oxygen therapy at least in the beginning of the recording. We will investigate the reliability of the S_pO_2 levels based on different ΔS_pO_2 limits: $\Delta S_pO_2 \geqslant 3$ $\%$, 4 $\%$, and 5 $\%$. So, the one-minute segment is classified as unreliable if the absolute difference between the maximum and minimum S_pO_2 values obtained in the one-minute segment exceeded 3 $\%$ (same procedure is done with 4 $\%$, or 5 $\%$).

Accelerometer threshold: To detect a certain movement during a recording, the magnitude of the resultant vector is used. The resultant vector is a net acceleration, which can be used as an indicator of overall body movements. The net accelerations is given by the following equation:

$$a_{net} = \sqrt{a_x^2 + a_y^2 + a_z^2} - 1 \tag{7.2}$$

where the magnitude of the static acceleration (gravity) is subtracted. Furthermore, the signal is further smoothed over time (window size of 0.5 seconds). After inspection of all the recordings a difference between motion and non-motion is clear when using a static threshold of 0.1 g. So we chose to define this value as a threshold to distinguish between motion or non-motion. Therefore, all S_pO_2 values calculated in the 20-seconds segments where the magnitude of the net acceleration is greater than 0.1 g, are classified to be not reliable.

Upper and lower limits of the S_pO_2 level: S_pO_2 values outside a range of 100 %-80 % are classified to be not reliable. This is because it is impossible to have values greater than 100 % and based on previous experiments it was not observed that any patients had a S_pO_2 level less than 80 %.

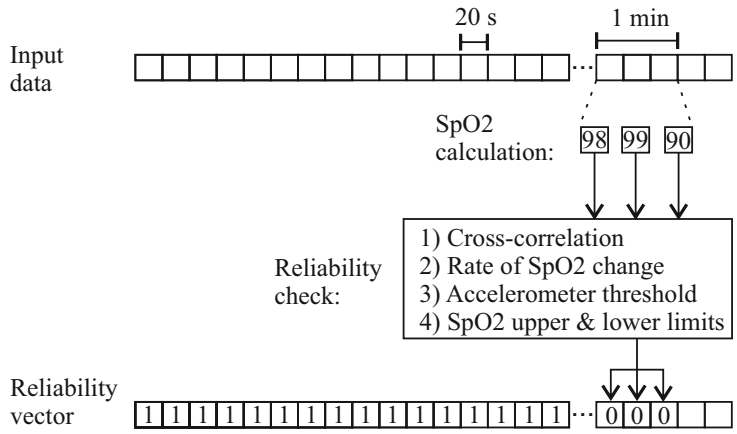

Figure 7.4: Schematic overview of the analysis. The reliability is checked based on the S_pO_2 levels calculated from three consecutive 20-second windows (corresponding to a one-minute data segment). If the input data from the one-minute segment is classified as unreliable, all three corresponding 20-second windows are also classified as unreliable and they are excluded from further analysis (illustrated by zeros in the reliability vector).

The reliability check was conducted as a sliding window with an overlap of two 20-second windows. This implies that each 20-second window is included in three different runs of the reliability check. If it is classified unreliable in at least one of the three checks, the 20-second segment is considered unreliable. Figure 7.5a shows all the calculated S_pO_2 values from one patient in a five hour recording sequence during the night. Each marker is a value calculated from a 20-second segment. The performance of the reliability check of the $\Delta S_pO_2 \geqslant 3$ % (red markers) and the accelerometer threshold (green markers) is also illustrated in Fig. 7.5b. These markers are classified to be non reliable. Removing those non reliable S_pO_2 values gives a more stable time course as seen in Fig. 7.5c. Fig. 7.5(d-e) shows the band-pass filtered red and infrared PPG signals. Fig. 7.5f shows the overall acceleration. The dashed red line corresponds to 0.1 g as described previously. Over time

the segments have a certain variation around a baseline S_pO_2 level. To estimate this variation, we introduce an estimated reference S_pO_2 trend curve. This curve is calculated with an average filter with 30 points (corresponding to 10 minutes). All unreliable segments were excluded for calculation of this reference trend curve. An example of the trend curve (red line) is provided in Fig. 7.5(c). We then defined the long-term accuracy of the S_pO_2 calculation as the Root Mean Squared error (RMSE) between this reference curve and the S_pO_2 values that were classified as reliable.

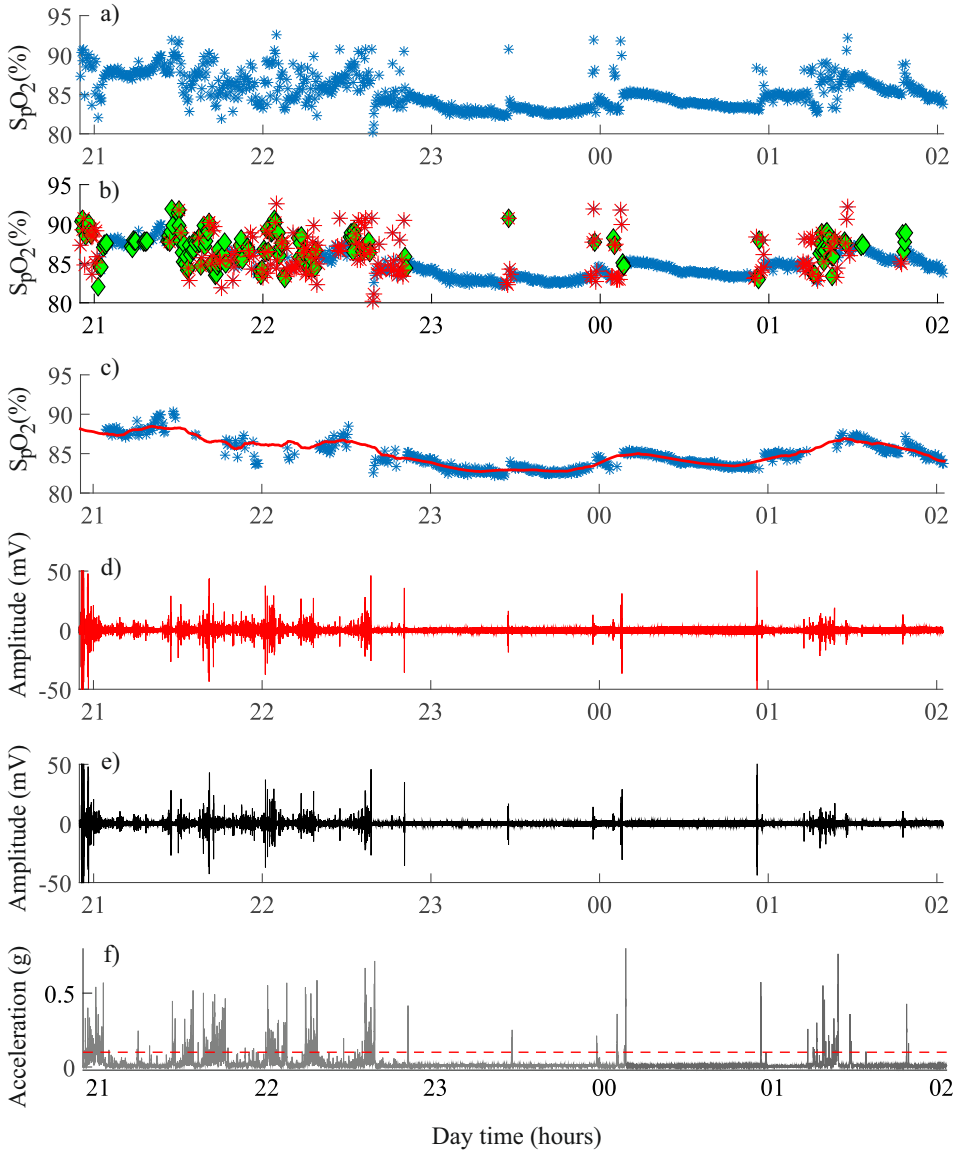

Figure 7.5: (a) An example of the time course of all calculated S_pO_2 values for five hours during the night for one patient. (b) An illustration of the reliable segments (blue markers) and the unreliable segments (red markers). These markers are detected due to the second criteria where in this particular example $\Delta S_pO_2 \geqslant 3$ % between the minimum the maximum value within a one-minute segment. The green markers are also from unreliable segments detected due to the accelerometer criteria. (c) The time course of all the extracted reliable segments (blue marks) together with the estimated average reference curve (red line). (d-e) Time course of the band-pass filtered red and infrared PPG signals are shown. Furthermore, it is observed how segments with high amounts of artifacts in the PPG signals are considered unreliable and therefore excluded from the S_pO_2 analysis. (f) Time course of the magnitude of the net accelerometer signal. Segments with accelerations above 0.1 g (dashed red line) are classified as unreliable.

Reliability of Sternal PPG in terms of the RR

Investigating the RR over a long-term recording without any reference is not a trivial task. The RR can fluctuate a lot during a recording. For instance while, talking, eating or walking. However, the RR during these circumstances will be treated as unreliable calculations due to the applied conditions.

The infrared PPG signal was used and was filtered using a Butterworth band-pass filter with two 4th order slopes at 0.1 Hz and 0.7 Hz corresponding to RRs from 6 to 42 breaths/min. The upper limits is chosen because it was seen in the previous study that COPD and asthma patients can have higher RRs than 30 breaths/min. Afterwards, a simple peak detection method was applied with two criteria: The height of the peaks must be more than 50 $\%$ of the root mean square value of the signal. And the inter-peak distance is minimum 1.4 seconds, corresponding to a maximum RR of 42 breaths/min. Now the calculated RR can be given by the inverse of the mean inter-peak distance in the 20-second segment.

In terms of the reliability check the same procedure as described in the previous section was used. So the RR is calculated in three 20-seconds segments in one-minute, giving three values of the RR. Then the maximum and the minimum absolute RR value is compared within this one-minute. If the difference in RR is greater than 3 breaths/min within one-minute then the value is classified as unreliable estimate of RR. Additionally, the acceleration criteria will also be used in the reliability check. It was chosen not to set any lower and upper limit check of the RR. Because this constrain is already applied in the peak detector algorithm. An example of the time course where the described conditions are applied is illustrated in Fig. 7.6. The segment is exactly at the same time as shown in Fig. 7.5, except that now in Fig. 7.6b the red markers corresponds to the unreliable RR values. It is assessed due to RR stability and low accelerometer activity that the time segment shows a transition to bedtime. During the night it is expected that the ΔRR is low, which seems like that in this example from 23:00 to 02 o'clock.

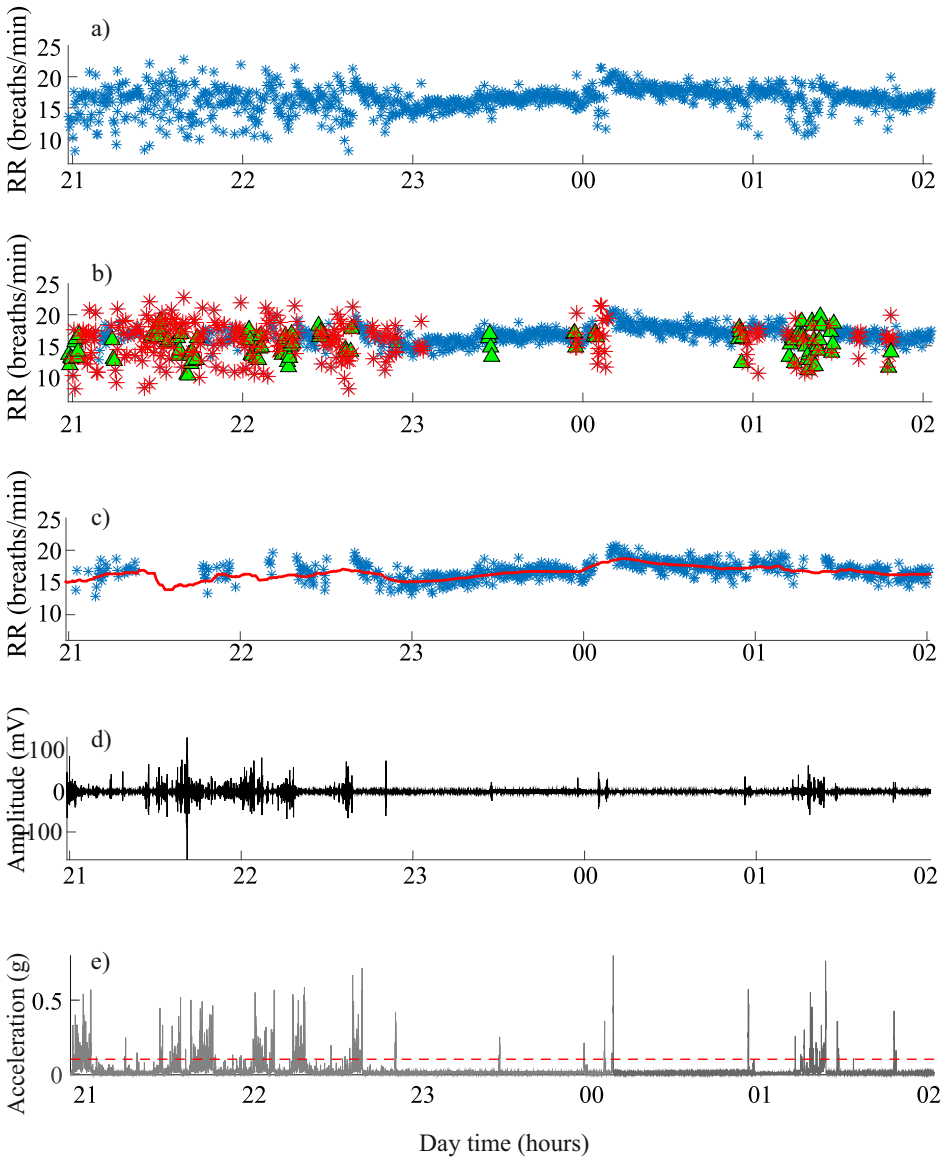

Figure 7.6: (a) An example of the time course of all calculated RR values in a five hour recording segment.(b) An illustration of the reliable segments (blue markers) and the unreliable segments (red markers). These markers are detected due to $\Delta RR \geqslant 3$ breaths/min within a one-minute segment. The green marks are also from unreliable segments detected due to the accelerometer criteria. (c) An illustration of the time course of all the reliable RR values (blue marks) together with the estimated average reference curve (red line). This curve is applied to calculate the long-term accuracy of the calculated reliable RR values. (d) Time course of the band-pass filtered infrared PPG signal are shown. (e) Time course of the magnitude of the resultant accelerometer signal. Segments with accelerations above 0.1 g (dashed red line) are classified as unreliable.

The variation over time is also used by introducing an estimated reference RR trend curve. This curve is calculated with an average filter with 30 points (corresponding to 10 minutes). All unreliable segments were excluded for calculation of this reference trend curve. The trend curve (red lines) is illustrated in Fig. 7.6(c). The long-term accuracy of the RR calculation is then defined as the Root Mean Squared error (RMSE) between this reference curve and the reliable RR values.

7.3 Results

The result will be presented in two sections, the first section is related to the S_pO_2 level and the second is related to the RR. In each section the result will be presented with and without the accelerometer criteria.

7.3.1 Long-term Monitoring of the S_pO_2 Level

For the group of patients the RMSE between the S_pO_2 values calculated from sternal PPGs in the beginning of the recording and the S_pO_2 values obtained from the conventional finger pulse oximeter was only 2.3 $\%$. No reference value was taken for the healthy group because it was expected that the S_pO_2 level is above 95 $\%$. For each hour in the recordings the percentage of reliable segments (defined as the percentage uptime) is calculated when all the previously mentioned conditions are applied.

The effect of different values of ΔS_pO_2 on the average percentage uptime and the RMSE is presented in appendix A. It is chosen to use the $\Delta S_pO_2 \geqslant 3$ $\%$ for further analysis because it is assessed that this constrain is applicable for the type of patients used in this study. Without including the accelerometer criteria the average percentage uptime during the whole recording for the patients and the healthy subjects is 57.6 $\%$ and 58.1 $\%$ respectively. The RMSE is accordingly 2.5 $\%$ and 2 $\%$. Figure 7.7 and Fig. 7.8 shows the uptime for every hour during the recordings. Interestingly, how the percentage uptime is almost the same for the group of patients while there is a remarkable increase during the night for the group of healthy subject. For the patients, the recording started in between 09 and 11 o'clock in the morning. While it was between 10 and 13 o'clock for the healthy subjects and therefore the percentage uptime decreases in the last hour because of activity.

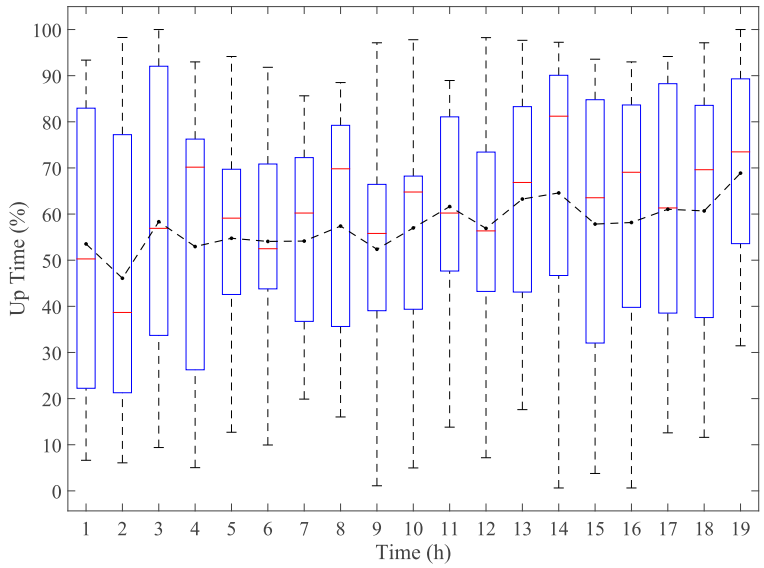

Figure 7.7: A box-plot of the percentage uptime for every hour of the calculated S_pO_2 values for the **patients**, when using all the conditions except the accelerometer condition. The horizontal dashed line corresponds to the average. The recordings started between 9 and 11 o'clock.

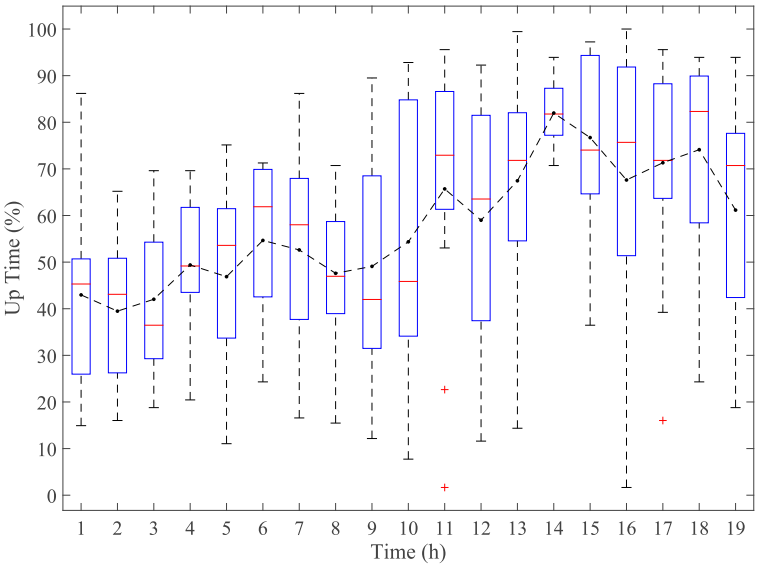

Figure 7.8: A box-plot of the percentage uptime for every hour of the calculated S_pO_2 values for the **healthy subjects**, when using all the conditions except the accelerometer condition. The horizontal dashed line corresponds to the average. A noticeable difference of the increase uptime between day and night. The recordings started between 10 and 13 o'clock.

Instead of only looking at the percentage uptime, we can also look at the span distribution of unreliable time segments for each patient. This is illustrated in a box plot in Fig. 7.9. Almost all the excluded time periods are less than ten minutes. For patient number 12, it is seen that there has been a segment of approximately 70 minutes where there has not been any reliable S_pO_2 levels.

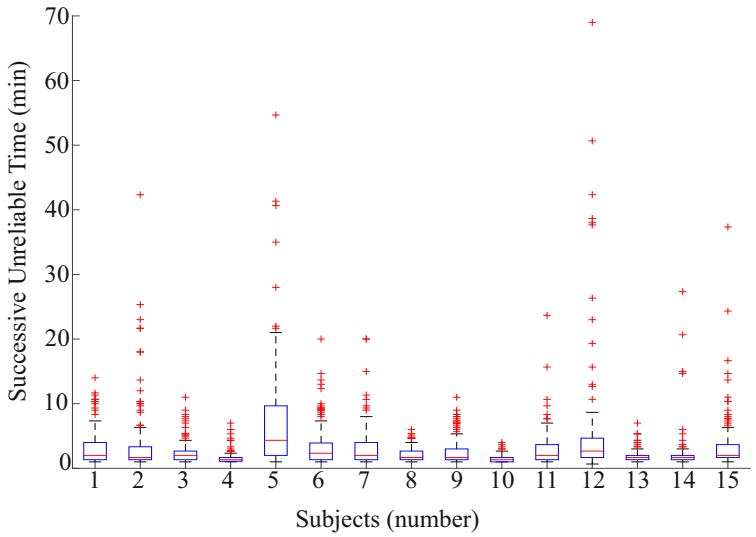

Figure 7.9: A box-plot of the distribution of the length of unreliable (excluded) time segments in terms of the S_pO_2 level for each patient. The red marks indicate outliers.

Now looking at the accelerometer condition without including the $\Delta S_pO_2 \geqslant 3$ % criteria. The average percentage reliable S_pO_2 values for the patients and for the healthy group is 50.2 % and 43.4 % respectively and the RMSE is accordingly 3.06 % and 2.4 %. For both groups it is seen in Fig. 7.10 and Fig. 7.11 that the percentage uptime during the day has decreased when the accelerometer criteria was applied, whereas during the night no remarkable differences is seen.

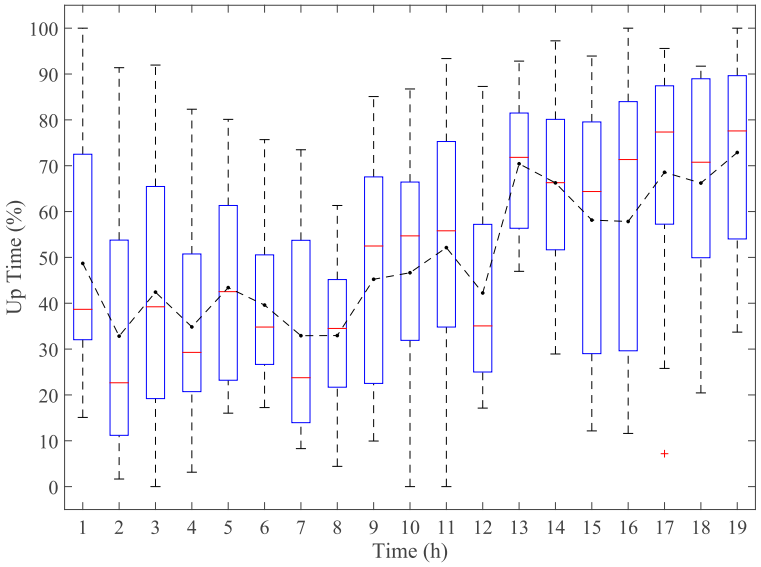

Figure 7.10: A box-plot of the percentage uptime for every hour of the calculated S_pO_2 values for the **patients**. The classification of reliable data is based on all the conditions except the $\Delta S_pO_2 \geqslant 3$ % criteria. The horizontal dashed lines corresponds to the average. The recordings started between 9 and 11 o'clock.

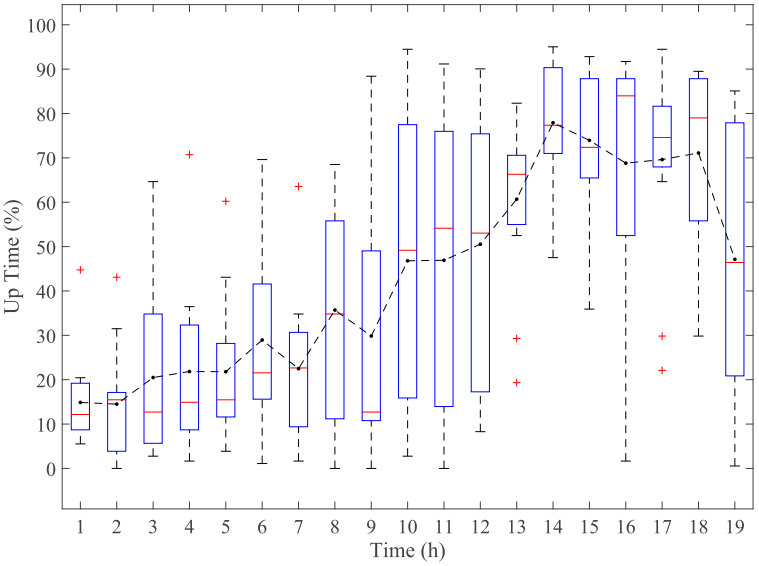

Figure 7.11: A box-plot of the percentage uptime for every hour of the calculated S_pO_2 values for the **healthy subjects**. The classification of reliable data is based on all the conditions except the $\Delta S_pO_2 \geqslant 3$ % criteria. The horizontal dashed line corresponds to the average. The recordings started between 10 and 13 o'clock.

Applying all the conditions on both groups gives an average reliable uptime of 37.6 % and 37 % for the patients and the group of healthy subjects respectively. And the RMSE is 2.7 % and 1.7 %. The progression over time is shown in Fig. 7.12 and Fig. 7.13 for each group.

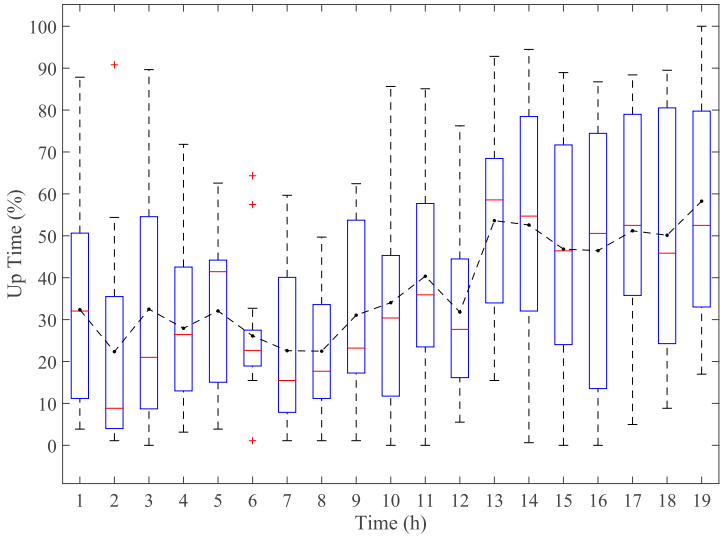

Figure 7.12: A box-plot of the percentage uptime for every hour of the calculated S_pO_2 values for the **patients**. The classification of reliable data is based on all the conditions: $\Delta S_pO_2 \geqslant 3$ %, cross-correlation, limited S_pO_2 range and accelerometer conditions. The horizontal dashed line corresponds to the average. The recordings started between 9 and 11 o'clock.

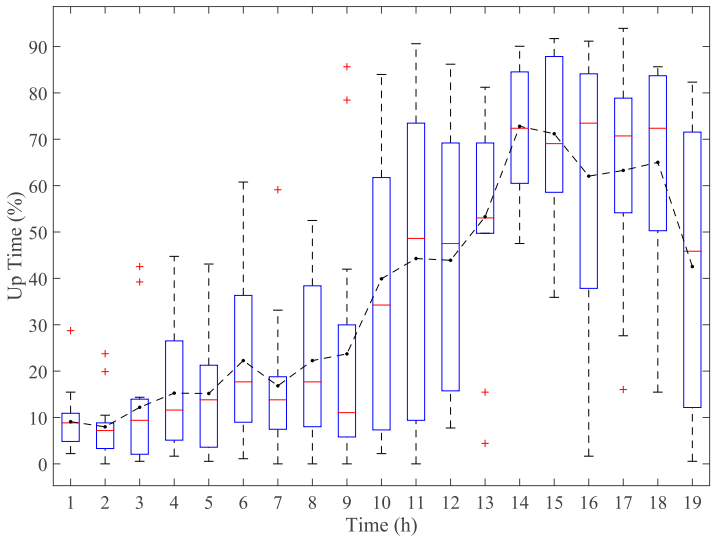

Figure 7.13: A box-plot of the percentage uptime for every hour of the calculated S_pO_2 values for the **healthy subjects**. The classification of reliable data is based on all the conditions: $\Delta S_pO_2 \geqslant 3$ %, cross-correlation, limited S_pO_2 range and accelerometer conditions. The horizontal dashed lines corresponds to the average. The recordings started between 10 and 13 o'clock.

7.3.2 Long-term Monitoring of the RR

The same calculations procedure was conducted in terms of the RR. For each hour in the recordings the percentage of the reliable segments is calculated when all the previously mentioned conditions are applied. The result when the $\Delta RR \geqslant 3$ breath/min, criteria is applied is shown in Fig. 7.15 and Fig. 7.16. The average percentage of reliable RRs for the patients group and the group of healthy subjects is 58 % and 59 %, respectively. The RMSE is 2.9 breaths/min and 3 breaths/min correspondingly.

The distribution of unreliable time segments for each patient is illustrated in a box plot in Fig. 7.14. Almost all excluded time periods are less than ten minutes, meaning that most likely we can obtain a reliable RR measure six times per hour. As seen before patient number 12 has an unreliable segment of approximately 70 min in terms of the S_pO_2 level. The same result is obtained in terms of the RR. By further inspection of the PPG segment it was seen that the signal in this 70 minutes was very noisy and it was not possible to detect any valid PPG signal.

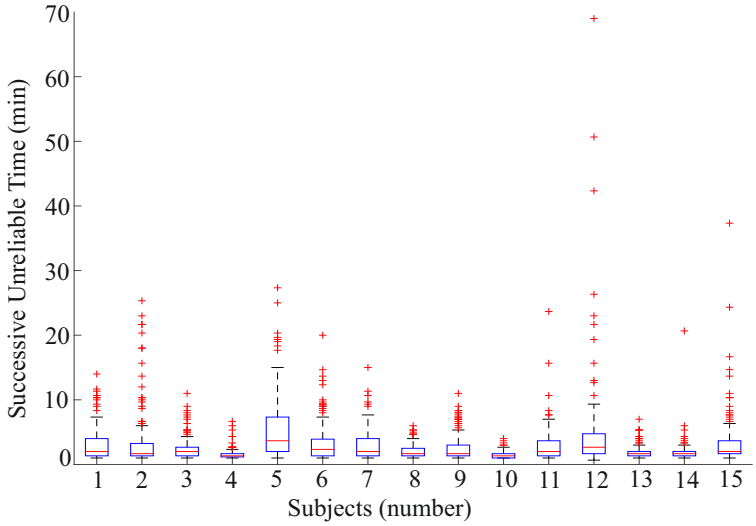

Figure 7.14: A box-plot of the distribution of the length of unreliable (excluded) time segments in terms of the RR for each patient. The red marks indicate outliers.

Adding the accelerometer condition changes the percentage uptime to 37.9 % for the patients and 38.1 % for the healthy subjects. The RMSE becomes 2.6 breaths/min and 2.8 breaths/min respectively. The percentage uptimes is shown in Fig. 7.17 and Fig. 7.18.

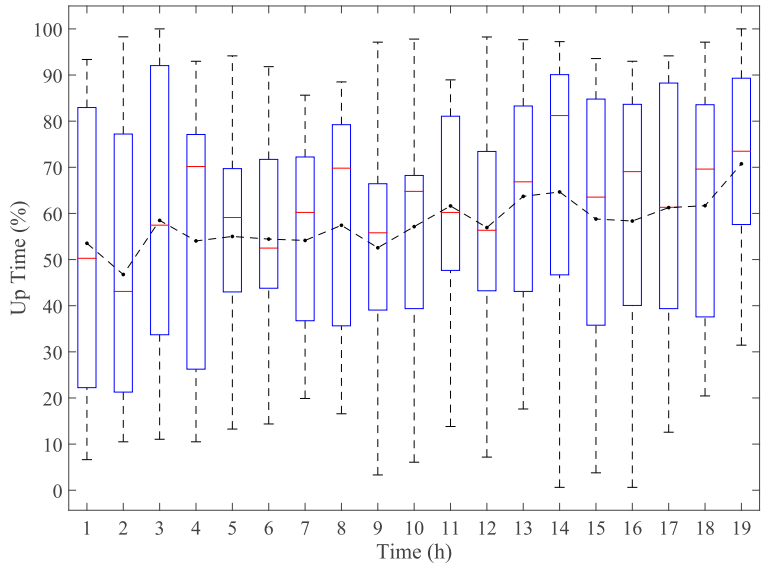

Figure 7.15: A box-plot of the percentage uptime for every hour of the calculated RRs for the **patients**, when using all the conditions except the accelerometer condition. The horizontal dashed lines corresponds to the average. The recordings started between 09 and 11 o'clock.

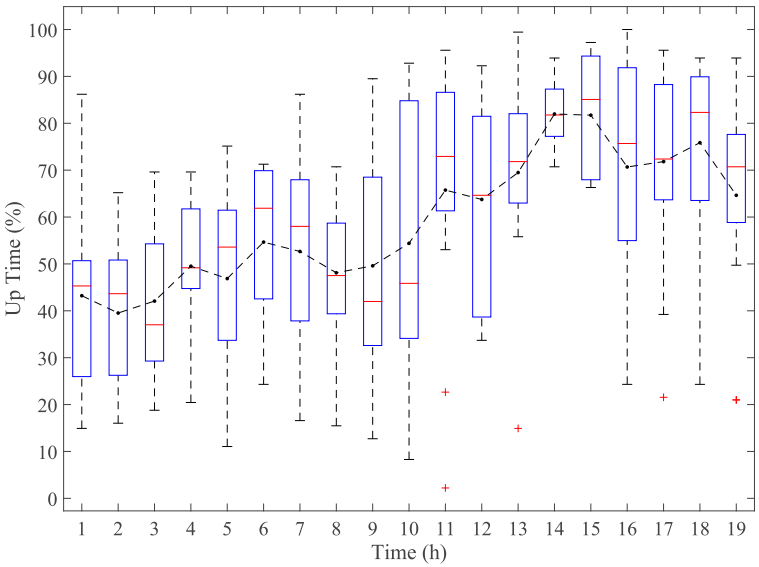

Figure 7.16: A box-plot of the percentage uptime for every hour of the calculated RRs for the **healthy subjects**, when using all the conditions except the accelerometer condition. The horizontal dashed lines corresponds to the average. A noticeable difference of the increase uptime between day and night. The recordings started between 10 and 13 o'clock.

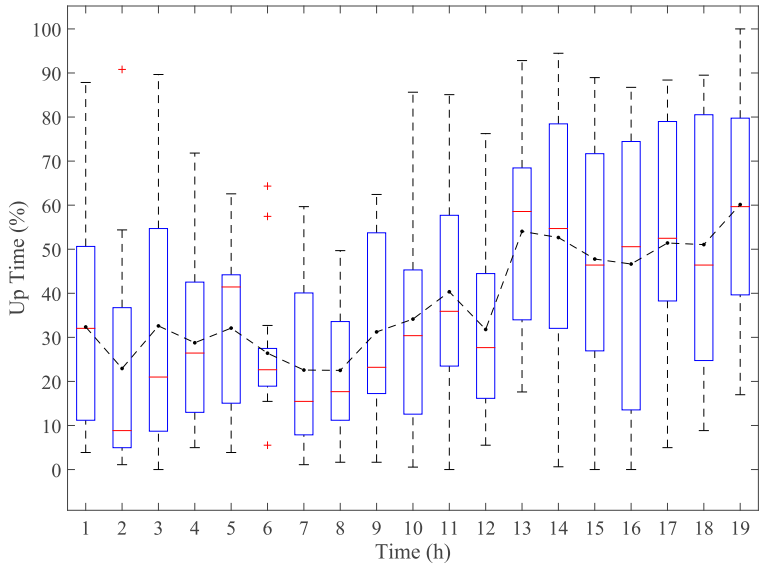

Figure 7.17: A box plot of the percentage uptime for every hour of the calculated RRs for the **patients**. The classification of reliable data is based on $\Delta RR \geqslant 3$ breaths/min and accelerometer conditions. The horizontal dashed line corresponds to the average. The recordings started between 9 and 11 o'clock.

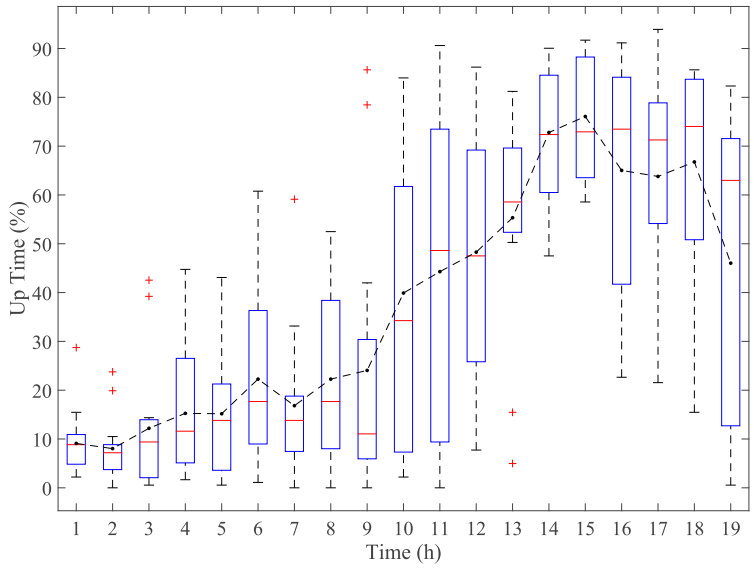

Figure 7.18: A box-plot of the percentage uptime for every hour of the calculated RRs for the **healthy subjects**. The classification of reliable data is based on the $\Delta RR \geqslant 3$ breaths/min and the accelerometer conditions. The horizontal dashed line corresponds to the average. The recordings started between 10 and 13 o'clock.

7.4 Discussion

In this long-term clinical study, it was important to restrict the patients' and the healthy participants' daily activity as little as possible. For the patients this ensures a realistic impression of the possibilities for future quasi-continuous calculation of the S_pO_2 level and the RR in the presence of artifacts arising from normal daily or in-hospital activities. It was therefore not feasible to compare the calculated values with conventional vital sign monitors throughout the recording length.

The Long-Term S_pO_2 Recording

As a baseline accuracy measure, we compared the S_pO_2 values calculated from sternal PPGs with a conventional finger pulse oximeter in the beginning of the recordings. Based on our findings from the previous study and the very low RMSE between the two methods, we presume that the S_pO_2 levels calculated from the long-term sternal PPGs are reliable in segments of sufficient data quality. For the rest of the recording time, we therefore investigated the reliability based on knowledge about the inherent physiological regulation of the S_pO_2 levels and the basic theory of pulse oximetry. By visual inspection of challenging data segments, we found that the $\Delta S_pO_2 \geqslant 3\ \%$ criteria seems reliable for this patient population. Taking the accuracy of the calibration for the PPG-patch into account this limit seems also reliable for the healthy participants. It is observed from Fig. 7.5 how the reliability classification correctly removes outliers. These outliers are expected to be caused by poor data quality due to motion artifacts or poor light and tissue interface. This finding is confirmed when using the accelerometer criteria to determine which of the segments that can be considered reliable. Generally, it was seen that the accelerometer criteria slightly underestimated the reliability percentage of the recordings compared to the $\Delta S_pO_2 \geqslant 3\ \%$ condition. As for the patient group the accelerometer condition resulted in a percentage uptime of 50.2 $\%$ and with the $\Delta S_pO_2 \geqslant 3\ \%$ condition it was 57.6 $\%$. And the difference was even larger between the two conditions (approximately 14 $\%$ difference) for the healthy subjects. This is because the activity levels between the two population are different. During the day time the activity level of the healthy subjects is expected to be larger compared to the night. This is also confirmed when looking at the percentage uptime for each hour during the entire recording. The uptime was larger during the night than the day. As expected the difference in the uptime during the night and day was not significant for the patients.

Generally, it is experienced that the accelerometer condition results in more false negative error. More interestingly, it is found that segments of reliable S_pO_2 values could be extracted throughout the recording length. This indicates that when the S_pO_2 level calculation temporarily becomes unreliable due to artifacts, it becomes reliable again after the artifact event. This is also the fact for the RR and it is also observed in the raw signals illustrated in Fig. 7.3. Another interesting outcome

is seen in Fig. 7.13. From recording hour 10 to 12 corresponding to approximately 19 to 22 o'clock the variability of the data is relatively large compared to the rest of the recording time for the group of healthy subjects. The reason to this may be "getting prepared just before bedtime". The same thing is seen at hour 19 corresponding to clock time between five and eight o'clock in the morning. Another interesting result is the lengths of successively unreliable segments. The maximum length was 70 min in terms of the S_pO_2 calculation. However, the average for all the patients is 23 min and most of the lengths are under 10 min. This is very promising for quasi-continuous measuring of the S_pO_2 level.

The Long-Term RR Recording

As described earlier the RR is measured by manual inspection of the thorax. A nurse holds the hand of a patient and acts like s/he is measuring the heart rate, while s/he actually is looking at the thorax and counting the movements. The main idea is not to bias the patient's breathing pattern during the measurement. So in order to calculate a reliable RR on any patient the person should not be moving. Furthermore, talking or eating should be avoided during the measurement. All these factors are of course impossible to apply during long-term recordings. The most important is to find the segments where the patient is at rest and then calculate the RR. For this reason the accelerometer threshold criteria is convenient in regarding the calculation of the RR compared to the S_pO_2 level. If there is good contact between the PPG sensor and the skin it is still possible to measure the S_pO_2 level while moving. This is however not possible with the RR because the inherent variation would be large. This is also what was reflected in the results. During the night, the percentage uptime was clearly higher compared to the rest of the day. This was seen for both groups. What should be noticed is that although the used peak detection method is not a robust and verified algorithm it was still possible to find a trend and to show a possibility of quasi-continuous calculation of the RR. It was shown in the previous study how accurate the RR can be estimated when a medical doctor annotated the data. However, automated calculation of the RR in long-term recordings still needs a lot of attention in terms of reliability. As it was noticed the variability of data is somehow stable for the patients during the whole recording time, while it was at specific times for the group og healthy subjects. Just before, bedtime and in the early morning the interquartile range is large compared to the rest of the recording time. The reliability estimates for the S_pO_2 level and the RR was almost the same (58 $\%$) which may indicate that the quality of the PPG signal is sufficient to calculate both parameters throughout a long-term recording and most importantly, it was also observed from Fig. 7.9 and Fig. 7.14 that it would be possible to measure the S_pO_2 level and the RR at least six times per hour. This is very promising for future quasi-continuous calculation of the S_pO_2 levels and the RRs from sternal PPGs.

Experimental Remarks

As experienced from study I and II the optical window does not make good contact with the skin when the modified adhesive electrode is used. Therefor the quality of the PPG signals may be compromised in this study. Furthermore, the data collection was very challenging. All the patients included in this study had severe COPD or athma. Temporary exacerbation occurred in almost all the enrolled patients during the day or night recordings. This was very challenging for a prototype sensor. Twenty-eight patients were enrolled in order to get 15 full recordings. The problems can be grouped into three categories: The first category is the hardware/software problems because of the lack of DC calibration during the recordings, which may result in a high percentage of saturated data. Furthermore, the device has a fixed gain, which makes it difficult to adapt to the tissue interfaces when for example a patient is sweating. The second category is the adhesive problem. Sweating makes the adhesive electrode less adhesive and the optical interface with the skin changes, which requires new calibration. The last category, the diversity of thorax anatomy makes it challenging to attach the sensor at the sternum, where on some patients it was impossible to position the PPG-patch because of the sternal curvature.

7.5 Conclusive Remarks

In this preliminary study, it was thus demonstrated the ability to calculate clinically relevant and reliable S_pO_2 levels and RR from long-term sternal PPG recordings obtained from patients suffering from obstructive lung diseases and from healthy participants. This finding is very promising for future implementation of the S_pO_2 and the respiratory measures in a sternum based vital sign patch. In the future, such a patch might assist in early detection of worsening in the condition of these patients (or other patient groups with chronic diseases) and thereby ensure timely treatment of the patients. Furthermore, it might be possible to design new algorithms for automatic detection of data segments that would provide a reliable S_pO_2 and RR measures. The low RMSE between the included S_pO_2 values and the estimated average reference curves as well for the RRs indicates a high long-term accuracy of the calculated values. It also indicates that we have obtained a high attenuation of artifacts in the originally calculated values. It might be possible to increase the uptime even further, e.g. by optimizing the sensor design, implementing adaptive noise cancellation from additional recording modalities, or implementing more advanced algorithms for calculation.

CHAPTER

EIGHT

CONCLUSION

The main purpose of this Ph.D project is to investigate the possibility of making reliable long-term monitoring of the respiratory rate and the oxygen saturation of the blood from sternal PPG. We have pursued this through four studies that each contributed to the overall investigation of sternal PPG. The project started with a pre-clinical proof of principle study to acquire knowledge about sternal PPG in terms of the RR and the S_pO_2 level. Afterwards, three clinical studies were designed and conducted to increase the currently limited amount of knowledge about the clinical applicability of sternal PPG. In the first study, we desaturated a group of healthy subjects and calculated the S_pO_2 level in a clinically relevant range between 100 $\%$-70 $\%$. In the second study, the aim was to validate the reliability of sternal PPG in short-term recordings on COPD and asthma patients. In the third study we focused on the clinical reliability of long-term recordings on the same group of patient (different people) and we extended the recording to a healthy group of subjects. Giving a total number of 82 included participants used in this research project.

For the purpose of conducting the clinical studies, two different designed PPG sensors were developed and used for the PPG recordings along with other modalities. In order to conduct the clinical studies, applications were written to the Danish regional ethical community (H-6-2014-013), the Danish Health and Medicines Authority (CIV-15-01-013029), and the Danish Data Protection Agency. All three studies were approved and monitored by the regional good clinical practice (GCP) unit.

The developed PPG sensor (PPG-patch) can operate in two modes; a mode where it is connected to a data acquisition system and a wireless mode. This utilizes short and long-term recordings. In the second mode the PPG-patch used DELTA's ePatch® framework to save the recorded PPG signals along with ECG and triaxial accelerometry from the sternum. Moreover, it also uses the ePatch® adhesive electrode to be positioned at the sternum. Both operation modes were very useful for the understanding of the clinical applicability of sternal PPG. However, it should be noticed that the

signal quality is 80 $\%$ better when the electrode is not used and the PPG-patch is directly attached to the sternum.

From the pre-clinical proof of principle study, it was shown that the respiratory component in the power spectral content of the sternal PPG signal was 76 $\%$ and the cardiac component was 22 $\%$. Moreover, the respiratory and cardiac component was highly correlated with the corresponding respiratory fCO_2 reference signal and the ECG signal, respectively. In regards to the RR no significant difference was between the PPG signal and the respiratory fCO_2 reference signal during spontaneous or paced breathing in the range from 6 to 27 breaths/min. Furthermore, the quality of the PPG signal was superior in terms of the signal morphology. For example the dicrotic notch was observable in the AC part of the signal, verifying the quality of the recorded signal. Finally, we have demonstrated the ability of pulse wave analysis in terms of pulse rate variability, which can be used in the assessment of cardiovascular diseases [15].

The first clinical study was a controlled desaturation study. For all the 14 subject the oxygen saturation was gradually reduced within the region of clinical interest (100 $\%$ - 70 $\%$). The results showed that there is good agreement between the calculated S_pO_2 values and the measured S_aO_2 reference values (n=324 blood samples). The accuracy of the sternal PPG system was found to be Arms = 1.75 $\%$. This accuracy is acceptable according to the ISO 80601-2-61:2011 guidelines that allows Arms values of up to 4 $\%$. Commercially available pulse oximeters such as Masimo R25-L and NellCore Oximax N-65 reports accuracies of 1.79$\%$ and 1.3$\%$, respectively. This study served as a calibration of the PPG-patch in terms of the S_pO_2 level.

In the second clinical study we conducted short-term PPG recordings on 30 COPD and asthma patients being in a semi-supine position. In regards to the S_pO_2 level the Pearson correlation between S_pO_2 level measured on the finger with a conventional pulse oximeter and the S_pO_2 level calculated from the sternal PPGs was found to be 0.89 ($p < 0.05$). Furthermore, the Blandt-Altman analysis showed good agreement between the two methods. Taking the individual accuracy of the two systems into account, we thus consider the agreement to be excellent. This shows that PPGs recorded on the sternum is reliable for estimation of S_pO_2 levels in admitted COPD and asthma patients. In terms of the RR the sternal PPG signal and the respiratory fCO_2 reference signal from a conventional patient monitor system was compared. The signals were divided into one-minute segments and a medical doctor annotated the data. The RR obtained from the patients ranged from 11 to 36 breaths/min and was highly correlated ($r = 0.93$, $p < 0.001$) with the referent signal.

In the third and last clinical study, we used the wireless version of the PPG-patch. We recorded 19 hours PPG, ECG and triaxial accelerometer signals on 15 COPD and asthma patients and on a group of 13 healthy participants. We implemented a check to assess the reliability of long-term sternal PPG recordings. Overall, the average percentage of reliable PPG segments from the patients

and the healthy participants was 58%. In terms of the RR the percentage of reliable PPG segments was 58 % and 59% for the patients and the healthy participants. More importantly, we generally found that segments of reliable S_pO_2 and RR values could be extracted throughout the recording length. The average longest period of time with unreliable data was 23.6 min in terms of the S_pO_2 level and 20 min in terms of the RR. In this clinical study, we have thus demonstrated the ability to calculate clinically relevant and reliable S_pO_2 values in long-term sternal PPG recordings obtained from patients suffering from obstructive lung diseases and on a group of healthy subjects. This finding is very promising for future implementation of S_pO_2 and RR measures in a sternum based vital sign patch. In the future, such a patch might assist in early detection of worsening in the condition of these patients and thereby ensure timely treatment of the patients.

Thus, all four hypotheses of this research project have been confirmed.

8.0.1 Future Perspectives

In the future, it might be possible to design new algorithms for automatic detection of data segments that would provide a reliable S_pO_2 and RR measures. This would allow for a real-time quasi-continuous setup for long-term monitoring in chronically ill patients. Furthermore, we suggest the following future work to improve the applicability of the sternal PPG:

1. Optimizing the sensor design in terms of good skin contact with the challenging anatomy of the sternum. The curvature of the sternum is very challenging and needs much more attention.
2. Implementing algorithms that use the multi-modality approach. Including the ECG signal and triaxial accelerometer signals in the algorithm is highly recommended. Moreover, adaptive noise cancellation can be utilized by the use of the accelerometer signal. PPG recording with other wavelengths may also be very useful for adaptive noise cancellation.
3. Electrical optimization by using recently available front-end electronics.

BIBLIOGRAPHY

[1] D. B. Saadi, H. B. D. Sørensen, I. H. Hansen, K. Egstrup, P. Jennum, and K. Hoppe, *ePatch® - A Clinical Overview*. 2014.

[2] H. D. Hummler, A. Engelmann, F. Pohlandt, J. Högel, and A. R. Franz, "Decreased accuracy of pulse oximetry measurements during low perfusion caused by sepsis: Is the perfusion index of any value?," *Intensive care medicine*, vol. 32, no. 9, pp. 1428–31, 2006.

[3] A. Louw, C. Cracco, C. Cerf, A. Harf, P. Duvaldestin, F. Lemaire, and L. Brochard, "Accuracy of pulse oximetry in the intensive care unit," *Intensive Care Medicine*, vol. 27, no. 10, pp. 1606–1613, 2001.

[4] H. Gehring, C. Hornberger, and H. Matz, "The effects of motion artifact and low perfusion on the performance of a new generation of pulse oximeters in volunteers undergoing hypoxemia," *Respiratory care*, vol. 47, no. 1, pp. 48–60, 2002.

[5] A. Boussuges, P. Rossi, M. Gouitaa, and E. Nussbaum, "Alterations in the peripheral circulation in COPD patients," *Clinical Physiology and Functional Imaging*, vol. 27, no. 5, pp. 284–290, 2007.

[6] A. M. Yañez, D. Guerrero, R. Pérez de Alejo, F. Garcia-Rio, J. L. Alvarez-Sala, M. Calle-Rubio, R. M. de Molina, M. Valle Falcones, P. Ussetti, J. Sauleda, E. Z. García, J. M. Rodríguez-González-Moro, M. Franco Gay, M. Torrent, and A. Agustí, "Monitoring Breathing Rate at Home Allows Early Identification of COPD Exacerbations," *Chest*, vol. 142, no. 6, pp. 1524–1529, 2012.

[7] K. H. Groenewegen, A. M. Schols, and E. F. Wouters, "Mortality and Mortality-Related Factors After Hospitalization for Acute Exacerbation of COPD*," *Chest*, vol. 124, no. 2, pp. 459–467, 2003.

[8] M. E. R. F. V. J. Eriksen N., Hansen E.F., "Chronic obstructive pulmonary disease. Admission, course and prognosis," *Ugeskr. Laeger*, vol. 165, no. 37, pp. 3449–502, 2003.

[9] S. C. Gandevia and D. K. McKenzie, "Respiratory rate: the neglected vital sign.," *The Medical journal of Australia*, vol. 189, no. 9, p. 532, 2008.

[10] S. B. Duun, R. G. Haahr, K. Birkelund, and E. V. Thomsen, "A ring-shaped photodiode designed for use in a reflectance pulse oximetry sensor in wireless health monitoring applications," *IEEE Sensors Journal*, vol. 10, no. 2, pp. 261–268, 2010.

[11] M. H. Crawford, S. J. Bernstein, P. C. Deedwania, J. P. DiMarco, K. J. Ferrick, A. Garson, L. A. Green, H. L. Greene, M. J. Silka, P. H. Stone, C. M. Tracy, R. J. Gibbons, J. S. Alpert, K. A. Eagle, T. J. Gardner, A. Garson, G. Gregoratos, R. O. Russell, T. J. Ryan, and S. C. Smith, "ACC/AHA Guidelines for Ambulatory Electrocardiography: Executive Summary and Recommendations : A Report of the American College of Cardiology/American Heart Association Task Force on Practice Guidelines (Committee to Revise the Guidelines for Ambulatory E," *Circulation*, vol. 100, no. 8, pp. 886–893, 1999.

[12] R. E. Klabunde, *Cardiovascular Physiology Concepts*, p. 256. Lippincott Williams & Wilkins, 2 ed., 2011.

[13] J. G. Webster, *Design of Pulse Oximeters*. CRC Press, 1997.

[14] P. R. Mathieu Lemay, Mattia Bertschi, Josep Sola, Jakub Parak, and I. Korhonen, "Application of Optical Heart Rate Monitoring," in *Wearable Sensors: Fundamentals, Implementation and Applications*, ch. 2.3, pp. 105–133, 1 ed., 2014.

[15] J. Allen, "Photoplethysmography and its application in clinical physiological measurement.," *Physiological measurement*, vol. 28, pp. R1–39, Mar. 2007.

[16] F. Scholkmann, S. Kleiser, A. J. Metz, R. Zimmermann, J. Mata Pavia, U. Wolf, and M. Wolf, "A review on continuous wave functional near-infrared spectroscopy and imaging instrumentation and methodology," *NeuroImage*, vol. 85, pp. 6–27, 2014.

[17] T. Tamura, Y. Maeda, M. Sekine, and M. Yoshida, "Wearable Photoplethysmographic Sensors—Past and Present," *Electronics*, vol. 3, no. 2, pp. 282–302, 2014.

[18] J. T. Moyle, *Pulse Oximetry*, p. 182. BMJ Books, 2 ed., 2002.

[19] M. Nogawa, T. Kaiwa, and S. Takatani, "A novel hybrid reflectance pulse oximeter sensor with improved\nlinearity and general applicability to various portions of the body," *Proceedings of the 20th Annual International Conference of the IEEE Engineering in Medicine and Biology Society. Vol.20 Biomedical Engineering Towards the Year 2000 and Beyond (Cat. No.98CH36286)*, vol. 4, no. 4, pp. 1858–1861, 1998.

[20] R. Vetter, L. Rossini, A. Ridolfi, J. Sola, O. Chetelat, M. Correvon, J. Krauss, O. Dossel, and W. C. Schlegel, "Frequency domain spo2 estimation based on multichannel photoplethysmographic measurements at the sternum," vol. 25, pp. 326–329, 2009.

[21] C. Schreiner, P. Catherwood, J. Anderson, and J. McLaughlin, "Blood oxygen level measurement with a chest-based Pulse Oximetry prototype system," *Computers in Cardiology*, vol. 37, pp. 537–540, 2010.

[22] K. H. Shelley, D. H. Jablonka, A. a. Awad, R. G. Stout, H. Rezkanna, and D. G. Silverman, "What Is the Best Site for Measuring the Effect of Ventilation on the Pulse Oximeter Waveform?," *Anesthesia & Analgesia*, vol. 103, no. 2, pp. 372–377, 2006.

[23] P. Leonard, T. F. Beattie, P. S. Addison, and J. N. Watson, "Standard pulse oximeters can be used to monitor respiratory rate.," *Emergency medicine journal : EMJ*, vol. 20, no. 6, pp. 524–5, 2003.

[24] D. Clifton, J. G. Douglas, P. S. Addison, and J. N. Watson, "Measurement Of Respiratory Rate From the Photoplethysmogram In Chest Clinic Patients," *Journal of Clinical Monitoring and Computing*, vol. 21, no. 1, pp. 55–61, 2007.

[25] L. G. Lindberg, H. Ugnell, and P. Å. Öberg, "Monitoring of respiratory and heart rates using a fibre-optic sensor," *Medical & Biological Engineering & Computing*, vol. 30, no. 5, pp. 533–537, 1992.

[26] "Combined photoplethysmographic monitoring of respiration rate and pulse: a comparison between different measurement sites in spontaneously breathing subjects," *Acta Anaesthesiologica Scandinavica*, vol. 51, no. 9, pp. 1250–7, 2007.

[27] H. Kronberg and H. Leist, "Apparatus and method for monitoring respiration," 1997. US Patent 5,273,036.

[28] V. König, R. Huch, and A. Huch, "Reflectance Pulse Oximetry – Principles and Obstetric Application in the Zurich System," *The Journal of Clinical Monitoring and Computing*, vol. 14, no. 6, pp. 403–412, 1998.

[29] Y. Mendelson, R. M. Lewinsky, and Y. Wasserman, "Multi-wavelength reflectance pulse oximetry.," *Anesthesia and analgesia*, vol. 94, no. 1, pp. 26–30, 2002.

[30] Y. Mendelson and M. McGinn, "Skin reflectance pulse oximetry: In vivo measurements from the forearm and calf," *Journal of Clinical Monitoring and Computing*, vol. 7, no. 1, pp. 7–12, 1991.

[31] M. Vegfors, H. Ugnell, B. Hök, P. a. Oberg, and C. Lennmarken, "Experimental evaluation of two new sensors for respiratory rate monitoring.," *Physiological measurement*, vol. 14, no. 2, pp. 171–81, 1993.

[32] a. Johansson and P. a. Oberg, "Estimation of respiratory volumes from the photoplethysmographic signal. Part I: Experimental results.," *Medical & biological engineering & computing*, vol. 37, no. 1, pp. 42–7, 1999.

[33] a. Johansson and P. Å. Öberg, "Estimation of respiratory volumes from the photoplethysmographic signal. Part 2: a model study," *Medical & Biological Engineering & Computing*, vol. 37, no. 1, pp. 48–53, 1999.

[34] L. Nilsson, A. Johansson, and S. Kalman, "Respiratory variations in the reflection mode photoplethysmographic signal. Relationships to peripheral venous pressure," *Medical & Biological Engineering & Computing*, vol. 41, no. 3, pp. 249–254, 2003.

[35] L. Nilsson, A. Johansson, and S. Kalman, "Macrocirculation is not the sole determinant of respiratory induced variations in the reflection mode photoplethysmographic signal.," *Physiological measurement*, vol. 24, no. 4, pp. 925–37, 2003.

[36] Y. Mendelson, J. C. Kent, B. L. Yocum, and M. J. Birle, "Design and evaluation of a new reflectance pulse oximeter sensor.," *Medical instrumentation*, vol. 22, pp. 167–73, aug 1988.

[37] L. Nilsson, A. Johansson, and S. Kalman, "Respiration can be monitored by photoplethysmography with high sensitivity and specificity regardless of anaesthesia and ventilatory mode," *Acta Anaesthesiologica Scandinavica*, vol. 49, no. 8, pp. 1157–1162, 2005.

[38] A. Camm, M. Malik, J. Bigger, and G. Breithardt, "Heart rate variability. Standards of measurement, physiological interpretation, and clinical use. Task Force of the European Society of Cardiology and the North American Society of Pacing and Electrophysiology.," *European heart journal*, vol. 17, no. 3, pp. 354–81, 1996.

[39] "A comparative study of pulse rate variability and heart rate variability in healthy subjects," *Journal of Clinical Monitoring and Computing*, vol. 26, no. 2, pp. 107–114, 2012.

[40] J. Pan and W. J. Tompkins, "A real-time QRS detection algorithm.," *IEEE transactions on bio-medical engineering*, vol. 32, no. 3, pp. 230–6, 1985.

[41] A. Schäfer and J. Vagedes, "How accurate is pulse rate variability as an estimate of heart rate variability? A review on studies comparing photoplethysmographic technology with an electrocardiogram.," *International journal of cardiology*, vol. 166, no. 1, pp. 15–29, 2013.

[42] W. New and J. Corenman, "Calibrated optical oximeter probe," 1987. US Patent 4,700,708. 33.

[43] H. Secker, "Sensor, apparatus and method for non-invasive measurement of oxygen saturation," 1993. US Patent 5,188,108.

[44] S. Takatani, H. Noda, H. Takano, and T. Akutsu, "A miniature hybrid reflection type optical sensor for measurement of hemoglobin content and oxygen saturation of whole blood," *IEEE Transactions on Biomedical Engineering*, vol. 35, no. 3, pp. 187–198, 1988.

[45] P. Mannheimer, "Isolated layer pulse oximetry," 1998. US Patent 5,746,206.3.

[46] a. C. M. Dassel, R. Graaff, M. Sikkema, A. Meijer, W. G. Zijlstra, and J. G. Aarnoudse, "Reflectance pulse oximetry at the forehead improves by pressure on the probe," *Journal of Clinical Monitoring*, vol. 11, no. 4, pp. 237–244, 1995.

[47] Y. Mendelson and B. D. Ochs, "Noninvasive pulse oximetry utilizing skin reflectance photoplethysmography.," *IEEE transactions on bio-medical engineering*, vol. 35, no. 10, pp. 798–805, 1988.

[48] Y. Mendelson, C. Pujary, and M. Savage, "Minimization of led power consumption in the design of a wearable pulse oximeter," *Proceedings of the Iasted International Conference on Biomedical Engineering, Proc. Iasted Internat. Conf. Biomed. Eng*, pp. 249–254, 2003.

[49] S. Takatani, C. Davies, N. Sakakibara, A. Zurick, E. Kraenzler, L. R. Golding, G. P. Noon, Y. Nose, and M. E. DeBakey, "Experimental and clinical evaluation of a noninvasive reflectance pulse oximeter sensor.," *Journal of clinical monitoring*, vol. 8, no. 4, pp. 257–66, 1992.

[50] J. Solà, O. Chételat, C. Sartori, Y. Allemann, and S. F. Rimoldi, "Chest pulse-wave velocity: a novel approach to assess arterial stiffness.," *IEEE transactions on bio-medical engineering*, vol. 58, no. 1, pp. 215–23, 2011.

[51] G. S. Agashe, J. Coakley, and P. D. Mannheimer, "Forehead Pulse Oximetry," *Anesthesiology*, vol. 105, no. 6, pp. 1111–1116, 2006.

[52] S. Takatani and J. Ling, "Optical oximetry sensors for whole blood and tissue," *IEEE Engineering in Medicine and Biology Magazine*, vol. 13, no. 3, pp. 347–357, 1994.

[53] M. Hickey and P. A. Kyriacou, "Optimal spacing between transmitting and receiving optical fibres in reflectance pulse oximetry," *Journal of Physics: Conference Series*, vol. 85, p. 012030, 2007.

[54] Y. Mendelson and C. Pujary, "Measurement site and photodetector size considerations in optimizing power consumption of a wearable reflectance pulse oximeter," in *Proceedings of the 25th Annual International Conference of the IEEE Engineering in Medicine and Biology Society (IEEE Cat. No.03CH37439)*, vol. 4, pp. 3016–3019, IEEE, 2003.

[55] A. C. M. Dassel, R. Graaff, A. Meijer, W. G. Zijlstra, and J. G. Aarnoudse, "Reflectance pulse oximetry at the forehead of newborns: The influence of varying pressure on the probe," *Journal of Clinical Monitoring*, vol. 12, no. 6, pp. 421–428, 1996.

[56] X. F. Teng and Y. T. Zhang, "The effect of contacting force on photoplethysmographic signals," *Physiological Measurement*, vol. 25, no. 5, pp. 1323–1335, 2004.

[57] J. Spigulis, "Optical noninvasive monitoring of skin blood pulsations," *Applied Optics*, vol. 44, no. 10, p. 1850, 2005.

[58] R. P. Dresher and Y. Mendelson, "Reflectance Forehead Pulse Oximetry: Effects of Contact Pressure During Walking," *International Conference of the IEEE Engineering in Medicine and Biology Society*, vol. 1, pp. 3529–3532, 2006.

[59] H. Ding, J. Q. Lu, W. a. Wooden, P. J. Kragel, and X.-H. Hu, "Refractive indices of human skin tissues at eight wavelengths and estimated dispersion relations between 300 and 1600 nm," *Physics in Medicine and Biology*, vol. 51, no. 6, pp. 1479–1489, 2006.

[60] S. Ghoochan, "Investigation of Signals Measured From a Sternal Photoplethysmographic Sensor: The Effect of Pressure, Coupling Media and Attachment Method," *Technical University of Denmark, Department of Micro- and Nanotechnology, M.Sc Thesis*, 2015.

[61] R. M. Tobin, J. a. Pologe, and P. B. Batchelder, "A characterization of motion affecting pulse oximetry in 350 patients.," *Anesthesia and analgesia*, vol. 94, no. 1, pp. S54–61, 2002.

[62] J. Lee, W. Jung, I. Kang, Y. Kim, and G. Lee, "Design of filter to reject motion artifact of pulse oximetry," *Computer Standards & Interfaces*, vol. 26, no. 3, pp. 241–249, 2004.

[63] H. Asada, Hong-Hui Jiang, and P. Gibbs, "Active noise cancellation using MEMS accelerometers for motion-tolerant wearable bio-sensors," 2004.

[64] T. Guo, Z. Cao, Z. Zhang, D. Li, and M. Yu, "Reflective oxygen saturation monitoring at hypothenar and its validation by human hypoxia experiment," *BioMedical Engineering OnLine*, vol. 14, no. 1, p. 76, 2015.

[65] B. Venema, N. Blanik, V. Blazek, H. Gehring, A. Opp, and S. Leonhardt, "Advances in Reflective Oxygen Saturation Monitoring With a Novel In-Ear Sensor System: Results of a Human Hypoxia Study," *IEEE Transactions on Biomedical Engineering*, vol. 59, no. 7, pp. 2003–2010, 2012.

[66] L. Wang, B. P. Lo, and G.-Z. Yang, "Multichannel Reflective PPG Earpiece Sensor With Passive Motion Cancellation," *IEEE Transactions on Biomedical Circuits and Systems*, vol. 1, no. 4, pp. 235–241, 2007.

[67] C. Baker, E. Karst, and C. Hoarau, "Pulse oximetry signal correction using near infrared absorption by water," 2012. US Patent 8,175,670.

[68] T. Rusch, R. Sankar, and J. Scharf, "Signal processing methods for pulse oximetry," *Computers in Biology and Medicine*, vol. 26, no. 2, pp. 143–159, 1996.

[69] M. Diab, "Systems and methods for determining blood oxygen saturation values using complex number encoding," 2006. US Patent App. 11/288,812.

[70] B. Kim and S. Yoo, "Motion Artifact Reduction in Photoplethysmography Using Independent Component Analysis," *IEEE Transactions on Biomedical Engineering*, vol. 53, no. 3, pp. 566–568, 2006.

[71] J. Foo, "Use of Independent Component Analysis to Reduce Motion Artifact in Pulse Transit Time Measurement," *IEEE Signal Processing Letters*, vol. 15, pp. 124–126, 2008.

[72] T. Jensen, S. Duun, J. Larsen, R. Haahr, M. Toft, B. Belhage, and E. Thomsen, "Independent component analysis applied to pulse oximetry in the estimation of the arterial oxygen saturation - a comparative study," 2009.

[73] J. Graybeal and M. Petterson, "Adaptive filtering and alternative calculations revolutionizes pulse oximetry sensitivity and specificity during motion and low perfusion," *The 26th Annual International Conference of the IEEE Engineering in Medicine and Biology Society*, vol. 4, pp. 5363–5366, 2004.

[74] I. Fine and A. Weinreb, "Multiple scattering effect in transmission pulse oximetry," *Medical & Biological Engineering & Computing*, vol. 33, no. 5, pp. 709–712, 1995.

[75] L. Nilsson, T. Goscinski, A. Johansson, L.-G. Lindberg, and S. Kalman, "Age and Gender Do Not Influence the Ability to Detect Respiration by Photoplethysmography," *Journal of Clinical Monitoring and Computing*, vol. 20, no. 6, pp. 431–436, 2006.

[76] D. Barschdorff and Wei Zhang, "Respiratory rhythm detection with photoplethysmographic methods," *Proceedings of 16th Annual International Conference of the IEEE Engineering in Medicine and Biology Society*, pp. 912–913, 1994.

[77] W. Johnston and Y. Mendelson, "Extracting breathing rate information from a wearable reflectance pulse oximeter sensor," *The 26th Annual International Conference of the IEEE Engineering in Medicine and Biology Society*, vol. 4, pp. 5388–5391, 2004.

[78] P. S. Addison, J. N. Watson, M. L. Mestek, J. P. Ochs, A. a. Uribe, and S. D. Bergese, "Pulse oximetry-derived respiratory rate in general care floor patients," *Journal of Clinical Monitoring and Computing*, vol. 29, no. 1, pp. 113–120, 2015.

[79] S. Fleming and L. Tarassenko, "A comparison of signal processing techniques for the extraction of breathing rate from the photoplethysmogram," *International Journal of Biological and Life Sciences*, vol. 2, no. 4, pp. 233–237, 2007.

[80] M. Folke, L. Cernerud, M. Ekstrom, and B. Hok, "Critical review of non-invasive respiratory monitoring in medical care.," *Medical & biological engineering & computing*, vol. 41, no. 4, pp. 377–83, 2003.

[81] W. LIM, S. CARTY, J. MACFARLANE, R. ANTHONY, J. CHRISTIAN, K. DAKIN, and P. DENNIS, "Respiratory rate measurement in adults—how reliable is it?," *Respiratory Medicine*, vol. 96, no. 1, pp. 31–33, 2002.

[82] M. Diab, E. Kiani-Azarbayjany, I. Elfadel, R. McCarthy, W. Weber, and R. Smith, "Signal processing apparatus," 1997. US Patent 5,632,272.

[83] K. O. Hadeli, E. M. Siegel, D. L. Sherrill, K. C. Beck, and P. L. Enright, "Predictors of Oxygen Desaturation During Submaximal Exercise in 8,000 Patients," *Chest*, vol. 120, no. 1, pp. 88–92, 2001.

[84] E. Crisafulli, A. Iattoni, E. Venturelli, G. Siscaro, C. Beneventi, A. Cesario, and E. M. Clini, "Predicting Walking-Induced Oxygen Desaturations in COPD Patients: A Statistical Model," *Respiratory Care*, vol. 58, no. 9, pp. 1495–1503, 2013.

[85] M.-L. Chuang, I.-F. Lin, and S.-P. Chen, "Kinetics of Changes in Oxyhemoglobin Saturation During Walking and Cycling Tests in COPD," *Respiratory Care*, vol. 59, no. 3, pp. 353–362, 2014.

APPENDIX

A

APPENDIX: DATA OF STUDY III

A.1 Long-Term S_pO_2

The effect of the reliability during the recording is shown when using different values of the ΔS_pO_2 criteria. Fig. A.1a shows a box-plot of the percentage of the reliable S_pO_2 levels (uptime) during a recording when the ΔS_pO_2 criteria is set to 3 $\%$, 4 $\%$, and 5 $\%$ respectively for the patient group. In this case the accelerometer criteria is not included. Correspondingly, the RMSE values is shown in Fig. A.1b. It is seen how the uptime increases when larger ΔS_pO_2 is allowed. Whereas the RMSE value does not have a remarkable increase. However, the interquartile range decreased remarkably, which means less variability in RMSE when higher ΔS_pO_2 is used. As for the group of healthy subjects the $\Delta S_pO_2 \geqslant 2$ $\%$ is added to the plots shown in Fig. A.2a and b. Clearly it is seen how the uptime increase with larger ΔS_pO_2.

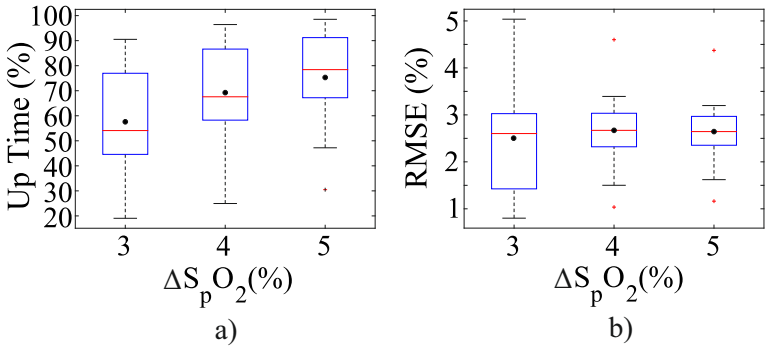

Figure A.1: (a) Shows the percentage of reliable S_pO_2 values (uptime) of all the recordings from the patients, when using all the conditions except the accelerometer condition. The red line corresponds to the median value and the dot corresponds to the mean value. (b) Shows the RMSE between the reliable S_pO_2 values and the calculated reference.

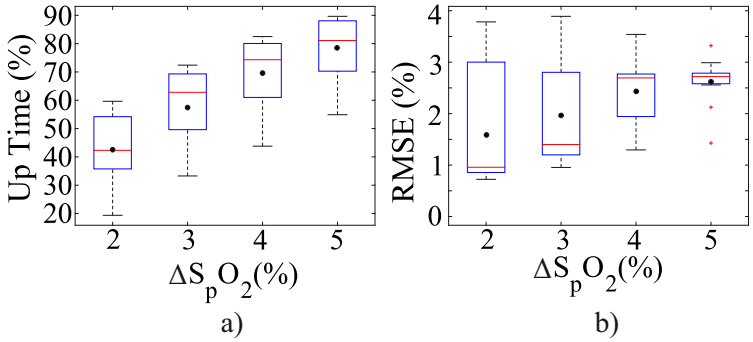

Figure A.2: (a) Shows the percentage of reliable S_pO_2 values (uptime) of all the recordings from the healthy participants, when using all the conditions except the accelerometer condition. (b) Shows the RMSE between the reliable S_pO_2 values and the calculated reference. The red line corresponds to the median value and the dot corresponds to the mean value.

APPENDIX

B

APPENDIX: DATASHEETS

Silicon PIN Photodiode

VBP104S

VBP104SR

FEATURES

- Package type: surface mount
- Package form: GW, RGW
- Dimensions (L x W x H in mm): 6.4 x 3.9 x 1.2
- Radiant sensitive area (in mm^2): 4.4
- High photo sensitivity
- High radiant sensitivity
- Suitable for visible and near infrared radiation
- Fast response times
- Angle of half sensitivity: $\varphi = \pm 65°$
- Floor life: 168 h, MSL 3, acc. J-STD-020
- Lead (Pb)-free reflow soldering
- Compliant to RoHS Directive 2002/95/EC and in accordance to WEEE 2002/96/EC
- Halogen-free according to IEC 61249-2-21 definition

Pb-free

e3

RoHS COMPLIANT

HALOGEN FREE

DESCRIPTION

VBP104S and VBP104SR are high speed and high sensitive PIN photodiodes. It is a surface mount device (SMD) including the chip with a 4.4 mm^2 sensitive area detecting visible and near infrared radiation.

APPLICATIONS

- High speed photo detector

PRODUCT SUMMARY			
COMPONENT	I_{ra} (µA)	φ (deg)	$\lambda_{0.1}$ (nm)
VBP104S	35	± 65	430 to 1100
VBP104SR	35	± 65	430 to 1100

Note

- Test conditions see table “Basic Characteristics”

ORDERING INFORMATION			
ORDERING CODE	PACKAGING	REMARKS	PACKAGE FORM
VBP104S	Tape and reel	MOQ: 1000 pcs, 1000 pcs/reel	Gullwing
VBP104SR	Tape and reel	MOQ: 1000 pcs, 1000 pcs/reel	Reverse gullwing

Note

- MOQ: minimum order quantity

ABSOLUTE MAXIMUM RATINGS (T_{amb} = 25 °C, unless otherwise specified)				
PARAMETER	TEST CONDITION	SYMBOL	VALUE	UNIT
Reverse voltage		V_R	60	V
Power dissipation	$T_{amb} \leq 25$ °C	P_V	215	mW
Junction temperature		T_j	100	°C
Operating temperature range		T_{amb}	- 40 to + 100	°C
Storage temperature range		T_{stg}	- 40 to + 100	°C
Soldering temperature	Acc. reflow solder profile fig. 8	T_{sd}	260	°C
Thermal resistance junction/ambient		R_{thJA}	350	K/W

Burr-Brown Products from Texas Instruments

OPA381
OPA2381

SBOS313B − AUGUST 2004 − REVISED NOVEMBER 2004

Precision, Low Power, 18MHz Transimpedance Amplifier

FEATURES

- **OVER 250kHz TRANSIMPEDANCE BANDWIDTH**
- **DYNAMIC RANGE: 5 Decades**
- **EXCELLENT LONG-TERM STABILITY**
- **LOW VOLTAGE NOISE: 10nV/$\sqrt{Hz}$**
- **BIAS CURRENT: 3pA**
- **OFFSET VOLTAGE: 25μV (max)**
- **OFFSET DRIFT: 0.1μV/°C (max)**
- **GAIN BANDWIDTH: 18MHz**
- **QUIESCENT CURRENT: 800μA**
- **FAST OVERLOAD RECOVERY**
- **SUPPLY RANGE: 2.7V to 5.5V**
- **SINGLE AND DUAL VERSIONS**
- ***Micro*PACKAGE: DFN-8, MSOP-8**

APPLICATIONS

- **PRECISION I/V CONVERSION**
- **PHOTODIODE MONITORING**
- **OPTICAL AMPLIFIERS**
- **CAT-SCANNER FRONT-END**
- **PHOTO LAB EQUIPMENT**

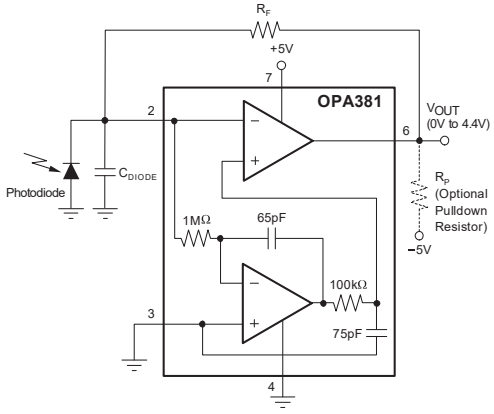

DESCRIPTION

The OPA381 family of transimpedance amplifiers provides 18MHz of Gain Bandwidth (GBW), with extremely high precision, excellent long-term stability, and very low 1/f noise. The OPA381 features an offset voltage of 25μV (max), offset drift of 0.1μV/°C (max), and bias current of 3pA. The OPA381 far exceeds the offset, drift, and noise performance that conventional JFET op amps provide.

The signal bandwidth of a transimpedance amplifier depends largely on the GBW of the amplifier and the parasitic capacitance of the photodiode, as well as the feedback resistor. The 18MHz GBW of the OPA381 enables a transimpedance bandwidth of > 250kHz in most configurations. The OPA381 is ideally suited for fast control loops for power level measurement on an optical fiber.

As a result of the high precision and low-noise characteristics of the OPA381, a dynamic range of 5 decades can be achieved. This capability allows the measurement of signal currents on the order of 10nA, and up to 1mA in a single I/V conversion stage. In contrast to logarithmic amplifiers, the OPA381 provides very wide bandwidth throughout the full dynamic range. By using an external pulldown resistor to –5V, the output voltage range can be extended to include 0V.

The OPA381 and OPA2381 are both available in MSOP-8 and DFN-8 (3mm x 3mm) packages. They are specified from –40°C to +125°C.

OPA381 RELATED DEVICES

PRODUCT	FEATURES
OPA380	90MHz GBW, 2.7V to 5.5V Supply Transimpedance Amplifier
OPA132	16MHz GBW, Precision FET Op Amp ±15V
OPA300	150MHz GBW, Low-Noise, 2.7V to 5.5V Supply
OPA335	10μV V_{OS}, Zero-Drift, 2.5V to 5V Supply
OPA350	500μV V_{OS}, 38MHz, 2.5V to 5V Supply
OPA354	100MHz GBW CMOS, RRIO, 2.5V to 5V Supply
OPA355	200MHz GBW CMOS, 2.5V to 5V Supply
OPA656/7	230MHz, Precision FET, ±5V

EPO-TEK® 302-3M

Technical Data Sheet

For Reference Only

Optically Transparent Epoxy

Number of Components	Two
Mi Ratio By eight	100 4
Specific ravity	
Part A	1.20
Part B	0. 6
Pot Life	1 our
Shelf Life	One year at room temperature

Minimum Bond Line Cure Schedule	
6 C	3 ours
23 C	24 ours

*Note: Container(s) should be kept closed when not in use. *Please see Applications Note available on our website.*
- TOTAL MASS SHOULD NOT EXCEED 25 GRAMS -

Product Description:

EPO TE 302 3M is a two component epo y used for optical, medical, fiber optic, and semiconductor applications. The epo y is good for adhesive oining, sealing, potting, or as a coating.

EPO-TEK® 302-3M Advantages & Application Notes:

- Low viscosity, clear and colorless epo y is well suited for potting applications, and for transmitting IS or NIR light in opto circuits.
- E cellent water, chemical, and solvent resistant properties including 10 nitric acid, acetone, he ane, and dicholormethane.
- Suggested Applications
  - Fiber Optic Optical
    - Potting and encapsulation lens and prism bonding for Scientific OEM instruments LED encapsulant.
    - Transmission in the IS NIR range from 3 0 – 1 0 nm. Can be used in the optical pathway.
    - Potting or sealing the fiber into the snout of the opto pac age.
    - Adhesive for groove, fiber arrays or lens arrays.
    - Bonding optical fibers into ferrules. Fibers of glass or plastic. Ferrules of glass, uart , stainless steel, ovar, or ceramic.
  - Semiconductor
    - Recommended for underfilling of flip chips or SMDs on PCB can also be used for COB glob top process using a DAM FILL method can resist 8 8 moisture soa s, as well as Tcycles and Tshoc s.
  - Medical
    - ic ing into fiber optic bundles for endoscopes or light guides very good autoclave resistance.
    - Adhesion to stainless steel metal, ceramic, titanium and most plastics.
    - SP Class I bio compatible.
- Passes NASA low outgassing standard ASTM E with proper cure http outgassing.nasa.gov
- This product has been tested and satisfies low halogen re uirements.

Typical Properties: ***(To be used as a guide only, not as a specification. Data below is not guaranteed. Different batches, conditions and applications yield differing results; Cure condition: varies as required; * denotes test on lot acceptance basis)***

Physical Properties:	
***Color:** **Part A:** Clear Colorless **Part B:** Clear Colorless	**Weight Loss:**
***Consistency:** Pourable Li uid	**@ 200°C:**
***Viscosity (@ 100 RPM/23°C):** 800 – 1,600 cPs	**@ 250°C:** 0.
Thixotropic Index: N A	**@ 300°C:** 1.22
***Glass Transition Temp.(Tg):** ≥ C Dynamic Cure 20—200 C ISO 2 Min Ramp 10—200 C 20 C Min	**Operating Temp:** **Continuous:** C to 1 C **Intermittent:** C to 2 0 C
Coefficient of Thermal Expansion (CTE):	**Storage Modulus @ 23°C:** 2 1, 32 psi
Below Tg: 6 10^{6} in in C	**Ions:** Cl^- 42 ppm
Above Tg: 1 3 10^{6} in in C	Na^+ 10 ppm
Shore D Hardness: 80	NH_4^+ 1 ppm
Lap Shear Strength @ 23°C: 2,000 psi	K^+ 4 ppm
Die Shear Strength @ 23°C: ≥ 10 g 3,400 psi	***Particle Size:** N A
Degradation Temp. (TGA): 3 1 C	
Optical Properties @ 23°C:	
Refractive Index @ 23°C (uncured): 1. 446 8 nm	**Spectral Transmission:** 460 1620 nm
Electrical & Thermal Properties:	
Thermal Conductivity: N A	**Volume Resistivity @ 23°C:** ≥ 1 10^{13} Ohm cm
Dielectric Constant (1KHz): 3.3	**Dissipation Factor (1KHz):** 0.0061

EPOXY TECHNOLOGY, INC.
14 Fortune Drive, Billerica, MA 01821 3 2 **Phone** 8.66 .380 **Fax** 8.663. 82
www.EPOTE .com

Epoxies and Adhesives for Demanding Applications™

Rev. III
Apr 2010

PAPER I

TITLE Sternal pulse rate variability compared with heart rate variability on healthy subjects

AUTHORS Shadi S. Chreiteh, Bo Belhage, Karsten Hoppe, Jens Branebjerg, and Erik V. Thomsen

JOURNAL Engineering in Medicine and Biology Society (EMBC), 2014 Annual International Conference of the IEEE

PUBLICATION HISTORY Published in August 2014.

Sternal Pulse Rate Variability Compared with Heart Rate Variability on Healthy Subjects

Shadi S. Chreiteh, Bo Belhage, Karsten Hoppe, Jens Branebjerg, and Erik V. Thomsen

Abstract— **The heart rate variability (HRV) is a commonly used method to quantify the sympathetic and the parasympathetic modulation of the heart rate. HRV is mainly conducted on electrocardiograms (ECG). However, the use of photoplethysmography (PPG) as a marker of the autonomic tone is emerging. In this study we investigated the feasibility of deriving pulse rate variability (PRV) using PPG signals recorded by a reflectance PPG sensor attached to the chest bone (sternum) and comparing it to HRV. The recordings were conducted on 9 healthy subjects being in a relaxed supine position and under forced respiration, where the subjects were asked to breathe following a visual scale with a rate of 27 breaths/min.**
HRV parameters such as the mean intervals (meanNN), the standard deviation of intervals (SDNN), the root mean square of difference of successive intervals (RMSSD), and the proportion of intervals differing more than 50 ms (pNN50) were calculated from the R peak-to-R peak (R-R) and pulse-to-pulse (P-P) intervals. In the frequency domain the low and high frequency ratio of the power spectral density (LF/HF) was also computed. The Pearson correlation coefficient showed significant correlation for all the parameters ($r > 0.95$ with $p < 0.001$) and the Bland-Altmann analysis showed close agreement between the two methods for all the parameters during resting and forced respiration condition. Thus, PRV analysis using sternal PPG can be an alternative to HRV analysis on healthy subjects at rest.

I. INTRODUCTION

The heart rate variability (HRV) obtained from electrocardiographic (ECG) recordings is a commonly used method that reflects the balance between sympathetic and parasympathetic modulation of the heart rate [1]. HRV is used in many clinical areas especially in the research of diabetes, cardiovascular diseases, and stress management [1]. Predominance of sympathetic activity and reduced parasympathetic cardiac control have been seen in patients with acute myocardial infarction [2]. As a complication of diabetes mellitus, autonomic neuropathy occurs and this often affects the autonomic control of the heart. Pontet et al. [3] reported that a depressed autonomic modulation may be an early indication of deterioration of septic patients in the intensive care unit. This finding was confirmed by Barnaby et al. [4] and in addition they reported that HRV may predict significant morbidity and mortality rates for septic patients in the emergency department.

Currently, HRV parameters are derived by analysis of the temporal relationship between successive heart beats (R-R intervals) in the ECG signal. From these intervals we can compute time and frequency domain, and nonlinear dynamics analysis to extract features to assess the autonomic nervous system (ANS) modulation of the heart rate [1].

A wide range of studies have investigated the use of Photoplethysmography (PPG) to quantify the cardiac autonomic tone as an alternative to ECG. PPG is a low-cost noninvasive optical technique for monitoring beat to beat relative blood volume changes in the microvascular bed of peripheral tissues [5]. The PPG signal contains two components; a small pulsatile component (AC), which corresponds to arterial pulsations from the cardiac cycle. The AC component is superimposed onto a large quasi-DC component that relates to the optical character of the underlying tissue, the ambient light, and the average blood volume. The DC component also varies due to respiration [6]. The morphology of the PPG signal is useful for the study of autonomic control of the peripheral vascular tone [5]. In fact, Wong et al. [7] reported that the PPG signal might have an additional information in regards to cardiac autonomic tone compared to the ECG, because the peripheral vasculature is also modulated by the ANS. The physiological information derived from the R-R intervals can also be derived from the pulse-to-pulse (P-P) intervals of the PPG signal. Studies on pulse rate variability (PRV) have been conducted on the peripheral location of the body, mainly at the fingertip and the earlobe using a traditional pulse oximetry probe [8]. Lu et al. [9] have shown that PRV obtained from a finger can be used as surrogate for HRV. However, Wong et al. [7] reported the opposite finding and reported that it could be due to the pulse wave modification in the arterial system. Constant and colleagues [10] conducted a study on pulse wave recordings on the 3rd finger of the right hand, and showed that the PRV did not precisely reflect HRV in healthy subjects.

In the literature there is a lack of results about the influence of sensor location, when extracting HRV parameters using the PPG. However, Johnston et al. [11] and Schafer et al. [12] reported that an approach to place a PPG sensor on a more central location could be beneficial for the assessment of the cardiac autonomic tone. To our knowledge the PRV has not been investigated at the sternum. Thus, in this study we examine whether the PRV at the chest bone (sternum) can be used as a marker of the cardiac autonomic tone when

The study was supported by the Danish Business Innovation Fund, the Danish Ministry of Science, Innovation and Higher Education.

Shadi S. Chreiteh is with the Department of Micro- and Nanotechnology, Technical University of Denmark, 2800 Kgs. Lyngby, Denmark and also with DELTA Microelectronics, Venlighedsvej 4, 2970 Hørsholm, Denmark (e-mail: ssc@delta.dk).

Bo Belhage is with the Bispebjerg Hospital, University of Copenhagen, 2400 Copenhagen NV, Denmark.

Karsten Hoppe and Jens Branebjerg are with DELTA Microelectronics, Venlighedsvej 4, 2970 Hørsholm, Denmark.

Erik V. Thomsen is with the Department of Micro- and Nanotechnology, Technical University of Denmark, 2800 Kgs. Lyngby, Denmark.

978-1-4244-7929-0/14/$26.00 ©2014 IEEE

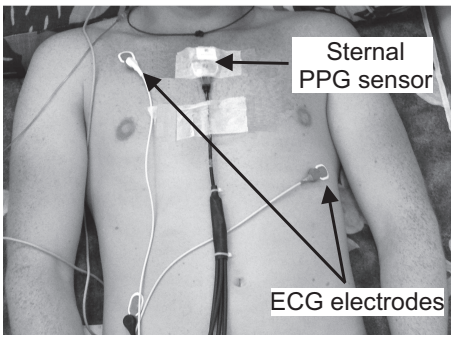

Fig. 1. Placement of the PPG sensor on the sternum. For this controlled experiment the sensor is positioned using adhesive tape.

comparing to traditional HRV in healthy subjects at rest and under paced respiration.

II. Methods & Materials

A. Data acquisition

A group of 9 healthy volunteers (8 males, 1 female) with mean age of 41.1±11.7 years and a mean Body Mass Index of 24.7±3.2 kg/m^2 were recruited for this preliminary study. The Danish Law and the Helsinki Declaration does not require a clinical protocol for this setup. The room temperature was $20-22\,^{\circ}\mathrm{C}$. A novel infrared reflective PPG prototype sensor was used to obtain the PPG signals. The sensor was positioned on the skin over the sternum with adhesive tape, cf. Fig 1. ECG electrodes were attached to the subject and used to record standard lead-II ECG signals. All analog signals were collected simultaneously and digitized with a sampling rate of 1000 Hz (Powerlab 8/35, 16 bit ADC, ADInstruments, USA) and stored on a laptop computer using Lab Chart 7 Pro (Lab Chart Version 7.3.7, ADInstruments, USA) as data acquisition software. For each subject being in supine position 10 min recordings has been conducted under natural respiration and under paced respiration frequency of 27 breaths/min. However, a 5 min segment of each recording was used for HRV analysis. The analysis was computed using MATLAB (MATLAB R2012b, The MathWorks, Inc., USA).

B. Heart rate and pulse rate analysis

Prior to the extraction of R-R and P-P intervals, the ECG signals were bandpass filtered using a second order Butterworth filter with cut-off frequencies of 0.05 Hz and 40 Hz. As for the PPG signals the cut-off frequencies were 0.05 Hz and 15 Hz. The QRS detection was performed using Pan and Tompkins QRS detection algorithm [13]. The R-R intervals were extracted from the located R peaks. As for the PPG signals, the systolic peaks were located using a custom made peak detection algorithm, cf. Fig. 2. The systolic peaks were then used to produce the P-P intervals. Fig. 3, shows a P-P and R-R interval from one of the subjects.

To compare the HRV and PRV methods, the commonly used time and frequency domain parameters were computed according to the standard definitions of HRV parameters [1]. As for the time domain parameters, the mean value of the R-R and P-P intervals (mean NN), the standard deviation of NN intervals (SDNN), the square root of the mean of the squares of differences between successive NN intervals (RMSSD), and the pNN50, which is the proportion of differences of successive intervals differing more than 50 ms was calculated. Prior to the frequency domain calculations the R-R and P-P intervals were resampled at 4 Hz and cubic spline interpolated [1]. From the power spectrum density the normalized low frequency (LF) power (0.04-0.15 Hz), the normalized high frequency (HF) power (0.15-0.4 Hz), and the LF/HF ratio has been computed. The time domain parameters are related mostly with the overall variability of the heart rate. The LF components represents the sympathetic and parasympathetic tones, while the HF components is more related to parasympathetic modulation.

C. Statistics

The Pearson correlation coefficient was used to correlate the calculated parameters derived from the ECG and PPG respectively. In addition the lower and the upper limits of agreement (LOA) and the mean system bias between the two methods is compared using a Bland-Altman analysis. Furthermore, the mean squared error is computed between the values of the HRV parameters derived from the R-R and P-P intervals.

III. Results

Fig. 2 shows a 10 seconds segment of a typical recording. The upper graph represents the PPG signal and the lower represents the ECG signal. Fig. 3, shows a time series of R-R and P-P intervals derived from the PPG and the ECG respectively. For all subjects the derived parameters obtained from PRV and HRV are represented in Table I. All the computed parameters derived from the PRV had correlation coefficients of $> 95\%$ (p <0.001) when compared to HRV. The error analysis showed insignificant differences between the parameters derived from the two methods (p <0.05). The Bland-Altmann analysis showed close agreement between the parameters derived from ECG and PPG. During natural respiration the average system bias for the mean NN interval was -0.03 ms and the lower and upper LOA was -0.561 ms and 0.501 ms respectively, cf. Fig. 4. As for the LF/HF ratio, the average system bias was -0.0064 ms and the lower and upper LOA was -0.27 ms and 0.25 ms respectively as seen in Fig. 5. Similarly, high degree of agreement was found for the rest of the parameters under natural respiration. During forced respiration the average system bias increased in the same direction for all parameters. It is also seen in Table I, that the LF/HF ratio increased from 1.045 to 2.99 for HRV and from 1.05 to 2.76 for PRV.

IV. Discussion

The results of this study clearly showed a close agreement between the HRV parameters derived from the PPG signals

TABLE I

THE TIME AND FREQUENCY DOMAIN PARAMETERS, CORRELATION COEFFICIENTS AND BLAND-ALTMANN ANALYSIS DERIVED FROM P-P AND R-R INTERVALS RESPECTIVELY.

	Parameters	HRV (Mean±SD)	PRV (Mean±SD)	Bias	Lower LOA	Upper LOA	Correlation coefficient	Absolute error
Natural respiration	*Time domain:*							
	Mean NN (ms)	1011.49±133.95	1011.52±133.86	-0.03	-0.56	0.5	0.999	0.000
	SDNN (ms)	63.25±34	63.43±34.58	-0.178	-2.50	2.15	0.999	0.0028
	RMSSD (ms)	50.51±41.23	50.64±41.58	-0.132	-5.79	5.53	0.998	0.0026
	pNN50 (%)	21.01±23.65	20.97±23.27	0.041	-5.86	5.94	0.993	0.0019
	Frequency domain:							
	LF/HF	1.045±0.61	1.05±0.65	-0.0064	-0.27	0.25	0.98	0.006
Forced respiration	*Time domain:*							
	Mean NN (ms)	953.34±111.86	953.48±112	-0.13	-1.35	1.07	0.999	0.000
	SDNN (ms)	51.68±23.6	54.74±23	-3.07	-9.09	2.96	0.992	0.056
	RMSSD (ms)	45.12±32.8	53.78±35.68	-8.65	-23.2	5.89	0.98	0.16
	pNN50 (%)	22.5±21.7	29.45±24.62	-6.93	8.83	-22.69	0.95	0.24
	Frequency domain:							
	LF/HF	2.99±1.86	2.76±1.68	0.23	-0.89	1.35	0.95	0.08

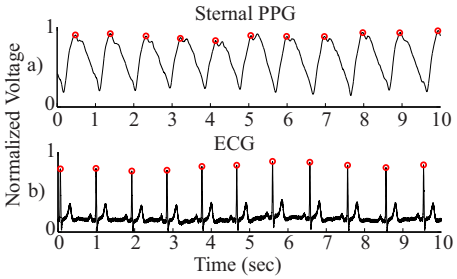

Fig. 2. A characteristic block of signals: (a) The sternal PPG signal. Note the signal waveform is inverted, upside deflection represents the systole. (b) the ECG signal. The circular markers corresponds to the detected peaks.

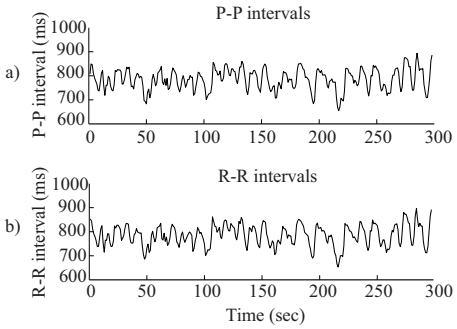

Fig. 3. Comparison of the (a) P-P interval derived from the sternal PPG signal and (b) R-R interval derived from the ECG signal.

and the ECG signals on a healthy group of subjects at rest and under forced respiration. Although, the average system bias increased between the parameters derived from PRV and HRV, the absolute values changed in the same direction as

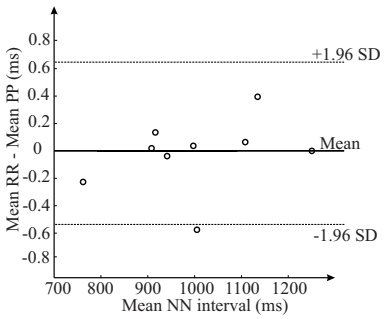

Fig. 4. Bland-Altman plot of the Mean NN derived from the sternal PPG signal and the Mean NN derived from the ECG signal. The majority of points are close to zero and within the 95% confidence interval showing a close agreement between the two methods.

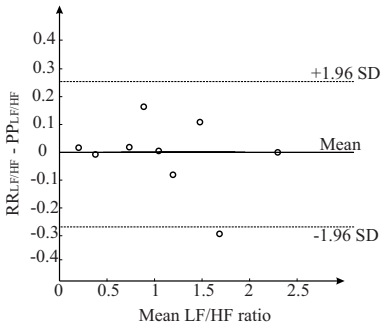

Fig. 5. Bland-Altman plot of the LF/HF ratio derived from the sternal PPG signal and the LF/HF ratio derived from the ECG signal. The majority of points are close to zero and within the 95% confidence interval showing a close agreement between the two methods.

seen in Table I. The LF/HF ratio derived from PRV increased during forced respiration, confirming that the change in the autonomic tone was also reflected in the PRV as it did in the HRV. The sternal PPG sensor is reliable for recording a PPG signal from, which HRV parameters can be derived, at least in healthy subjects at rest. The morphology of the PPG signal acquired at the sternum has also a clear systolic, end-diastolic and diacrotic notch as seen in Fig. 2. This might be useful for different types of pulse wave analysis since other clinically relevant features may be extracted. As explained in the introduction, recent studies have reported that the use of PPG recordings might be a more convenient method for the measurement of HRV in clinical environments and for ambulatory recordings than ECG. However, there has been a difference in the accuracy between the PRV derived from finger PPG and HRV both at rest and during physical and mental tasks [12]. Furthermore, there is a clear uncertainty regarding the measuring site [12].

We suggest that the reason behind the close agreement of both methods in our study is the proximal measuring site relative to the heart. This is in agreement with Johnson and Mendelson [11], who reported similar correlations between heart rate intervals derived from ECG and reflective forehead PPG. Our findings are also in agreement with [14], who reported high accuracy between the two methods when measuring on the earlobe. Although, the PPG also reflects the cardiac rhythm, the pulse wave and the heart rate are different by nature. The ECG signals are electrical signals originating from the SA node, while the pulse waves are mechanical signals mainly measured in the periphery. The blood vessels can be considered as transmission lines rather than a (rigid) pipe system. So when the pulse waves propagate from the heart to the periphery it undergoes significant changes in the arterial system due to for example the ANS modulation on the blood vessels and the viscosity of the blood. These factors will impact the pulse waveform, resulting in difference between the HRV and PRV. We expect that most of these factors are minimal when measuring at the sternum because of the relative location to the heart. However, it is worth to notice the change in the average system bias and limits of agreements when the subjects were asked to breathe with a rate of 27 breath/min.

It is known that motion artifacts impact PPG signals [5]. Therefore, future perspectives are to examine the correlation between the HRV and the PRV parameters in more demanding conditions like; during different body motion; in different postural positions and in long-term recordings. This can be useful in sleep studies. Additionally, elderly people who suffer from cardiovascular diseases might also be an interesting group to examine the similarities between the two approaches.

The concept of PPG and pulse oximetry at the sternum is has been demonstrated recently by [15]. Our findings showed that the parasympathetic and sympathetic autonomic modulation of the heart rate can be measured from PRV analysis using sternal PPG on a healthy group of subjects at rest. Thus, being able to monitor these physiological parameters using a low-cost sternal PPG sensor will simplify many aspects of monitoring systems.

ACKNOWLEDGMENT

The study was supported by the Danish Business Innovation Fund, the Danish Ministry of Science, Innovation and Higher Education. The authors would like to thank the test subjects who participated in the study.

REFERENCES

[1] A. Camm, M. Malik, J. Bigger, and G. Breithardt, "Heart rate variability. Standards of measurement, physiological interpretation, and clinical use. Task Force of the European Society of Cardiology." *European heart journal*, vol. 17, no. 3, pp. 354–81, 1996.

[2] R. E. Kleiger, P. K. Stein, and J. T. Bigger, "Heart rate variability: measurement and clinical utility." *Journal of the International Society for Holter and Noninvasive Electrocardiology, Inc*, vol. 10, no. 1, pp. 88–101, 2005.

[3] J. Pontet, P. Contreras, A. Curbelo, J. Medina, S. Noveri, S. Bentancourt, and E. R. Migliaro, "Heart rate variability as early marker of multiple organ dysfunction syndrome in septic patients." *Journal of critical care*, vol. 18, no. 3, pp. 156–63, 2003.

[4] D. Barnaby, K. Ferrick, D. T. Kaplan, S. Shah, P. Bijur, and E. J. Gallagher, "Heart rate variability in emergency department patients with sepsis." *Journal of the Society for Academic Emergency Medicine*, vol. 9, no. 7, pp. 661–70, 2002.

[5] J. Allen, "Photoplethysmography and its application in clinical physiological measurement." *Physiological measurement*, no. 3, pp. R1–39, Mar. 2007.

[6] L. M. Nilsson, "Respiration signals from photoplethysmography." *Anesthesia and analgesia*, vol. 117, no. 4, pp. 1–7, Feb. 2013.

[7] J.-S. Wong, W.-A. Lu, K.-T. Wu, M. Liu, G.-Y. Chen, and C.-D. Kuo, "A comparative study of pulse rate variability and heart rate variability in healthy subjects." *Journal of clinical monitoring and computing*, vol. 26, no. 2, pp. 107–14, 2012.

[8] N. Selvaraj, a. Jaryal, J. Santhosh, K. K. Deepak, and S. Anand, "Assessment of heart rate variability derived from finger-tip photoplethysmography as compared to electrocardiography." *Journal of medical engineering & technology*, vol. 32, no. 6, pp. 479–84, 2008.

[9] S. Lu, H. Zhao, K. Ju, K. Shin, M. Lee, K. Shelley, and K. H. Chon, "Can photoplethysmography variability serve as an alternative approach to obtain heart rate variability information?" *Journal of clinical monitoring and computing*, vol. 22, no. 1, pp. 23–9, 2008.

[10] I. Constant, D. Laude, I. Murat, and J.-L. Elghozi, "Pulse rate variability is not a surrogate for heart rate variability," *Clinical Science*, vol. 97, no. 4, p. 391, 1999.

[11] W. Johnston and Y. Mendelson, "Extracting heart rate variability from a wearable reflectance pulse oximeter," *Proceedings of the IEEE 31st Annual Northeast Bioengineering Conference, 2005.*, pp. 157–158, 2005.

[12] A. Schäfer and J. Vagedes, "How accurate is pulse rate variability as an estimate of heart rate variability? A review on studies comparing photoplethysmographic technology with an electrocardiogram." *International journal of cardiology*, vol. 166, no. 1, pp. 15–29, 2013.

[13] J. Pan and W. J. Tompkins, "A real-time QRS detection algorithm." *IEEE transactions on bio-medical engineering*, vol. 32, no. 3, pp. 230–6, 1985.

[14] G. Lu, F. Yang, J. a. Taylor, and J. F. Stein, "A comparison of photoplethysmography and ECG recording to analyse heart rate variability in healthy subjects." *Journal of medical engineering & technology*, vol. 33, no. 8, pp. 634–41, 2009.

[15] J. Solà, O. Chételat, and J. Krauss, "On the reliability of pulse oximetry at the sternum." *IEEE Engineering in Medicine and Biology Society.*

PAPER II

TITLE Estimation of respiratory rates based on photoplethysmographic measurements at the sternum

AUTHORS Shadi S. Chreiteh, Bo Belhage, Karsten Hoppe, Jens Branebjerg, Sune Duun, Rasmus Haahr, and Erik V. Thomsen

JOURNAL Engineering in Medicine and Biology Society (EMBC), 2015 Annual International Conference of the IEEE

PUBLICATION HISTORY Status: Published in August 2015.

Estimation of Respiratory Rates based on Photoplethysmographic Measurements at the Sternum

Shadi S. Chreiteh, Bo Belhage, Karsten Hoppe, Jens Branebjerg, Rasmus Haahr, Sune Duun and Erik V. Thomsen

***Abstract*— The respiratory rate (RR) is a clinically important vital sign and is a frequently used parameter in the general hospital wards. In current clinical practice, the monitoring of the RR is by manual count of the chest movement for one minute. This paper addresses a new approach where the respiratory rate is extracted using photoplethysmography (PPG) on the chest bone (sternum).**

Sternal PPG signals were acquired from 10 healthy subjects resting in a supine position. As reference signals, finger PPG, electrocardiogram (ECG), and capnography were simultaneously recorded during spontaneous and paced breathing. The sternal PPG signals were then compared with the reference signals in terms of Bland-Altman analysis, the power spectrum analysis and the magnitude squared coherence.

The Bland-Altman analysis showed an average bias of 0.21 breaths/min between RR extracted from sternal PPG and capnography. The respiratory power content at the sternum was 78.8 (38) $\%$ in terms of the median and (the interquartile range). The cardiac content was 19 (18.4) $\%$ within the cardiac region. The results from the magnitude squared coherence analysis was 0.97 (0.09) in the respiratory region (6 to 27 breaths/min) and 0.98 (0.01) in the cardiac pulse region (30-120 beats/min).

This preliminary study demonstrates the possibility of monitoring the RR from sternal PPG on a healthy group of subjects during rest.

I. INTRODUCTION

The respiratory rate (RR) is known to be an early indicator of disease. A change in RR is one of the earliest and most important indicators of clinical complications such as hypercarpnia, hypoxia and chronic obstructive pulmonary disease. Besides being a valuable early warning indicator, changes in RR may often precede changes in other monitored vital signs such as heart rate (HR) or reduction in peripheral oxygen saturation (S_PO_2) [1]. In current clinical practice, the standard technique for monitoring the RR (particularly outside the emergency units) is by manual count through observation of the rib cage for one minute. This method requires direct observation and may influence the patient's respiration rhythm. Furthermore, the observer can have difficulties in the detection of distinct breaths [2]. Current automatic RR measurement requires either an airflow detection method such as nasal air flow monitoring, end tidal fCO_2 volume ($ETCO_2$) using a capnograph, or a measurement of movement, e.g. trans-thoracic impedance or inductance plethysmography. These methods are obtrusive and time consuming to setup for a general ward patient usage. Other techniques have been proposed for RR monitoring, including acoustic measurement of respiratory sound and extraction of RR from photoplethysmography (PPG) [3].

Monitoring of the RR from PPG has previously been studied through analysis of peripheral PPG. Leonard et al. [4] and Clifton et al. [5] have described the derivation of RR from finger PPG. Shelley et al. [6] have found that the respiratory component is significantly larger in the regions of the head (the ear and forehead) compared to the component derived from the finger. This indicates that the measuring site has a significant importance for the magnitude of the respiratory component in the PPG signal. Furthermore, it may also indicate that the smaller the distance to the chest, the less attenuation of the respiratory component by the vasculature. This is supported by Nilsson et al. [7] who found that the respiratory and cardiac induced variations in the PPG were different at different measuring sites (finger, forearm, wrist, forehead, and shoulder). The application of pulse oximetry using PPG at the sternum has recently been demonstrated [8]. However, the extraction of the RR from sternal PPG has not been investigated. It is therefore interesting to investigate whether the combined monitoring of pulse oximetry and respiratory rate at the sternum may be a clinically useful approach.

The sternal body location is expected to be robust for acquiring PPG signals, because of the central body location. Additionally, PPG signals from the sternum might have a different composition with a stronger respiratory component than peripherally sampled signals, due to local pressure variations. During inhaling/exhaling the pressure variations in the thoracic cavity change and affect the blood volume in the internal thoracic arteries and the anterior perforating branches of intercostal vessels. Hence, we hypothesize that RR estimated from sternal PPGs are equal to RR estimated from capnography. The aim of this study is therefore to examine whether the sternal PPG produces a reliable estimate of the RR compared to gold standard capnography.

The study was supported by the Danish Business Innovation Fund, the Danish Ministry of Science, Innovation and Higher Education.

Shadi S. Chreiteh is with the Department of Micro- and Nanotechnology, Technical University of Denmark, 2800 Kgs. Lyngby, Denmark and also with DELTA Microelectronics, Venlighedsvej 4, 2970 Hørsholm, Denmark (e-mail: ssc@delta.dk).

Bo Belhage is with the Bispebjerg Hospital, University of Copenhagen, 2400 Copenhagen NV, Denmark.

Karsten Hoppe and Jens Branebjerg are with DELTA Microelectronics, Venlighedsvej 4, 2970 Hørsholm, Denmark.

Rasmus Haahr, Sune Duun and Erik V. Thomsen are with the Department of Micro- and Nanotechnology, Technical University of Denmark, 2800 Kgs. Lyngby, Denmark.

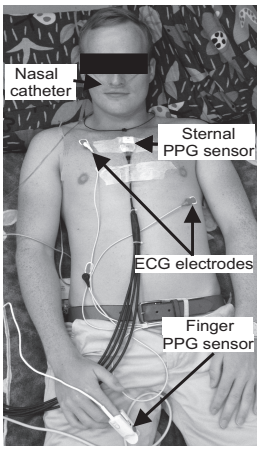

Fig. 1. Schematic overview of the measurement setup. For each subject, the sternal PPG sensor, lead-II ECG, finger PPG, and nasal (fCO_2) were acquired simultaneously. The test subject is positioned in a supine position during the experiment.

II. Methods & Materials

A. Data acquisition

A group of 10 healthy volunteers (9 males, 1 female) with mean age of 39.2±12.6 years and a mean Body Mass Index of 24.5±3.2 kg/m^2 were recruited for this preliminary study. The Danish Law and the Helsinki Declaration does not require a clinical protocol for this setup. The room temperature was $20 - 22\,^{\circ}$C. A custom build infrared light (940 nm) reflective PPG sensor was positioned on the skin over the sternum. A transmission PPG was obtained using a standard finger probe (Datex-Ohmeda AS/3, GE Healthcare, USA) and lead-II electrocardiogram (ECG) was also acquired and used as a cardiac reference signal. As a reference signal to the RR derived from sternal PPG, the inspiratory and expiratory fraction of carbon dioxide (fCO_2) was acquired via a nasal catheter. The reference signals and the sternal PPG signal were collected simultaneously and digitized with a sampling rate of 1000 Hz (Powerlab 8/35, 16 bit ADC, ADInstruments, USA) and stored on a laptop computer using Lab Chart 7 Pro (Lab Chart Version 7.3.7, ADInstruments, USA) data acquisition software. Fig. 1 outlines the experimental setup. For each subject being in a supine position data were collected in two stages:

1) Spontaneous respiration: The subjects were instructed to relax and breathe with natural respiratory rate for 10 min.
2) Paced respiration: The subjects were instructed to breathe in time with a visual scale. The pace was set to 6, 17, 24, 12, and 27 breaths/min for 3 min. each.

The subjects were instructed not to make any unnecessarily body movements to avoid motion artifacts.

B. Data analysis

In order to quantify the respiratory and cardiac contents of the sternal PPG and compare them with the reference signals we used three methods: (1) Power spectrum analysis, (2) Magnitude squared coherence analysis, and (3) time-domain RR estimation. All three methods have been applied on data acquired during the first stage of the experiments. However, only the last method has been used for the second stage of the experiment. The analysis of the acquired signals was conducted using MATLAB (MatLab R2012b, The MathWorks, Inc., USA).

1) Power spectrum analysis: The power spectral density (PSD via Welch's averaged, modified periodogram- method, 50% overlap, 160-s Hamming window) for the sternal PPG signal was calculated and the power $(\%)$ within the range of 0.1 to 0.45 Hz (6 to 27 breaths/min) was used as a measure of the respiratory component. The same procedure was used to estimate the cardiac content within the range of 0.5 to 2 Hz (30 to 120 beats/min) for the sternal PPG. The same PSD for the reference signals has also been calculated for comparison. 8 minutes recording periods were used in the analysis.

2) Mangitude squared coherence analysis: The similarity between the fCO_2 reference signal and the sternal PPG signal as well as between the ECG reference signal and the sternal PPG signal is calculated using the magnitude squared coherence analysis [7]. The magnitude squared coherence $C_{xy}(f)$ is given by (1)

$$C_{xy}(f) = \frac{|Pxy(f)|^2}{Px(f)Py(f)}. \quad (1)$$

The result is a normalized measure between 0 and 1 of the correlation between the frequency content of two signals x and y at the frequency f, where $P_{xy}(f)$ is the cross-spectral density between x and y, and $P_x(f)$ and $P_y(f)$ are the power spectra densities of x and y respectively. $C_{xy}(f)$ was calculated at the frequency of the reference respiratory rate and heart rate, respectively.

3) Extraction of the sternal PPG respiratory rate: The sternal PPG signal was filtered using a zero-phase 3rd order Butterworth band-pass filter with cut-off frequencies at 0.1-0.5 Hz (6 to 30 breaths/min) [9]. These cut-off values are chosen to suppress the cardiac-related variations and the frequencies below the respiratory frequency in the PPG signals. After the filtering process MATLAB's peak detection algorithm has been applied. The same procedure was applied to the capnographic reference fCO_2 signal. The RR was estimated using 1-min, non-overlapping segments.

III. Results

A typical example of a 1 min recording is shown in Fig. 2. It is clearly seen that spike like pulses is appearing in the PPG signals and the variations are beat-by-beat synchronous with the heartbeats in the ECG signal and the finger PPG signal. At the same time the respiratory variations in the sternal PPG signal can be identified clearly breath-by-breath, corresponding to the respiration reference fCO_2 signal.

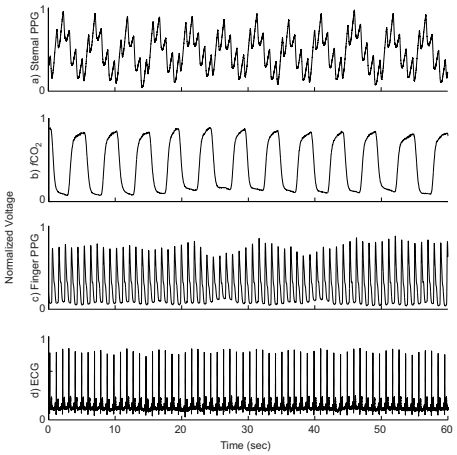

Fig. 2. Example of the acquired signals: a) PPG signal acquired from the sternal PPG sensor. It is observed that the PPG signals include a high frequency and a low frequency component, due to the cardiac and the respiratory cycle, respectively. b) Nasal fCO_2 signal, c) finger PPG signal, and d) ECG signal.

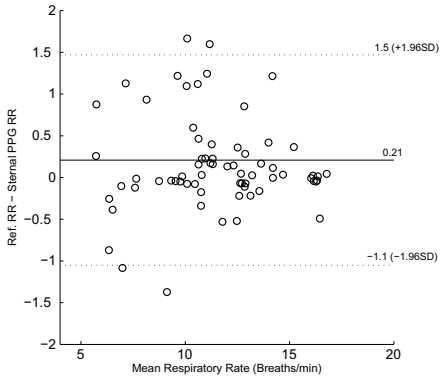

Fig. 3. Bland-Altman plot of RR derived from the sternal PPG signal and the reference signal during spontaneous respiration. The dashed lines represent the 95% confidence interval (lines of agreement). For each one-min segment RR is calculated for each subject (n=80).

TABLE I

SUMMARY OF THE RESPIRATORY RATES DURING PACED RESPIRATION. THE RESULTS ARE EXPRESSED IN MEDIAN (INTERQUARTILE RANGE).

Visual scale RR (breaths/min)	fCO_2 RR (breaths/min)	Sternal PPG RR (breaths/min)
6	6.10 (0.14)	6.03 (0.15)
12	12 (0.14)	11.95 (0.12)
17	17.01 (0.55)	16.97 (0.12)
24	23.99 (0.15)	23.86 (0.24)
27	26.98 (0.01)	26.98 (0.13)
Correlation Coefficient		0.99

During spontaneous respiration the median and (interquartile range) of RR was estimated to 10.99 (3.68) breaths/min and 11.41 (3.32) breaths/min from sternal PPG and the reference signal respectively. The overall difference between RR estimated from sternal PPG and the reference fCO_2 signal during spontaneous respiration is summarized in a Bland-Altman plot, Fig. 3. The average system bias is 0.21 breaths/min between the measurement methods. Fig. 4 shows a typical result of the power spectral analysis for all three acquired signals. The figure shows that the sternal PPG signal contains both a respiratory and a cardiac component. The power spectral content of the respiratory variations in the sternal PPG is larger than the power spectral content of the cardiac variations. The median and (interquartile range) of the respiratory spectral power at the sternum is 78.8 (38) %, while the pulse spectral power is 19 (18.4) %. The respiration coherence is 0.97 (0.09) and the pulse coherence is 0.98 (0.01). The results for the paced respirations are summarized in Table I. RRs derived from sternal PPG are significantly correlated with reference RRs.

IV. DISCUSSION

The key findings of this preliminary study are that sternal PPG shows very strong coherence with the respiratory fCO_2 reference signal and the ECG signal, respectively. Furthermore, the power spectral analysis showed that the sternal PPG contains larger power spectral content of the respiratory variations than the cardiac variations. From the sternal PPG signal we were able to extract the RR with high accuracy, confirming the hypothesis of the study. The respiratory rates were derived within a mean absolute error of 0.04 breaths/min during spontaneous respiration. This is a key result, which illustrates that the RR can be derived at the sternum with high accuracy within a clinical relevant range (6-27 breaths/min). Additionally, the results showed a high correlation (99%) between the capnography derived RR and the PPG derived RR under both spontaneous respiration and paced respiration. The power spectral density and magnitude squared coherence analysis are widely used in the literature in order to quantify the respiratory content in the PPG signal. In this study we used similar approach as reported by L. Nilsson et al. (2007). These authors reported that the best site for measuring the respiratory rate is at the forearm. However, they did not investigate the PPG at the sternum. In this preliminary study the sternal PPG had a relatively larger respiratory component and a relative smaller cardiac component when compared to the peripheral PPG. Although, the respiratory component dominates the sternal PPG signal, the pulse spectral power is 19 % of the total spectral power. Furthermore, the magnitude squared coherence analysis showed a strong similarity (0.98) between the sternal PPG signal and the ECG reference signal.

The vascular properties of the skin differ between various locations on the body. The tissue at the sternum is less perfused when compared with the peripheral locations such as the fingertip [8]. Nevertheless, acquiring the RR from

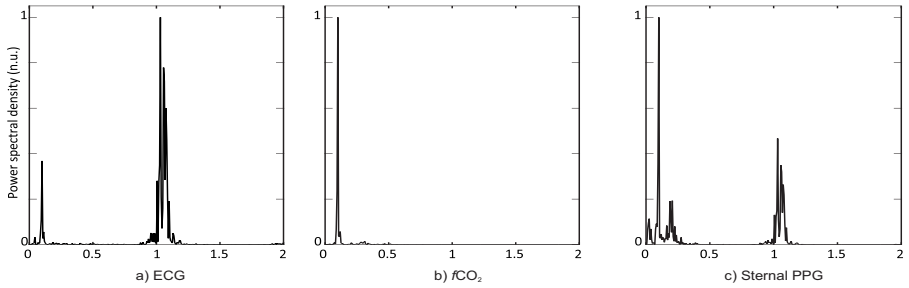

Fig. 4. Power spectrum analysis of one of the recordings. a) The ECG signal, b) The respiratory reference signal, and c) The sternal PPG signal. Notice that the respiratory component is also seen in the ECG signal.

sternal PPG has several advantages that make the sternum an appropriate sensor position. First of all, a probe placed at the sternum is less obtrusive than earlobe or finger probes. Secondly, the sternum can be used to monitor other clinically relevant parameter such as pulse wave variability [10] and pulse oximetry [11]. Respiratory pressure variations in the thoracic cavity affects the blood volume on the venous side and on the arterial side. We propose that the center location at the sternum and the anatomical structure of the thoracic cage is the main contributor to a pronounced respiratory effect. The perforating veins and arteries that surround the chest bone affect the PPG signal at the sternum.

In addition to this mechanism we propose that the mechanical tension over the sternum during inhalation/exhalation causes the skin to stretch. This affects the underlying vasculature of the skin and due to the thin wall of the veins, this mechanical effect is believed to be more prominent in the veins than in the arteries and therefore contributes to the respiratory component in the sternal PPG signal.

Pulse oximetry has recently been investigated by measuring the PPG at the sternum [11]. It is reported that even though the blood perfusion is low at the sternum the pulse oximetry is still possible. Pulse oximetry is currently used to detect hypoxemia and is used in many clinical settings as in emergency care, during patient transportation within the hospitals, etc. However, it does not detect hypo- or hypercapnoea which often precedes hypoxaemia [12]. Therefore monitoring the arterial oxygen saturation, the heart rate in combination with the respiratory rate at a single measuring site using the same sensor could prove to be clinically useful.

V. Conclusion

This preliminary study showed that the sternum is superior in regarding the estimation of the RR from PPG on healthy subjects. Future experiments will be conducted on patients with chronic obstructive pulmonary disease (COPD) or asthma. These patients have different respiration patterns and lower oxygen saturation in the blood. Additionally, how well the RR can be extracted in more demanding conditions like; during motion; in different body positions and in long-term recordings will also be examined.

Acknowledgment

The authors would like to thank the test subjects who participated in the study.

References

[1] D. J. Meredith, D. Clifton, P. Charlton, J. Brooks, C. W. Pugh, and L. Tarassenko, "Photoplethysmographic derivation of respiratory rate: a review of relevant physiology," *Journal of Medical Engineering & Technology*, vol. 36, no. 1, pp. 1–7, 2012.

[2] C. H. V. Leuvan and I. Mitchell, "Missed opportunities? An observational study of vital sign measurements." *Journal of the Australasian Academy of Critical Care Medicine*, vol. 10, no. 2, pp. 111–115, 2008.

[3] J. Allen, "Photoplethysmography and its application in clinical physiological measurement." *Physiological measurement*, no. 3, pp. R1–39, 2007.

[4] P. Leonard, T. F. Beattie, P. S. Addison, and J. N. Watson, "Standard pulse oximeters can be used to monitor respiratory rate." *Emergency medicine journal : EMJ*, vol. 20, no. 6, pp. 524–5, 2003.

[5] D. Clifton, J. G. Douglas, P. S. Addison, and J. N. Watson, "Measurement of respiratory rate from the photoplethysmogram in chest clinic patients." *Journal of clinical monitoring and computing*, vol. 21, no. 1, pp. 55–61, 2007.

[6] K. H. Shelley, D. H. Jablonka, A. a. Awad, R. G. Stout, H. Rezkanna, and D. G. Silverman, "What is the best site for measuring the effect of ventilation on the pulse oximeter waveform?" *Anesthesia and analgesia*, vol. 103, no. 2, pp. 372–7, 2006.

[7] L. Nilsson, T. Goscinski, S. Kalman, L.-G. Lindberg, and a. Johansson, "Combined photoplethysmographic monitoring of respiration rate and pulse: a comparison between different measurement sites in spontaneously breathing subjects." *Acta anaesthesiologica Scandinavica*, vol. 51, no. 9, pp. 1250–7, 2007.

[8] J. Solà, O. Chételat, and J. Krauss, "On the reliability of pulse oximetry at the sternum." *IEEE Engineering in Medicine and Biology Society.*, p. 1537, 2007.

[9] L. Nilsson, A. Johansson, and S. Kalman, "Respiration can be monitored by photoplethysmography with high sensitivity and specificity regardless of anaesthesia and ventilatory mode." *Acta anaesthesiologica Scandinavica*, vol. 49, no. 8, pp. 1157–62, 2005.

[10] S. S. Chreiteh, B. Belhage, K. Hoppe, J. Branebjerg, and E. V. Thomsen, "Sternal Pulse Rate Variability Compared with Heart Rate Variability on Healthy Subjects," *IEEE Engineering in Medicine and Biology Society.*, pp. 3394–7, 2014.

[11] R. Vetter, L. Rossini, A. Ridolfi, J. Sola, O. Chetelat, M. Correvon, and J. Krauss, "Frequency Domain SpO2 Estimation Based on Multichannel Photoplethysmographic Measurements at the Sternum," *World Congress on Medical Physics and Biomedical Engineering*, vol. 25/4, pp. 326–329, 2010.

[12] M. A. Cretikos, R. Bellomo, K. Hillman, J. Chen, S. Finfer, and A. Flabouris, "Respiratory rate: the neglected vital sign." *The Medical journal of Australia*, vol. 188, no. 11, pp. 657–659, 2008.

PAPER III

TITLE Monitoring of Respiratory Rate in COPD and Asthma Patients Using Sternal Photoplethysmography

AUTHORS Shadi S. Chreiteh, Bo Belhage, Nassim Nabipour, Karsten Hoppe, and Erik V. Thomsen

JOURNAL European Clinical Respiratory Journal

PUBLICATION HISTORY Submission date: 23-12-2015, Status: In review.

Title Page

Title:

Monitoring of Respiratory Rate in COPD and Asthma Patients Using Sternal Photoplethysmography

Authors:

Shadi Samir Chreiteh[1*], Bo Belhage[3], Nassim Nabipour[3], Karsten Hoppe[2] and Erik V. Thomsen[1]

Affiliations:

1Department of Micro- and Nanotechnology, Technical University of Denmark, 2800 Kgs. Lyngby, Denmark
2 Body sensors Department, DELTA, Danish Electronics, Light & Acoustics, Body Sensors, 2970 Hoersholm, Denmark
3 Department of Anesthesiology Bispebjerg Hospital, University of Copenhagen, 2400 Copenhagen NV, Denmark

Corresponding Author:

Shadi Samir Chreiteh
Email:shach@nanotech.dtu.dk
Address: Department of Micro- and Nanotechnology, Technical University of Denmark, DK-2800 Kgs. Lyngby

Conflict of interest

Karsten Hoppe is an employee of DELTA, Danish Electronics, Light & Acoustics, Body Sensors, 2970 Hoersholm, Denmark.

Abstract

Background: The respiratory rate (RR) is known to be an early indicator of exacerbations of Chronic Obstructive Pulmonary Disease (COPD). Currently, RR is most often monitored manually by the hospital staff and continuous evaluation of RR is seldom performed. RR is a central vital sign and pivotal for catching early sign of severe decline in health. Accordingly, a growing interest in alternative, continuous techniques for estimating RR have been shown.

Purpose: The aim of this study was to assess the use of sternal PPG (photoplethysmography)for estimating the RR on patients with pathologic RR patterns such as COPD or asthma.

Methods: Sternal Photoplethysmography recording conducted from 30 patients suffering from obstructive airway disease, either COPD or severe asthma. The recording duration was between 10 to 60 minutes. The patients were monitored through a nasal catheter obtaining the FCO_2 (capnography), from which the RR could be estimated. A custom build infrared PPG sensor was positioned on sternum. All the recording were divided into one minute segments (1250 segments) and annotated by a medical doctor.

Results: The RR obtained from the patients ranged from 11 to 36 brpm (breaths per minute). The mean rate was 20 brpm with a standard deviation of 5 brpm. Pearson's correlation coefficient between the two techniques showed a significant correlation ($r = 0.93$, $p<0.001$). The Blandt-Altmann analysis showed an excellent agreement between the two measuring techniques giving a mean system bias of 0.6 brpm and the 95% limits of agreement to be -2.8 to 4 brpm.

Conclusion: The results showed excellent agreement with capnography and may therefore be a future technique for RR estimation. Moreover, this may provide a useful clinical relevant improvement over manual or capnography estimated RR.

Key words: COPD; asthma; photoplethysmography; respiration rate; sternum

Introduction

Respiratory rate (RR) is a clinically important vital sign and is known to be an early indicator for detecting exacerbations and changes in the severity of Chronic Obstructive Pulmonary Disease (COPD) (1). According to the World Health Organization, COPD is currently the third leading cause of death globally. Exacerbation of COPD is not only one of the major causes of morbidity and mortality, but it also place a high economic burden on the healthcare system (2). In a small country like Denmark with around 6 million citizens, it is estimated that approximately 23,000 acute COPD-related patients are admitted to the hospital every year and the readmission rate is as high as 24% (3). The mortality rate during admission is furthermore 8 %, which is in line with the mortality in acute myocardial infarction (2).

It is generally recognized that one of the most important early warning signs indicating an exacerbation of COPD is a change in the respiration pattern of the patient. This change is among others characterized by an increased RR (1). In spite of this, recent studies have found that the RR, in particular, is often not recorded even in cases where the patient's primary problem is a respiratory challenge (4). The lack of consistent routine RR monitoring may be a consequence of shortcomings in today's measuring techniques. In current clinical practice, the standard method for monitoring the RR is by intermittent manual count of chest movement in one minute or by using the automatic capnography. The manual count is very time consuming and may even induce uncertainties by influencing the patient's breathing rhythm. The capnography method is obtrusive and requires either a nasal CO_2 detector or a face mask, both of which can be uncomfortable for the patient (5). Hence, the methods are therefore not ideal in the clinical setting. Other monitoring methods have been proposed. These methods include, among others, electrocardiography (ECG) derived respiration (6,7) and estimation of the RR from standard-pulse oximeters using photoplethysmography (PPG) (8–12) or chest impedance (5). Today, PPG is primarily performed peripherally and the most common measuring sites are the fingertip, earlobe, or the forehead (13). However, a number of other sites have also been investigated, e.g. the sternum (14) or the shoulder (15).

The PPG signal is generated when the light is modulated by blood volume changes in the vessels. It is known that the respiration modulates the baseline ("DC") component of the PPG signal (16). This is illustrated in Figure 1. The respiratory induced variations in the intrathoracic pressure are transferred to the central veins in the circulation system. During inspiration, the chest wall expands and the intrathoracic pressure decreases and causes a decrease in the central venous pressure. This results in an increase in the venous return. This is observed as an increase in the

baseline of the PPG signal (see Figure 1). During expiration the opposite occurs and the venous return will decrease. This is observed as a decrease in the PPG signal. Superposed on the DC component, there is a small intensity variation termed the AC component. This corresponds to blood volume changes due to the cardiac pulse.

The application of PPG has previously been studied and is well documented (17–20). Some of the advantages include that the PPG derived RR can be used regardless of age, gender, anesthesia, and mode of ventilation (21, 22). However, as mentioned, the measuring sites have previously been confined to the extremities. It seems that the measuring site has a significant effect on the respiratory component of the PPG signal and it is interesting to further investigate the RR derived from PPG measured at the sternum. Recently, we have shown in a preliminary study that sternal measurements are advantageous for RR estimation (14). The PPG signals differ from the peripherally obtained PPG signals by showing extremely clear respiratory oscillations in healthy subjects. Therefore, the aim of this study is to assess the RR from a clinical relevant patient group with pathologic RR patterns using sternal PPG.

Methods

Study population

The clinical study took place at two different departments; the department of pulmonary medicine and the medical admissions ward on Bispebjerg Hospital, Copenhagen University Hospital, Copenhagen, Denmark. The data was collected from 30 patients with obstructive airway disease, either COPD or asthma. One of the COPD patients was excluded due to missing data in the recording. The study was approved by the Danish regional ethical community (H-6-2014-013), the Danish Health and Medicines Authority (CIV-15-01-013029), and was monitored by the regional good clinical practice (GCP) unit. The patients provided written informed consent for study participation. The inclusion criteria required that the patients were diagnosed with COPD or asthma and were admitted to the hospital due to an exacerbation of their condition for at least 24 hours prior to their inclusion in the study. The patient demographics are listed in Table 1.

Study materials and procedure

The patients were monitored using a Datex-Ohmeda AS/3 Compact Patient Monitor, recording the fraction of carbon dioxide (FCO_2) via nasal catheter, from which the RR can be calculated. A

custom build infrared PPG sensor was positioned on the skin over the sternum using adhesive tape. Both signals were collected simultaneously and digitized with a sampling rate of 1000 Hz (Powerlab 8/35, 16 bit ADC, ADInstruments, USA) and stored on a laptop computer using Lab Chart 8 Pro (Lab Chart Version 8.0.8, ADInstruments, USA) as data acquisition software. During the experiment the patients were at rest in a semi-supine position and, since it is known that motion artefacts impact the PPG signals negatively, the patients were instructed not to make any unnecessarily body movements during the measurements (23). However, physiological artifacts, e.g. coughing, are unavoidable. The recording duration was intended to be between 10 and 60 minutes. However, the maximum recording length was 54 minutes, cf. Table 1.

Data analysis

The sternal PPG signal and the reference signal from the capnograph were filtered to suppress the cardiac related AC component and increase the respiratory related DC component (using a zero-phase 3rd order Butterworth band-pass filter with cut-off frequencies at 0.1-0.7 Hz which corresponds to accentuation of the part of the signal that represents 6 - 42 brpm). After the filtering, both the sternal PPG and the capnographic signal were divided into one-minute non-overlapping segments. This yields a total of 1250 segments (half from the PPG and half from the capnographic signals). The 1250 segments were randomized and a medical doctor was asked to visually go through all 1250 segments and manually detect the RR in each one-minute segment. After the manual detection of the RR in each segment, the segments were paired to allow a direct comparison of the RRs obtained with simultaneous measurements from the two recording systems. The statistical package for social sciences (SPSS) ver. 23 was used to analyze the data. The Bland-Altman assessment for agreement was used to compare the RRs estimated from the two methods. The 95 % limits of agreement were defined as mean bias ± 1.96 x standard deviation (SD) of the differences. The correlation between the two measurement techniques was calculated using Pearson's correlation coefficient. A p-value less than 0.05 was considered statistically significant.

Results

Figure 2 illustrates three filtered segments from sternal PPG (black) and the corresponding flow signal from capnography (blue) at different RRs. The distribution of all the RRs derived from the capnographic signals and the sternal PPG signals is shown in figure 3. The RRs are ranged from 11.3 to 35.5 brpm. The mean rate was 20.4 brpm with a standard deviation of 4.7 brpm. Figure 4 contains the distribution of the differences between the sternal PPG derived RRs and the RRs derived from simultaneous measurements obtained with the capnographic signals. The mean bias between the rates was 0.6 brpm with a standard deviation of 1.7 brpm. The accuracy of the measurement defined as the root mean squared (A_{rms}) difference between measured values of sternal PPG and the reference values from capnography was 1.9 brpm. This parameter is often used by manufactures in terms of accuracy and is often used as a key performance parameter when evaluating pulse oximetry (24). A more detailed view of the differences is further provided in Figure 5. The figure contains a Bland-Altman plot of the data. The Bland-Altman analysis demonstrated a mean system bias of 0.6 brpm and the 95% limits of agreement to be -2.8 to 4 brpm. Additionally, Pearson's correlation coefficient between the two techniques showed a significant correlation ($r = 0.93$, $p<0.001$).

Discussion

The purpose of this study was to examine whether the RRs derived from sternal PPGs can be used for reliable monitoring of patients with obstructive airway disease like COPD or asthma. Besides the importance of monitoring the RR on these patients, it was also important to evaluate how well sternal PPG derived respiration rate could be correctly identified in a clinical setting over a broad range of RRs.

The RR for a healthy adult at rest is between 9-16 brpm. Also it is known that COPD and asthma patients have higher RRs (1). This is reflected in the distribution plots provided in figure 3. Additionally, it is reflected in the figure that there are two main epochs in the distributions, one around 16 brpm and one around 24 brpm. By further inspection of the recorded data it was clear that the reason behind the two epochs is because the fact that the study took place at two different hospital wards having the majority of the patients with higher RR at the department of pulmonary medicine. One of the inclusion criteria of this study was that patients should be hospitalized for at least 24 hours prior to the measurement and when COPD or asthma patients are admitted to the medical admissions ward, they receive the needed treatment and some will be dismissed while other may need more medical attention. This means that we may have monitored a more stable group of COPD and asthma patients at the medical admissions ward than the patients at the pulmonary medicine. Usually when patients require more medical treatment they will be transferred to the pulmonary medicine ward. The majority of the segments (90%) with RRs above 28 brpm belong to the asthma patients. In conclusion, the patient population in this study seem to provide a realistic clinical basis for investigating the performance of sternal PPG obtained RRs.

The standard procedure of measuring the respiration rate at the pulmonary ward and the medical admission ward at Bispebjerg Hospital in Denmark is by physical assessment either by direct observation of the chest movement or via breath sounds with a stethoscope. This procedure is done at least once a day. However, in some rare cases the traditional capnography is used for continuous monitoring of the patients. In this study we compared RRs derived from the sternum with capnography measurements. Excellent agreement was found between the two measurement methods. The documented accuracy of the used capnograph (Datex Ohmeda AS/3 Compact Patient Monitor) is ± 5 brpm and the result from the Blandt-Altmann analysis showed that the upper 95% limits of agreement was 4 brpm and the lower limit was -2.8 brpm. This finding is considered to be clinical acceptable and within the accuracy range of the used “gold standard” method. Furthermore, the standard deviation of differences and the root mean square of the differences (A_{rms}) are 1.7 brpm

and 1.9, respectively, which indicates a very precise estimate by sternal PPG derived RR. These numbers can be compared to the performance of manual respiration counting as described in (25). Lim et al. (25) found that the repeatability coefficient for respiration rate monitoring made consecutively by the same observer is only 4.9 brpm and a repeatability coefficient as low as 5.7 brpm for respiration rate monitored consecutively by a different observer, and finally a repeatability coefficient of 4.2 brpm when simultaneous observers were investigated. Based on this reporting and compared to the results of this study we can say that the respiration rate monitoring using PPG at the sternum is well within the currently clinically accepted tolerance. Importantly, the distribution of the differences seems to follow a normal distribution with a small bias as seen on figure 4.

One of the limitations of this study is that the recording length for each patient is not equal. This means that one recording potentially may bias the results in a negative or positive direction. Furthermore, the different stages of COPD could be very useful to know in a future study as some patients contributed to a normal range of the RR and others to higher rates. If patients were screened using for example spirometry it would be possible to divide the COPD patients into subgroups during the analysis. The strength of this study is that the data covered a broad range of RR in a normal clinical setting on a relevant group of patients. The small group of severe asthma patients contributed to the high values of the respiration rates. This was very useful in our study. To our knowledge, no study has previously reported results regarding the possibility of deriving the RR from sternal PPG on COPD and asthma patients.

Respiratory dependent oscillations are also seen in PPG signals from more peripheral located detectors, in example the finger and forearm as shown by Nilsson et al. (26). However, the authors reported that the strength of the respiration component in the PPG signal depended on the measuring site. The authors reported that the largest respiratory induced variations seem to be more prominent proximal to the chest (the largest component was found on the forearm). Furthermore, the largest respiratory induced variations in the PPG signal are evident at low respiratory rates and high tidal volumes. This is not completely in line with the results of this study: As seen in the Bland-Altman analysis there was excellent agreement in the whole range of respiration rates from 11 to 35 brpm. We propose that the central location at the sternum and the anatomical structure of the thoracic cavity is the main contributor to this pronounced respiratory effect. Additionally, the respiratory variations affect both the blood volume in the venous side and on the arterial side, hence the pronounced respiratory component in the sternal PPG signal.

Sternum has recently been introduced as a novel measuring site for vital sign monitoring. Preliminary results from an hypoxia study conducted by Sola et al. (27) has demonstrated that even pulse oximetry measurement at the sternum is possible on a healthy group of subjects. Being able to measure the RR in combination with oxygen saturation level in the blood and the heart rate on a single measurement site using a small probe might lead to increased patient safety in terms of detecting earlier indication of developing respiratory exacerbations. The importance of continuous monitoring of the respiration rate in COPD patients has recently been reported by Yanez et al. (1).The authors found RR increases significantly few days before patients require hospital admission because of exacerbated COPD, this was the case for 70% of COPD patients (n=89). Interestingly, similar result was reported by Seemungal et al. (28), where COPD patients (n=101) reported an increased shortness of breathing during the days before formal diagnoses of exacerbated COPD is established. Early detection of worsening in the patient condition using sternal PPG may therefore possess the opportunity to increase early interventions.

Conclusion

In this clinical study we have demonstrated that the RR can be estimated from an unobtrusive sternal PPG probe placed on COPD and asthma patients. The results showed excellent agreement with capnography and may therefore be a future technique for respiration rate estimation. Moreover, this may provide a useful clinical relevant improvement over manual or capnography estimated respiratory rates.

References

1. Yañez AM, Guerrero D, Pérez de Alejo R, Garcia-Rio F, Alvarez-Sala JL, Calle-Rubio M, et al. Monitoring Breathing Rate at Home Allows Early Identification of COPD Exacerbations. CHEST J. 2012 Dec 1;142(6):1524.

2. Groenewegen KH. Mortality and Mortality-Related Factors After Hospitalization for Acute Exacerbation of COPD. Chest. 2003 Aug 1;124(2):459–67.

3. Eriksen N, Hansen EF, Munch EP, Rasmussen FV, Vestbo J. Chronic obstructive pulmonary disease. Admission, course and prognosis. Ugeskr Laeger. 2003;165(37):3499–502.

4. Cretikos MA, Bellomo R, Hillman K, Chen J, Finfer S, Flabouris A. Respiratory rate: the neglected vital sign. Med J Aust. 2008 Nov 3;188(11):657–9.

5. Folke M, Cernerud L, Ekström M, Hök B. Critical review of non-invasive respiratory monitoring in medical care. Med Biol Eng Comput. 2003 Jul;41(4):377–83.

6. Boyle J, Bidargaddi N, Sarela A, Karunanithi M. Automatic Detection of Respiration Rate From Ambulatory Single-Lead ECG. IEEE Trans Inf Technol Biomed. 2009 Nov;13(6):890–6.

7. Arunachalam SP, Brown LF. Real-time estimation of the ECG-derived respiration (EDR) signal using a new algorithm for baseline wander noise removal. In: 2009 Annual International Conference of the IEEE Engineering in Medicine and Biology Society. IEEE; 2009. p. 5681–4.

8. Nilsson LM. Special article: respiration signals from photoplethysmography. Anesth Analg. 2013 Oct 28;117(4):859–65.

9. Nilsson L. Respiratory monitoring using reflection mode photoplethysmography: clinical and physiological aspects. Acta Anaesthesiol Scand. 2007 Jan;51(1):130–130.

10. Addison PS, Watson JN, Mestek ML, Ochs JP, Uribe A a, Bergese SD. Pulse oximetry-derived respiratory rate in general care floor patients. J Clin Monit Comput. 2015;29(1):113-120.

11. Leonard P. Standard pulse oximeters can be used to monitor respiratory rate. Emerg Med J. 2003 Nov 1;20(6):524–5.

12. Lindberg L, Ugnell H, Öberg P. Monitoring of respiratory and heart rates using a fibre-optic sensor. Med Biol Eng. 1992 Sep;30(5):533–7.

13. Tamura T, Maeda Y, Sekine M, Yoshida M. Wearable Photoplethysmographic Sensors—Past and Present. Electronics. 2014 Apr 23;3(2):282–302.

14. Chreiteh SS, Belhage B, Hoppe K, Branebjerg J, Haahr R, Duun S, et al. Estimation of respiratory rates based on photoplethysmographic measurements at the sternum. In: 2015 37th Annual International Conference of the IEEE Engineering in Medicine and Biology Society (EMBC). IEEE; 2015. p. 6570–3.

15. Shelley KH, Jablonka DH, Awad A a, Stout RG, Rezkanna H, Silverman DG. What is the best site for measuring the effect of ventilation on the pulse oximeter waveform? Anesth Analg. 2006 Aug;103(2):372–7.

16. Webster JG. Design of Pulse Oximeters. 1st ed. Series in Medical Physics and Biomedical Engineering. CRC Press; 1997.

17. Vegfors M, Ugnell H, Hök B, Oberg P a, Lennmarken C. Experimental evaluation of two new sensors for respiratory rate monitoring. Physiol Meas. 1993 May;14(2):171–81.

18. Johansson a, Oberg P a. Estimation of respiratory volumes from the photoplethysmographic signal. Part I: Experimental results. Med Biol Eng Comput. 1999 Jan;37(1):42–7.

19. Nilsson L, Johansson A, Kalman S. Respiratory variations in the reflection mode photoplethysmographic signal. Relationships to peripheral venous pressure. Med Biol Eng Comput. 2003 May;41(3):249–54.

20. Nilsson L, Johansson a, Kalman S. Macrocirculation is not the sole determinant of respiratory induced variations in the reflection mode photoplethysmographic signal. Physiol Meas. 2003 Nov;24(4):925–37.

21. Nilsson L, Johansson a, Kalman S. Respiration can be monitored by photoplethysmography with high sensitivity and specificity regardless of anaesthesia and ventilatory mode. Acta Anaesthesiol Scand. 2005 Sep;49(8):1157–62.

22. Nilsson L, Goscinski T, Johansson A, Lindberg L-G, Kalman S. Age and gender do not influence the ability to detect respiration by photoplethysmography. J Clin Monit Comput. 2006 Dec;20(6):431–6.

23. Allen J. Photoplethysmography and its application in clinical physiological measurement.

Physiol Meas. 2007 Mar;28(3):R1–39.

24. ISO 80601-2-61:2011. Medical electrical equipment - Part 2-61: Particular requirements for basic safety and essential performance of pulse oximeter equipment. International Organization for Standardization. 2011;

25. LIM WS, CARTY SM, MACFARLANE JT, ANTHONY RE, CHRISTIAN J, DAKIN KS, et al. Respiratory rate measurement in adults—how reliable is it? Respir Med. 2002 Jan;96(1):31–3.

26. Nilsson L, Goscinski T, Kalman S, Lindberg L-G, Johansson a. Combined photoplethysmographic monitoring of respiration rate and pulse: a comparison between different measurement sites in spontaneously breathing subjects. Acta Anaesthesiol Scand. 2007 Oct;51(9):1250–7.

27. Solà J, Chételat O, Krauss J. On the reliability of pulse oximetry at the sternum. Conf Proc IEEE Eng Med Biol Soc. 2007 Jan;2007:1537.

28. SEEMUNGAL TAR, DONALDSON GC, BHOWMIK A, JEFFRIES DJ, WEDZICHA JA. Time Course and Recovery of Exacerbations in Patients with Chronic Obstructive Pulmonary Disease. Am J Respir Crit Care Med. 2000 May;161(5):1608–13.

Table 1. Patient demographics.

	All	COPD	Asthma
Gender (male/female)	11/18	9/15	1/4
Age (mean±SD[a]), years	64.3±14.4	64.4±14.2	62.4±15
BMI (mean±SD), m*Kg^-2	25.8±8.8	25.8±8.7	25.7±9.1
Recording length, min[b]	21.5 (10 – 54)	21 (10 – 54)	24.2 (13 – 32)

a Standard deviation
b Duration lengths are presented as mean (minimum – maximum)

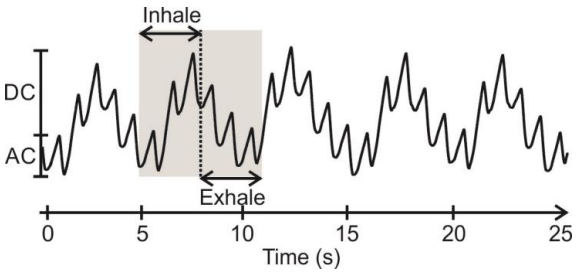

Fig. 1. Sternal PPG segment showing the two PPG components. The AC component reflects the cardiac pulses. The DC component reflects the respiratory induced variations which modulate the baseline of the PPG signal. The grey area shows one respiration cycle including an inhalation and an exhalation.

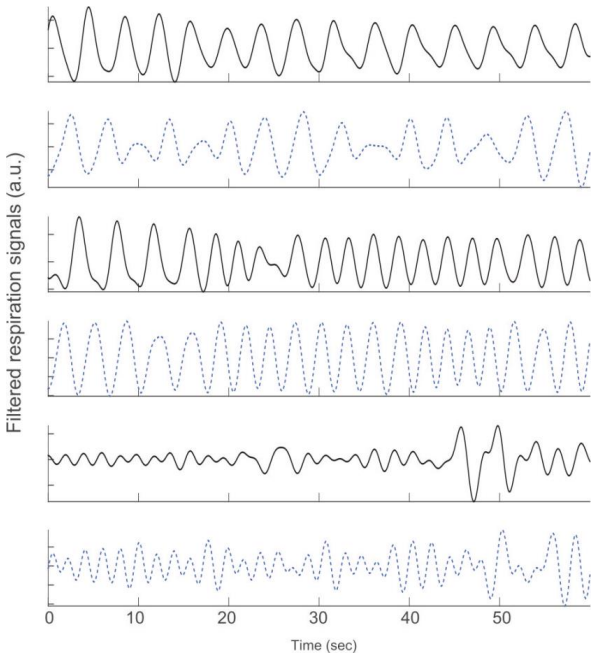

Fig. 2. Filtered respiration signals from sternal PPG (solid) and the reference flow signal from capnography (dashed) respectively. These segments are six of the 1250 segments that the medical doctor annotated.

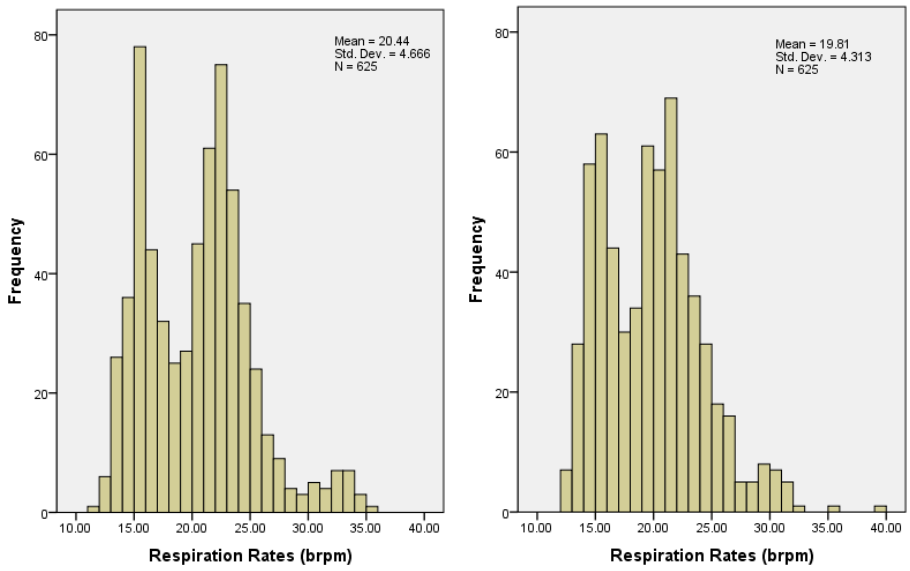

(a) (b)

Fig 3. Distribution of all the RR of the patients included in this study. (a) The RR are calculated from the capnographic signal (b) and derived from sternal PPG.

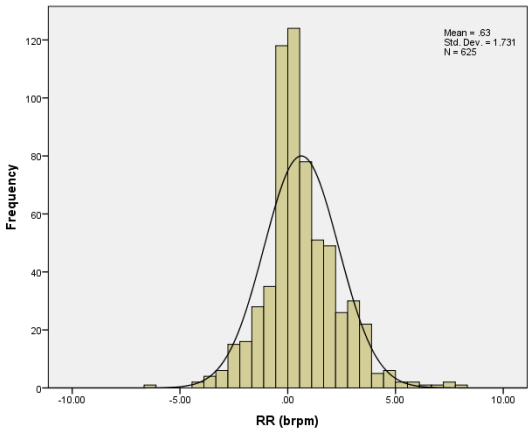

Fig 4. The distribution of all the differences between the sternal PPG derived respiratory rates and the respiratory rates estimated from the capnographic signal. The solid curve shows a normal distribution curve of the differences.

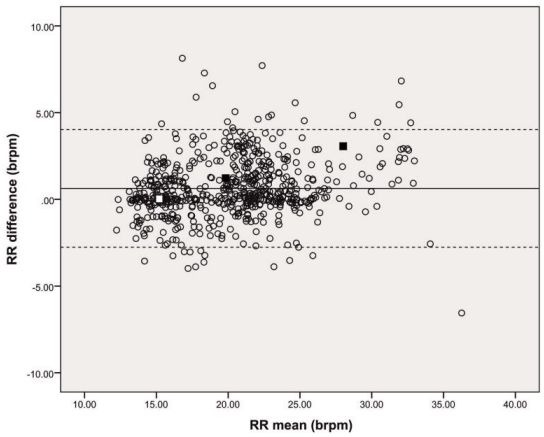

Fig. 5. The Blandt-Altman plot of the data. The dashed lines are the lines of agreement (mean±1.96SD) and the solid line is the mean bias. The three square markers represent the mean and differences for signals shown in figure 2.

PAPER IV

TITLE A Clinical Study of Short-Term Sternal Photoplethysmography: Recordings from Patients with Obstructive Airways Diseases

AUTHORS Shadi S. Chreiteh, Dorthe B. Saadi, Bo Belhage, Nassim Nabipour, Karsten Hoppe, and Erik V. Thomsen

JOURNAL Engineering in Medicine and Biology Society (EMBC), 2016 Annual International Conference of the IEEE

PUBLICATION HISTORY Submission date: 22-02-2016, Status: In review.

A Clinical Study of Short-Term Sternal Photoplethysmography: Recordings from Patients with Obstructive Airways Diseases*

Shadi S. Chreiteh, Dorthe B. Saadi, Bo Belhage, Nassim Nabipour, Karsten Hoppe, and Erik V. Thomsen

Abstract— **Traditionally, measurements of the oxygen saturation (S_pO_2) has been confound to the extremities. In this study, we therefore investigated the possibility for reliable estimation of clinically relevant S_pO_2 levels from photoplethysmography (PPG) obtained on the sternum of patients with obstructive airway diseases. We initiated the study with a calibration of a prototype sternal PPG sensor. In accordance with the ISO 80601-2-61:2011 guidelines, the calibration was conducted as a controlled desaturation study. We obtained a calibration accuracy of 1.75% which is well within the clinically and commercially accepted range. We then compared the S_pO_2 levels simultaneously obtained from the sternal PPGs and a commercially available finger pulse oximeter on 28 admitted patients with either asthma or Chronic Obstructive Pulmonary Disease (COPD). The Pearson correlation between the S_pO_2 levels estimated from the two body locations was found to be 0.89 ($p<0.05$) and the mean system bias was only 0.052% with upper and lower limits of agreement of 2.5% and -2.4%, respectively. This finding is very promising for the future design of new sternum based patch technologies that might be able to provide continuous estimates of the S_pO_2 levels on critically or chronically ill patients.**

I. Introduction

The oxygen saturation (S_pO_2) is known as a highly relevant vital sign that can be used to detect worsening in the condition of critically ill patients, e.g. patients suffering from Chronic Obstructive Pulmonary Disease (COPD) [1] [2]. According to the World Health Organization (WHO), COPD is the third leading cause of death globally. Furthermore, the readmission rate for this patient population is as high as 24% and the mortality during admissions is 8% [3]. These numbers indicate that it is highly relevant to be able to detect worsening in the condition of these patients in a timely manner and thereby be able to initiate treatment and prevent dangerous exacerbations in the patient's condition. As mentioned, the S_pO_2 level is an important vital sign in this context. Unfortunately, continuous levels of S_pO_2 are not routinely monitored on this patient population today. It is therefore desirable to design new methods for reliable continuous estimation of S_pO_2 levels. Traditionally, the S_pO_2 levels have been found using wired pulse oximeters placed on, for instance, the fingertip or the earlobe [4]. Our group has previously shown that photoplethysmographic (PPG) signals recorded on the sternum are clinically useful for analysis of the respiratory rate [5]. This parameter is another very important vital sign that is especially relevant when considering the condition of COPD patients [6]. Accordingly, it is important to investigate whether PPG signals recorded on the sternum are also suitable for calculation of the S_pO_2 levels. In combination with the currently emerging patch type electrocardiogram (ECG) recorders [7], the ability to add PPG analysis on the sternum might therefore open the possibility for a future vital sign patch that could assist in detecting any worsening in the condition of critically ill patients. The purpose of this study is therefore to investigate whether PPG recorded on the sternum is able to provide reliable and clinically relevant measures of S_pO_2 levels in patients suffering from obstructive airway diseases.

A. The PPG Signal

In relation to pulse oximetry, PPG is a method that estimates the relative variations in the blood volume by emitting light with different wavelengths into the tissue and detecting the reflected/transmitted light by a photo detector. It is generally accepted that the S_pO_2 values can be estimated from the optical ratio, R, between the normalized amplitude of the red (λ = 660nm) and the infrared (λ = 940nm) PPG signals, see Fig. 1 [8]. However, the exact mathematical relation between R and S_pO_2 needs to be established empirically with a controlled desaturation study. After this calibration, the recorded PPG signals can be used to estimate the S_pO_2 levels directly. A few other research groups have previously published results from successful calibrations of PPG sensors placed on the sternum [9] [10], but to our best knowledge, this is the first study that extends the investigation of sternal PPG to include an estimate of the performance on a clinically very important patient population.

II. Methods

For this study, we used a custom build PPG sensor that can be attached to the skin over the sternum with an adhesive tape, see Fig. 2. As mentioned, the first step was to calibrate the custom build prototype of a sternal PPG sensor. This was accomplished with a controlled desaturation study. The next step was to simultaneously measure S_pO_2 values from the prototype sternal PPG sensor and a commercially available finger PPG sensor on patients with obstructive airway disease. Finally, the last step was to compare the S_pO_2 values

*Research supported by the Danish Ministry of Higher Education and Science.

Shadi S. Chreiteh is with the Department of Micro- and Nanotechnology, Technical University of Denmark, 2800 Kgs. Lyngby, Denmark (e-mail: shach@nanotech.dtu.dk).

Dorthe B. Saadi and Karsten Hoppe are with DELTA Danish Electronics, Light & Acoustics, Venlighedsvej 4, 2970 Hørsholm, Denmark.

Bo Belhage and Nassim Nabipour are with the Department of Anesthesiology, Bispebjerg University Hospital, University of Copenhagen, 2400 Copenhagen NV, Denmark.

Erik V. Thomsen is with the Department of Micro- and Nanotechnology, Technical University of Denmark, 2800 Kgs. Lyngby, Denmark.

Preprint submitted to 38th Annual International Conference of the IEEE Engineering in Medicine and Biology Society. Received February 22, 2016.

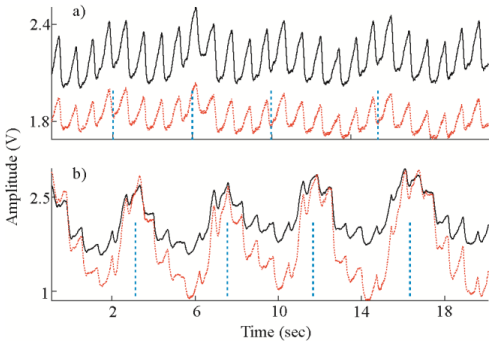

Figure 1. Examples of red (red dotted line) and infrared (black solid line) PPG signals recorded with the custom build PPG sensor placed on the sternum with an oxygen saturation of 98% (a) and 71% (b), respectively. Both the respiratory component (slow baseline changes indicated with vertical dashed blue lines) and the cardiac component (high frequency fluctuations) are clearly observed in both examples. Finally, it is observed how both the heart rate (HR) and the depth of the breathing are increased during low oxygen saturation.

obtained from the two systems. Each of these steps will be described in details in following section. The study was approved by the Danish Regional Ethical Community, the Danish Health and Medicines Authority, the Danish Data Protection Agency, and it was monitored by the regional Good Clinical Practice (GCP) unit. Furthermore, all subjects provided written informed consent to participate before they were enrolled in the study.

A. Data Acquisition for Calibration of the PPG Sensor

The protocol for the calibration was conducted in accordance with the recommendations stated in the ISO 80601-2-61:2011 guidelines. We enrolled a total of 14 healthy Caucasian volunteers. The demographics of the subjects are provided in Table I. During the desaturation study, the oxygen saturation in the blood was gradually reduced within the region of clinical interest (70% to 100%). The experimental setup is illustrated in Fig. 2. The calibration was based on invasive measures of the blood oxygen

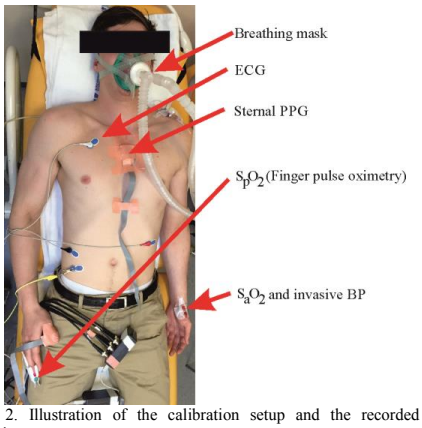

Figure 2. Illustration of the calibration setup and the recorded data modalities.

TABLE I. SUBJECT DEMOGRAPHICS FOR THE CALIBRATION STUDY.

Gender (male/female)	9 / 5
Age (years), mean ± SD[a]	30.3 ± 11
BMI[b] (kg/m^2), mean ± SD[a]	22.2 ± 3
Recording length[c] (min)	24.9 (18.1 - 50.1)

[a] SD is the standard deviation
[b] BMI is the body mass index
[c] The recording length is stated as mean (minimum – maximum)

saturation in the radial artery (S_aO_2). Therefore, a medical doctor (MD) performed an Allen's test on the hand before the subject was included. This test ensures that both the radial and the ulnar arteries are able to individually supply the hand with sufficient amount of blood during the experiment. If the Allen's test was passed, the MD placed a catheter in the radial artery under local anesthesia. This catheter is used for collection of arterial blood samples during the experiment. The desaturation was controlled with a closed-loop breathing system: The subjects were breathing in a mask with a manually controlled mixture of oxygen and nitrogen air from a 50 L container (a Douglas bag). The regulation of the air mixture was conducted by the MD. The subjects were lying in a supine position and, to avoid the influence of motion artifacts, they were instructed to move as little as possible. The patients were monitored using the prototype PPG sensor placed on the sternum and a 3-lead ECG. These recordings are used for the calibration procedure. To ensure the subject safety during the experiment, they were furthermore monitored using a Datex-Ohmeda AS/3 Patient Monitor (finger pulse oximetry, invasive blood-pressure (BP), and fraction of CO_2 in the breathing air). To ensure synchronization of all the modalities, all the equipment was connected to the same data acquisition device (Powerlab 8/35, 16 bit ADC ADInstruments, USA) and acquired simultaneously.

During the recordings, up to 25 blood samples of 2 ml each were taken from each test subject. The goal was to obtain a distribution of the S_aO_2 level from the blood samples in the range of 70% to 100%. The first five blood samples were taken when the subject was breathing outside the closed system (reference measurements). The experiment was stopped when 25 blood samples were obtained, when the subject reached an oxygen saturation of 70%, or when the MD decided to stop (whichever came first). During the experiment, we obtained a total of 324 blood samples from the 14 subjects. The blood samples were analyzed using a Radiometer blood gas analyzer (ABL 800 Flex, Radiometer Co.). Each time a blood sample was taken, a marker was placed in the data acquisition software. This ensures synchronization between the time instance for the blood samples and the recorded signals.

B. Calibration of the Sternal PPG sensor

The first step of the calibration is to estimate the optical ratio, R, between the normalized amplitude of the red and the infrared PPG signals. We estimated R as described below:

1. Extract the simultaneously recorded ECG and PPGs in a 20 second window centered on the time marker for each of the blood samples (corresponding to the window size of the finger pulse oximeter).

Preprint submitted to 38th Annual International Conference of the IEEE Engineering in Medicine and Biology Society. Received February 22, 2016.

2. Normalize the red and the infrared PPG signals according to (1), where x(t) is the original PPG and y(t) is the normalized PPG [8].
3. Extract the heart rate (HR) as the frequency bin with the largest amplitude in the power spectral density of the ECG. Consider only frequencies from 0.5 Hz to 4 Hz (corresponding to a HR of 30 to 240 beats per minutes).
4. Design a Butterworth band-pass filter of order 4 [11]. The low cut-off frequency for each window (corresponding to one blood sample) was found by subtracting 0.2 Hz from the detected HR and the high cut-off frequency was found by adding 2 Hz to the detected HR for this specific window.
5. Filter both the red and the infrared PPGs with the individually designed filter. The effect of the normalization and filtering is illustrated in Fig. 3.
6. Calculate R as defined in (2), where $y_r(t)$ is the normalized red PPG signal and $y_{ir}(t)$ is the normalized infrared PPG signal [8].

$$y(t) = \frac{x(t) - mean(x(t))}{mean(x(t))} \quad (1)$$

$$R = \frac{sqrt(mean(y_r{}^2(t)))}{sqrt(mean(y_{ir}{}^2(t)))} \quad (2)$$

The last step is to mathematically link the calculated R values to the measured S_aO_2 reference values. This provides a formula for future estimation of the oxygen saturation based on the PPG signals directly. In line with [8], we decided to use a simple linear regression defined in (3), where a and b are the regression coefficients. To ensure a high generalization performance of our calibration curve and to gain knowledge about the performance of the regression on new subjects, we used a leave-one-out scheme to fit the calibration curve. This implies that all blood samples from one subject were left out, while the calibration was conducted on all the blood samples from the remaining 13 subjects. This procedure was repeated with all 14 subjects as the test subject. For each of the 14 iterations, the values of a and b were found and the performance of the obtained calibration curve was evaluated as the root mean squared error (RMSE) between the measured S_aO_2 reference values and the levels estimated based on the calibration curve for the test subject. The final calibration curve was fitted as an average of the regression coefficients obtained in the 14 iterations.

$$S_pO_2 = aR + b \quad (3)$$

C. Data Acquisition for the Comparison Study

As mentioned, the purpose of this study was to investigate whether clinical relevant and reliable measures of the oxygen saturation can be obtained from PPG signals recorded on the sternum of relevant patients suffering from obstructive airway diseases. We therefore included a total of 30 patients with either COPD or asthma in this part of the study. All enrolled patients were admitted to the Department of Pulmonary Medicine or the Medical Admission Ward at Bispebjerg Hospital, Denmark. They were admitted for at least 24 hours prior to their inclusion due to a worsening in their condition. Two of the patients were excluded due to missing data in the recording. The demographics of the remaining 28 patients are provided in Table II. During the recording, the patients were monitored with the same commercial Patient Monitor as in the calibration part of the study. Furthermore, the prototype of the sternal PPG sensor was attached to the sternum using adhesive tape. This allows for a comparison between the S_pO_2 measures obtained from the commercially available finger pulse oximeter and the S_pO_2 levels estimated from the sternal PPG sensor. As in the calibration study, all signals were recorded with the same acquisition device. The patients were at rest in a semi-supine position. They were furthermore instructed not to make any unnecessary movements since this is known to cause motion artifacts in the recorded PPG signals.

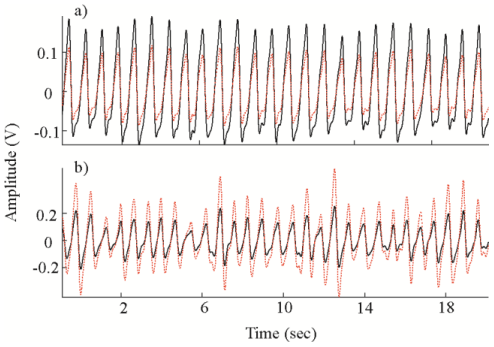

Figure 3. Illustration of the effect of normalization and filtering. For comparison, the raw unprocessed signals are provided in Fig. 1. It is observed how the relation between the amplitude of the red (dotted red line) and the infrared PPG (solid black line) signals shift for different oxygen saturation levels.

D. Performance of the Sternal PPG Signals

To estimate the performance of the sternal PPG signals on the patient population, we divided the recorded sternal PPGs and the ECGs into non-overlapping windows of 20 seconds (corresponding to the finger oximeter and the windows applied during the calibration). Then we repeated step 2 – 6 in the calibration procedure for each of the non-overlapping windows. The obtained R values were then used to estimate the S_pO_2 values from (3) with the calibrated regression coefficients. This provides a time course of the estimated S_pO_2 values. A representative example of this time course is illustrated in Fig. 4 together with the S_pO_2 values simultaneously obtained from the finger pulse oximeter. The S_pO_2 values obtained from the two systems were then compared to estimate the performance of the sternal PPG signals on clinically relevant patients.

III. Results

A. Calibration of the Sternal PPG Sensor

The relation between R estimated from the sternal PPG signals and the measured S_aO_2 reference values are provided in Fig. 5(a) together with the obtained calibration curve. For validation of the calibration, the final calibration curve was applied to estimate the S_pO_2 values based on the calculated R value for all 324 blood samples. In accordance with the ISO 80601-2-61:2011 guidelines, the accuracy of the sternal PPG sensor was then estimated according to (4), where n indicates

Preprint submitted to 38th Annual International Conference of the IEEE Engineering in Medicine and Biology Society. Received February 22, 2016.

TABLE II. PATIENT DEMOGRAPHICS FOR THE COMPARISON STUDY.

Gender (male/female)	10 / 18
Age (years), mean ± SD	64.25 ±14.65
BMI (kg/m^2), mean ± SD	25.99 ± 8.87
Recording length (min)	21 (10 - 54)

the number of blood samples (n = 324). The accuracy was found to be A_{rms} = 1.75%.

$$A_{rms} = sqrt\left(mean\left(\left(SpO2 - SaO2 \right)^2 \right) \right) \quad (4)$$

The Blandt-Altman plot of the comparison between the measured S_aO_2 reference values and the estimated S_pO_2 values are provided in Fig. 5(b). The mean system bias is -0.21% and the limits of agreements are 3.5% and -3.9% respectively. This shows slightly overestimated sternal derived S_pO_2.

B. *Performance of the Sternal PPG Signals*

The Pearson correlation between S_pO_2 measured on the finger and the S_pO_2 estimated from the sternal PPGs was found to be 0.89 ($p<0.05$). The Blandt-Altman plot of the comparison between the two methods is provided in Fig. 6.

IV. DISCUSSION

The first step was to calibrate the sternal PPG sensor through a controlled desaturation study. The results showed that there is an excellent agreement between the estimated S_pO_2 values and the measured S_aO_2 reference values in the clinical region of interest (70% to 100%). The accuracy of the sternal PPG system was found to be A_{rms} = 1.75%. This accuracy is acceptable according to the ISO 80601-2-61:2011 guidelines that allows A_{rms} values of up to 4%. Commercially available pulse oximeters such as Masimo R25-L and NellCore Oximax N-65 reports accuracies of 1.79% and 1.3%, respectively. Furthermore, another recent desaturation study conducted with a sternal PPG sensor has obtained an accuracy of 1.7% [9]. The calibration thus indicates an accuracy that is well within both the state of the art performance and the clinically acceptable range. We thus consider the calibration to be successful and we therefore find it reasonable to apply the estimated calibration curve to

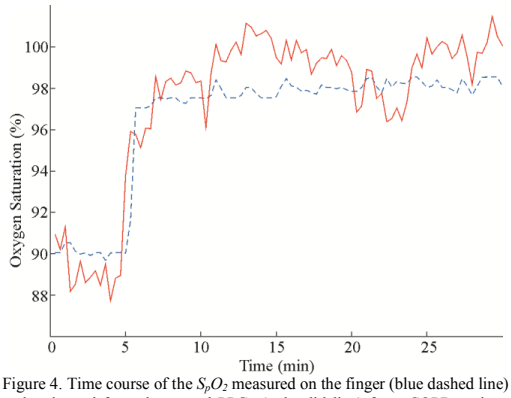

Figure 4. Time course of the S_pO_2 measured on the finger (blue dashed line) and estimated from the sternal PPGs (red solid line) for a COPD patient. The rapid increase in S_pO_2 observed from both systems is caused by the initiation of oxygen therapy.

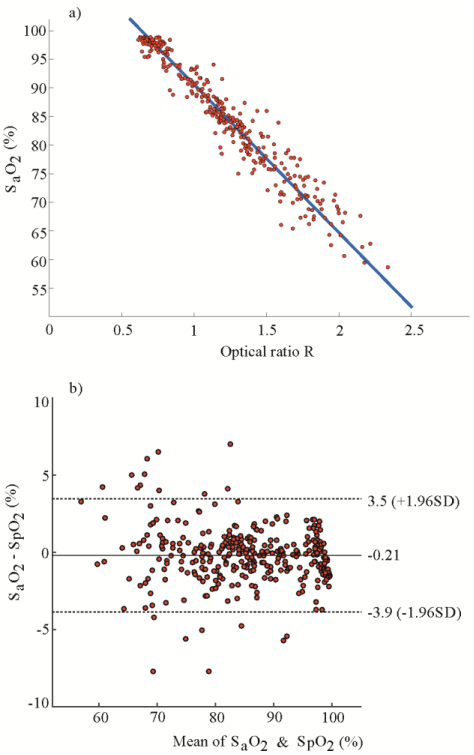

Figure 5. (a) Relation between the calculated R values and the measured S_aO_2 reference values (red dots) and the final calibration curve (blue line). The final calibration coefficients were a = -25.89 and b = 116.48. The average RMSE for the 14 calibration iterations was 1.73%. (b) The Blandt-Altman plot of the comparison between the measured S_aO_2 reference values and the estimated S_pO_2 values. The middle solid line represents the mean system bias, whereas the upper and lower dashed lines represent the limits of agreements ±1.96 standard deviations (SD).

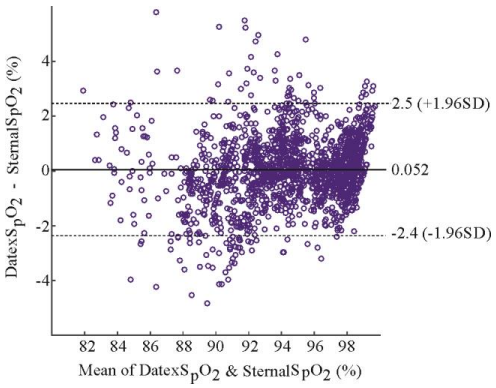

Figure 6. The Blandt-Altman plot of the comparison between the two measurement systems. Each dot corresponds to the difference between the obtained S_pO_2 in one of the 20 second analysis windows. The study included a total of 1784 non-overlapping 20 second analysis windows.

Preprint submitted to 38th Annual International Conference of the IEEE Engineering in Medicine and Biology Society. Received February 22, 2016.

investigate the clinical performance of the sternal PPG signals on the patient population.

As observed from Fig. 6 and the statistically significant correlation, there was a very high agreement between the results obtained from the commercially available Patient Monitor and the sternal PPGs. Furthermore, the Patient Monitor has a standard deviation in the estimation of S_pO_2 of ±2% points in the range of 80% to 100%. Taking the individual accuracy of the two systems into account, we thus consider the agreement to be excellent. This shows that PPGs recorded on the sternum are reliable for estimation of S_pO_2 levels in admitted COPD and asthma patients. Furthermore, it is observed from Fig. 4, that the sternal PPG sensor actually has a shorter response time for detection of changes in the S_pO_2 levels when oxygen therapy is initiated. However, the instantaneous deviations in the estimated S_pO_2 levels are observed to be slightly higher for the sternal PPGs. However, these minor fluctuations are within a very small range that is not considered to be critical for clinical applications. The high performance is expected to be caused by several factors. First of all, the signal quality was found to be excellent on the sternum and it was furthermore observed that the signal quality increased during episodes of hypoxia. This might be caused by an increase in the blood perfusion at the sternum. Furthermore, the temperature was observed to be higher on the sternum compared to the traditional finger or earlobe locations and the sensor might therefore obtain a better interface between the skin and tissue due to increased sweating and additional thermal insulation. These factors might contribute the high signal quality levels. Furthermore, the algorithm design contains several factors that are expected to increase the overall performance of the system, e.g. the window specific filter that was designed to maximize the attenuation of both movement artifacts and the influence of the respiratory component.

One of the major limitations in this study is that both the healthy volunteers and the patients were instructed to move as little as possible. In future studies, it could be highly relevant to investigate the ability to conduct and analyze long-term PPG recordings on the sternum. In this context, it is, of course, necessary to investigate the performance of the system in the presence of different amounts of artifacts. However, several studies have demonstrated a high performance of adaptive noise cancellation using active sensors such as accelerometers [12]. This possibility would be very interesting to investigate in a future study. Furthermore, many episodes of physiological artifacts, e.g. coughing, are present in the recordings obtained from the patient population. The designed method is thus evaluated in the presence of physiological artifacts. Another limitation is that only four of the admitted patients did not receive oxygen therapy during the comparison. This implies that 89% of all the data points from the patient recordings represent S_pO_2 levels of > 90%. It is expected that the uncertainty of the estimated S_pO_2 levels increases for both recording systems with decreased S_pO_2 levels. It might therefore be interesting to expand the comparison to include lower S_pO_2 levels as well. However, patients admitted with obstructive airway diseases are not normally allowed to reach S_pO_2 levels below 90% while in the hospital bed. We thus find the evaluated range of S_pO_2 levels adequate for estimating the in-hospital performance of the sternal PPGs in this patient population.

To our best knowledge, this is the first study addressing the possibility for reliable estimation of clinically relevant S_pO_2 levels from sternal PPGs on patients with obstructive airway diseases. We have thus demonstrated that S_pO_2 levels can be estimated from a prototype of a sternal PPG sensor placed on the sternum of COPD and asthma patients. The results show an excellent agreement with the gold standard (S_aO_2) and the accuracy is well within the range of commercially available S_pO_2 systems. This indicates that sternal PPG recordings might be incorporated into a vital sign patch together with e.g. ECG, accelerometer recordings, and estimation of the respiration rate. Such a patch may be able to assist in a timely detection of worsening of the condition of critical or chronically ill patients and improve the possibilities of treatment for this important patient population.

REFERENCES

[1] J. Allen, "Photoplethysmography and its application in clinical physiological measurement.," *Physiol. Meas.*, vol. 28, no. 3, pp. R1–39, Mar. 2007.

[2] N. Soguel Schenkel, L. Burdet, B. de Muralt, and J. W. Fitting, "Oxygen saturation during daily activities in chronic obstructive pulmonary disease.," *Eur. Respir. J.*, vol. 9, no. 12, pp. 2584–2589, 1996.

[3] N. Eriksen, E. F. Hansen, E. P. Munch, F. V. Rasmussen, and J. Vestbo, "[Chronic obstructive pulmonary disease. Admission, course and prognosis].," *Ugeskr. Laeger*, vol. 165, no. 37, pp. 3499–502, 2003.

[4] Y. Mendelson, R. J. Duckworth, and G. Comtois, "A wearable reflectance pulse oximeter for remote physiological monitoring.," *Conf. Proc. IEEE Eng. Med. Biol. Soc.*, vol. 1, pp. 912–5, Jan. 2006.

[5] S. S. Chreiteh, B. Belhage, K. Hoppe, J. Branebjerg, R. Haahr, S. Duun, and E. V Thomsen, "Estimation of respiratory rates based on photoplethysmographic measurements at the sternum," in *2015 37th Annual International Conference of the IEEE Engineering in Medicine and Biology Society (EMBC)*, 2015, pp. 6570–6573.

[6] A. M. Yañez, D. Guerrero, R. Pérez de Alejo, F. Garcia-Rio, J. L. Alvarez-Sala, M. Calle-Rubio, R. M. de Molina, M. Valle Falcones, P. Ussetti, J. Sauleda, E. Z. García, J. M. Rodríguez-González-Moro, M. Franco Gay, M. Torrent, and A. Agustí, "Monitoring Breathing Rate at Home Allows Early Identification of COPD Exacerbations," *Chest*, vol. 142, no. 6, pp. 1524–1529, Dec. 2012.

[7] D. B. Saadi, I. Fauerskov, A. Osmanagic, H. M. Sheta, H. B. D. Sorensen, K. Egstrup, and K. Hoppe, "Heart Rhythm Analysis using ECG Recorded with a Novel Sternum based Patch Technology - A Pilot Study," in *Proceedings of the International Congress on Cardiovascular Technologies*, 2013, pp. 15–21.

[8] J. G. Webster, *Design of Pulse Oximeters*, 1st ed. CRC Press, 1997.

[9] R. Vetter, L. Rossini, A. Ridolfi, J. Sola, O. Chetelat, M. Correvon, and J. Krauss, "Frequency Domain SpO2 Estimation Based on Multichannel Photoplethysmographic Measurements at the Sternum," in *World Congress on Medical Physics and Biomedical Engineering*, Springer Berlin Heidelberg, 2009, pp. 326–329.

[10] C. Schreiner, P. Catherwood, J. Anderson, and J. McLaughlin, "Blood oxygen level measurement with a chest-based Pulse Oximetry prototype system," *Comput. Cardiol.*, vol. 37, pp. 537–540, 2010.

[11] B. Venema, N. Blanik, V. Blazek, J. Schiefer, and S. Leonhardt, "A feasibility study evaluating innovative in-ear pulse oximetry for unobtrusive cardiovascular homecare monitoring during sleep," in *2013 IEEE Point-of-Care Healthcare Technologies (PHT)*, 2013, no. August, pp. 124–127.

[12] T. Tamura, Y. Maeda, M. Sekine, and M. Yoshida, "Wearable Photoplethysmographic Sensors—Past and Present," *Electronics*, vol. 3, no. 2, pp. 282–302, Apr. 2014.

Preprint submitted to 38th Annual International Conference of the IEEE Engineering in Medicine and Biology Society. Received February 22, 2016.

PAPER V

TITLE Long-Term Quasi-Continuous Oxygen Saturation Levels Obtained from Sternal Photoplethysmography on Patients with Obstructive Lung Diseases

AUTHORS Shadi S. Chreiteh, Dorthe B. Saadi, Bo Belhage, Nassim Nabipour, Karsten Hoppe, and Erik V. Thomsen

JOURNAL Engineering in Medicine and Biology Society (EMBC), 2016 Annual International Conference of the IEEE

PUBLICATION HISTORY Submission date: 14-03-2016, Status: In review.

Long-Term Quasi-Continuous Oxygen Saturation Levels Obtained from Sternal Photoplethysmography on Patients with Obstructive Lung Diseases*

Shadi S. Chreiteh, Dorthe B. Saadi, Bo Belhage, Nassim Nabipour, Karsten Hoppe, and Erik V. Thomsen

Abstract— **Calculation of long-term quasi-continuous oxygen saturation (S_pO_2) levels is highly relevant for critically ill patients. The purpose of this study is therefore to conduct a preliminary investigation of the clinical reliability of long-term photoplethysmography (PPG) recordings obtained from the *sternum* of patients admitted to the hospital with obstructive lung diseases. Due to the lack of a gold standard reference that is suitable for long-term monitoring without interfering with the patient's activity level, we extracted reliable segments based on knowledge from the basic pulse oximeter theory as well as knowledge about the inherent physiological regulation of the S_pO_2 levels. We included 15 admitted patients who were monitored with a prototype of a sternal PPG sensor for approximately 20 hours. On average, we found that clinically reliable S_pO_2 levels could be calculated for 58% of the recording time. Furthermore, the average longest period of time with unreliable data was only 23.6 minutes. This indicates a high potential for quasi-continuous calculation of S_pO_2 levels from sternal PPGs in many different clinical applications in the future.**

I. Introduction

Outside the intensive care unit, the oxygen saturation (S_pO_2) level is often only monitored manually a few times per day. For critically ill patients, e.g. patients with Chronic Obstructive Pulmonary Disease (COPD), this might not be enough to ensure timely detection of a potential worsening in the patient's condition [1][2]. Recently, the possibility for calculation of S_pO_2 levels from photoplethysmography (PPG) signals obtained from the sternum has been investigated [3]. Our group has furthermore previously shown that clinically relevant S_pO_2 levels can be obtained from short-term sternal PPGs recorded in a controlled environment on the sternum of admitted patients with COPD or asthma [4]. These findings show that sternal PPGs are highly applicable for reliable calculation of clinically relevant S_pO_2 levels in controlled conditions with a minimum influence of artifacts. However, in real-life applications, the recorded PPGs will be influenced by varying amounts of unavoidable artifacts. This includes for instance artifacts from motions, changes in the amounts of ambient light, and changes in the contact between the skin and the sensor. When the PPG signals are affected by these artifacts, the calculation of the S_pO_2 levels might be unreliable. From a clinical point-of-view, it is acceptable to estimate the S_pO_2 levels in quasi-continuous periods with sufficient signal quality, e.g. provide a reliable calculation of the S_pO_2 level six times per hour or provide a reliable S_pO_2 trend curve. This implies that periods of poor data quality are clinically acceptable as long as they alternate with periods of data that permits reliable calculation of the S_pO_2 levels. Due to the current lack of unobtrusive S_pO_2 measurement devices suitable for long-term monitoring, without impairment of normal activity levels, we utilize knowledge about the inherent physiological regulation of the S_pO_2 levels to investigate the reliability of the recorded PPGs. To our best knowledge, the long-term quasi-continuous reliability of S_pO_2 levels calculated from sternal PPGs has never been investigated in chronically ill patients before. The purpose of this study is thus to investigate this possibility using long-term sternal PPGs obtained from patients with obstructive lung diseases.

II. Methods

An overview of the analysis is provided in Fig. 1. The recorded signals are divided into non-overlapping windows of 20 seconds and the S_pO_2 level is calculated in each of these windows. The window length is chosen to represent enough physiological information to provide a reliable calculation of the changes in the S_pO_2 levels over time. We then investigated the reliability of each segment and excluded unreliable segments. This is described in details later.

A. Data Acquisition

We enrolled a total of 15 patients with obstructive lung diseases (two asthma patients and 13 COPD patients). The patient demographics are provided in Table I. All 15 patients were admitted to the Department of Pulmonary Medicine at Bispebjerg University Hospital, Denmark. The patients were admitted due to a worsening in their conditions for at least 24 hours prior to their inclusion in the study. Most of the patients received oxygen therapy. It is expected that these patients cause a relatively high amount of physiological artifacts, e.g. due to coughing, clearing of their throats, and their higher amount of muscle activation during respiration. The patients were furthermore instructed to follow their daily routines during the hospitalization (except showering). This ensures that the investigation is conducted on a clinically

*This Research was supported by the Danish Ministry of Higher Education and Science.

Shadi S. Chreiteh is with the Department of Micro- and Nanotechnology, Technical University of Denmark, 2800 Kgs. Lyngby, Denmark (e-mail: shach@nanotech.dtu.dk).

Dorthe B. Saadi and Karsten Hoppe are with DELTA Danish Electronics, Light & Acoustics, Venlighedsvej 4, 2970 Hørsholm, Denmark.

Bo Belhage and Nassim Nabipour are with the Department of Anesthesiology, Bispebjerg University Hospital, University of Copenhagen, 2400 Copenhagen NV, Denmark.

Erik V. Thomsen is with the Department of Micro- and Nanotechnology, Technical University of Denmark, 2800 Kgs. Lyngby, Denmark.

Preprint submitted to 38th Annual International Conference of the IEEE Engineering in Medicine and Biology Society. Received March 14, 2016.

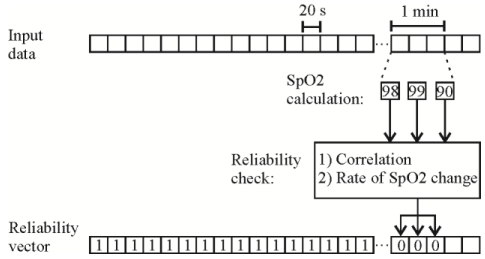

Figure 1. Schematic overview of the analysis. The reliability is checked based on the S_pO_2 levels calculated from three consecutive 20-second windows (corresponding to a one minute data segment). If the input data from the one-minute segment is deemed unreliable, all three corresponding 20-second windows are deemed unreliable and they are excluded from further analysis (illustrated by zeros in the reliability vector).

highly relevant patient population with a realistic amount of artifacts. The patients were monitored using a custom build prototype of a PPG sensor. The PPG sensor simultaneously records a red (λ = 660nm) PPG signal, an infrared (λ = 940nm) PPG signal, and a bipolar ECG signal. The PPG sensor was attached to the sternum of the patients using an adhesive electrode, see Fig. 2. The S_pO_2 level was also measured using a conventional finger pulse oximeter (Nellcor OxiMax N-65) in the beginning of each recording. This is used as a reference for comparison with the S_pO_2 levels obtained from the sternal PPGs in the beginning of the recording. The study was approved by the Danish Regional Ethical Community, the Danish Health and Medicines Authority, the Danish Data Protection Agency, and it was monitored by the regional Good Clinical Practice (GCP) unit. Furthermore, all patients provided informed written consent to participate before they were enrolled in the study.

B. Calculation of the S_pO_2 Levels

The S_pO_2 level was calculated as $S_pO_2 = -25.89 \cdot R + 116.48$, where R represents the relation between the amplitudes of the normalized and filtered red and infrared PPG signals and, in accordance with the ISO 80601-2-5-61:2011 guidelines, the calibration coefficients were found from a desaturation study recently conducted by our group [4]. A detailed description of the normalization and filtering is also provided in [4]. An example of the obtained time course of the S_pO_2 levels is provided in Fig. 3(a).

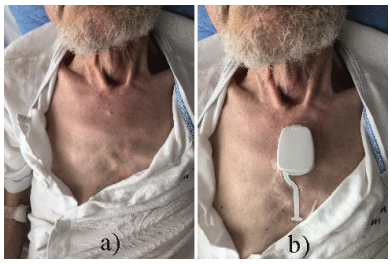

Figure 2. (a) Illustration of the chest of a patient before application of the prototype PPG sensor. (b) Illustration of the prototype PPG sensor attached to the sternum of the patient using an adhesive electrode. The ECG recording sites are embedded in the adhesive electrode.

TABLE I. DEMOGRAPHICS OF THE PATIENT POPULATION.

Gender (male/female)	3/12
Age (years), mean ± SD[a]	67.4 ± 19
BMI[b] (kg/m^2), mean ± SD[a]	25 ± 4.5
Recording length[c] (hours)	18-20

[a] SD is the standard deviation
[b] BMI is the body mass index
[c] The recording length is stated as minimum – maximum

C. Reliability of the Calculated S_pO_2 Levels

We applied two different criteria to check the reliability of every one-minute segment of the recorded data (see Fig. 1). The first check is related to the basic assumptions for calculation of the S_pO_2 level based on the red and the infrared PPG signals. Since the S_pO_2 level is calculated based on the relation between the amplitudes of the two signals, it is theoretically reasonable that a certain mathematical correlation is required between the two signals [5]. The first criteria was therefore that the one-minute segment was deemed unreliable if the Pearson correlation coefficient between the red and the infrared PPG signal in any of the three 20-second windows was below 0.75 [6]. The second part of the reliability check is related to knowledge about the inherent physiological regulation of the S_pO_2 levels. The S_pO_2 change observed within one minute is physiologically expected to vary very little [7]. Several research groups have investigated the response time to changes in S_pO_2 levels during low endurance walk in COPD patients and they generally found a decrease in the S_pO_2 level around 3% per minute [7][8][9]. We therefore deemed the one-minute segment unreliable if the absolute difference between the maximum and minimum S_pO_2 values obtained in the one-minute segment exceeded 3%. The reliability check was conducted as a sliding window with an overlap of two 20-second windows. This implies that each 20-second window is included in three different runs of the reliability check. If it is deemed unreliable in at least one of the three checks, the 20-second segment is considered unreliable. The performance of the reliability check is illustrated in Fig. 3(b).

D. Estimation of Long-Term Accuracy

As observed from Fig. 3(b), the included segments have a certain variation around a baseline S_pO_2 level. To estimate this variation, we calculated an estimated reference S_pO_2 trend curve. This curve is calculated with an average filter with 30 points (corresponding to 10 minutes). All unreliable segments were excluded for calculation of this reference trend curve. An example of the trend curve is provided in Fig. 3(c). We then defined the long-term accuracy of the S_pO_2 calculation as the Root Mean Squared (RMS) error between this reference curve and the S_pO_2 values that were deemed reliable.

III. RESULTS

The RMS error between the S_pO_2 values calculated from the sternal PPGs in the beginning of the recording and the S_pO_2 values obtained from the conventional finger pulse oximeter was only 2.3%. Fig. 4 contains a few examples of the time course of the calculated S_pO_2 values. It is observed from both Fig. 3 and Fig. 4 that several short periods of data are excluded. An overview of the lengths of all excluded

Preprint submitted to 38th Annual International Conference of the IEEE Engineering in Medicine and Biology Society. Received March 14, 2016.

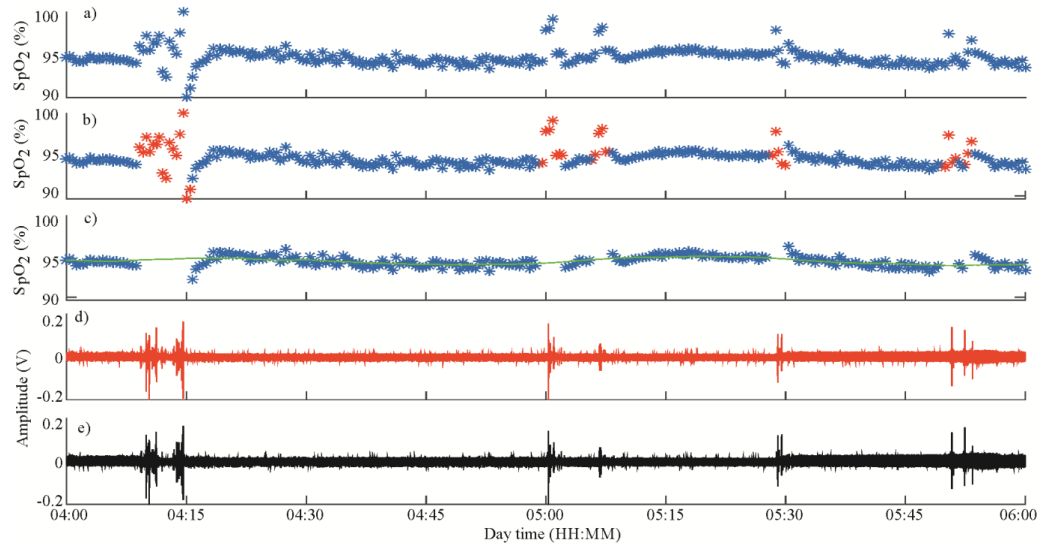

Figure 3. (a) Example of the time course of all calculated S_pO_2 values for two hours during the night for one patient. (b) Illustration of the reliable segments (blue marks) and the unreliable segments (red marks). (c) Illustration of the time course of all the extracted reliable segments (blue marks) together with the estimated average reference curve (green line). This curve is applied to calculate the long-term accuracy of the reliable S_pO_2 values. (d) Time course of the raw red PPG signal. (e) Time course of the raw infrared PPG signal. It is observed how segments with high amounts of artefacts in the PPG signals are considered unreliable and therefore excluded from the S_pO_2 analysis.

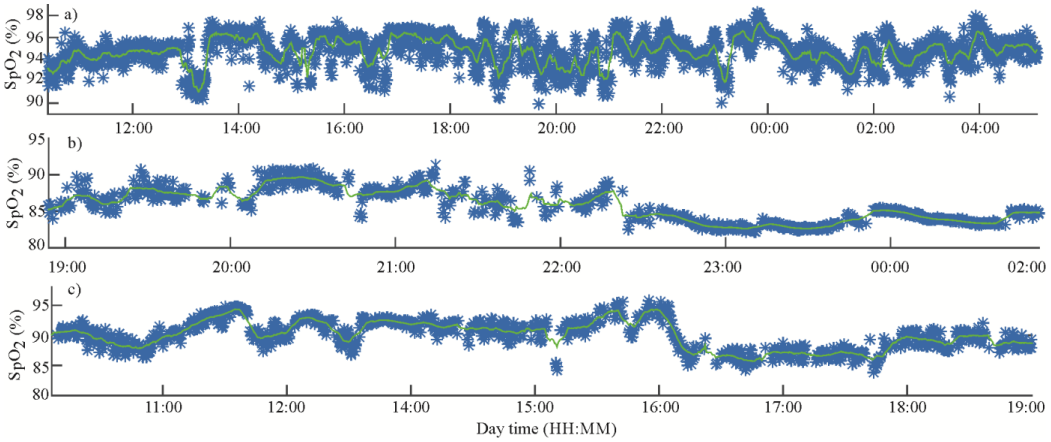

Figure 4. Three different examples of the time course of the calculated S_pO_2 segments that were deemed reliable (blue marks) and the estimated average reference curve (green line). (a) Illustration of a full 20-hour recording. It is observed how the S_pO_2 level temporarily decreases several times during the day. This might be caused by removal of the oxygen therapy, e.g. if the patient left the bed. (b) Illustration of the S_pO_2 level during the transmission between day and night. It is observed that the calculated S_pO_2 levels vary more during the day compared to the night. Furthermore, several segments are deemed unreliable right before bedtime (around 22:00). This might be caused by artifacts in the PPGs when the patient was getting ready for the night. (c) Example of slow variations in the S_pO_2 levels during the day.

successive windows from all 15 patients is provided in Fig. 5. On average, the longest period of unreliable data from the 15 patients was only 23.6 minutes. Overall, the average percentage of reliable PPG segments from the 15 patients was 58%. Finally, the average RMS error between the S_pO_2 values calculated directly from the sternal PPGs and the estimated average reference curves was only 2.5%.

IV. Discussion

This study is a preliminary investigation of the possibility for long-term quasi-continuous calculation of S_pO_2 levels based on sternal PPGs. We have previously shown the potential for calculation of clinically relevant and reliable S_pO_2 levels based on sternal PPGs obtained in controlled

Preprint submitted to 38th Annual International Conference of the IEEE Engineering in Medicine and Biology Society. Received March 14, 2016.

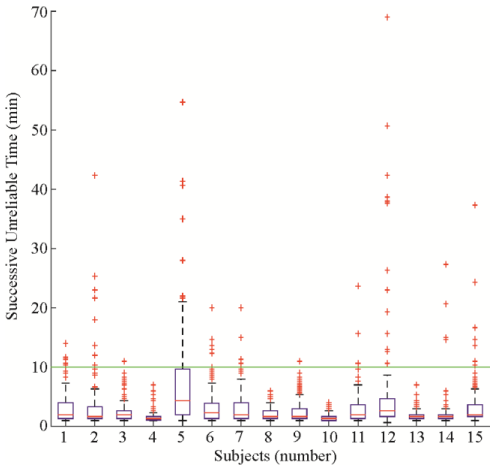

Figure 5. Illustration of the distribution of the lengths of unreliable (excluded) time segments for each patient. The red vertical lines indicate the median for each subject, the blue boxes indicate the interquartile ranges, and the red marks indicate outliers. The green vertical line indicates a threshold of 10 minutes (corresponding to obtaining an average of at least six reliable S_pO_2 measures every hour).

conditions [4]. In this preliminary long-term study, it was important to restrict the patient's daily activities as little as possible. This mimics a realistic impression of the possibilities for future quasi-continuous calculation of S_pO_2 levels in the presence of artifacts arising from normal in-hospital activities. It was therefore not feasible to compare the calculated S_pO_2 values with either the gold standard (arterial blood samples) or the conventional pulse oximeters (wired finger probes) throughout the recording length. Instead, we compared the S_pO_2 values obtained from the sternal PPGs with a conventional finger pulse oximeter in the beginning of the recordings. This comparison was applied to establish a baseline accuracy of the sternal PPGs. Based on our previous findings [4] and the very low RMS error between the two methods in the beginning of the recordings, we assume that the S_pO_2 levels calculated from the long-term sternal PPGs are reliable in segments of sufficient data quality. For the rest of the recording time, we therefore investigated the reliability based directly on knowledge about the inherent physiological regulation of the SpO2 levels and the basic theory of pulse oximetry. It is observed from Fig. 3 how the reliability check correctly removes many of the outliers. These outliers are expected to be caused by poor data quality. It should be mentioned that our limit of a maximum S_pO_2 difference of 3% in one minute is quite strict. This implies that the actual amount of reliable data segments might have been even higher. We selected the stricter limit because it is worse to include an unreliable segment and hereby provide the doctor with an erroneous S_pO_2 calculation than it is to exclude a segment that could have provided reliable calculation of the S_pO_2 level.

On average, we found the calculated S_pO_2 values to be reliable in 58% of the recording time. More importantly, we generally found that segments of reliable S_pO_2 values could be extracted throughout the recording length. This indicates that when the S_pO_2 calculation temporarily becomes unreliable due to artifacts, it becomes reliable again after the artifact event. This is observed from Fig. 4. Furthermore, it is observed from Fig. 5 that almost all excluded time periods are less than ten minutes. Looking at the S_pO_2 levels in one hour intervals, it is therefore indicated that it would be possible to measure the S_pO_2 level at least six times per hour. This is very promising for future quasi-continuous calculation of S_pO_2 values based on sternal PPGs.

In the future, it might be possible to design new algorithms for automatic detection of data segments that would provide a reliable S_pO_2 measure. This would allow for a real-time quasi-continuous setup for long-term monitoring of S_pO_2 values in chronically ill patients. The low RMS error between the included S_pO_2 values and the estimated average reference curves furthermore indicates a high long-term accuracy of the calculated S_pO_2 values. This indicates that we have obtained a high attenuation of artifacts in the originally calculated S_pO_2 values. In the future, it will be possible to increase the uptime even further, e.g. by optimizing the sensor design, implementing adaptive noise cancellation from additional recording modalities, or implementing more advanced algorithms for calculation of the S_pO_2 values.

In this preliminary study, we have thus demonstrated the ability to calculate clinically relevant and reliable S_pO_2 values in long-term sternal PPG recordings obtained from patients suffering from obstructive lung diseases. This finding is very promising for future implementation of S_pO_2 measures in a sternum based vital sign patch. In the future, such a patch might assist in early detection of worsening in the condition of these patients and hereby ensure timely treatment of the patients.

REFERENCES

[1] L. Fuhrmann, A. Lippert, and D. Østergaard, "Observation af kritisk syge patienter," *Ugeskr. læger*, pp. 502–506, 2009.

[2] N. Soguel Schenkel, L. Burdet, B. de Muralt, and J. W. Fitting, "Oxygen saturation during daily activities in chronic obstructive pulmonary disease.," *Eur. Respir. J.*, vol. 9, no. 12, pp. 2584–2589, 1996.

[3] R. Vetter, L. Rossini, A. Ridolfi, J. Sola, O. Chetelat, M. Correvon, and J. Krauss, "Frequency domain SpO2 estimation based on multichannel photoplethysmographic measurements at the sternum," in *IFMBE Proceedings*, vol. 25, no. 4, Springer Berlin Heidelberg, 2009, pp. 326–329.

[4] S. S. Chreiteh, D. B. Saadi, B. Belhage, N. Nabipour, K. Hoppe, and E. V Thomsen, "A Clinical Study of Short-Term Sternal Photoplethysmography : Recordings from Patients with Obstructive Airways Diseases," *Submitt. to 38th Annu. Int. Conf. IEEE Eng. Med. Biol. Soc.*, 2016.

[5] J. G. Webster, *Design of Pulse Oximeters*, 1st ed. CRC Press, 1997.

[6] R. A. S. Mohamed K. Diab, Esmaiel Kiani-Azarbayjany, Ibrahim M. Elfadel, Rex J. McCarthy, Walter M. Weber, "Signal processing apparatus," US Patent 5,632,2721997.

[7] K. O. Hadeli, E. M. Siegel, D. L. Sherrill, K. C. Beck, and P. L. Enright, "Predictors of Oxygen Desaturation During Submaximal Exercise in 8,000 Patients," *Chest*, vol. 120, no. 1, pp. 88–92, Jul. 2001.

[8] M.-L. Chuang, I.-F. Lin, and S.-P. Chen, "Kinetics of Changes in Oxyhemoglobin Saturation During Walking and Cycling Tests in COPD," *Respir. Care*, vol. 59, no. 3, pp. 353–362, Mar. 2014.

[9] E. Crisafulli, A. Iattoni, E. Venturelli, G. Siscaro, C. Beneventi, A. Cesario, and E. M. Clini, "Predicting Walking-Induced Oxygen Desaturations in COPD Patients: A Statistical Model," *Respir. Care*, vol. 58, no. 9, pp. 1495–1503, Sep. 2013.

Preprint submitted to 38th Annual International Conference of the IEEE Engineering in Medicine and Biology Society. Received March 14, 2016.

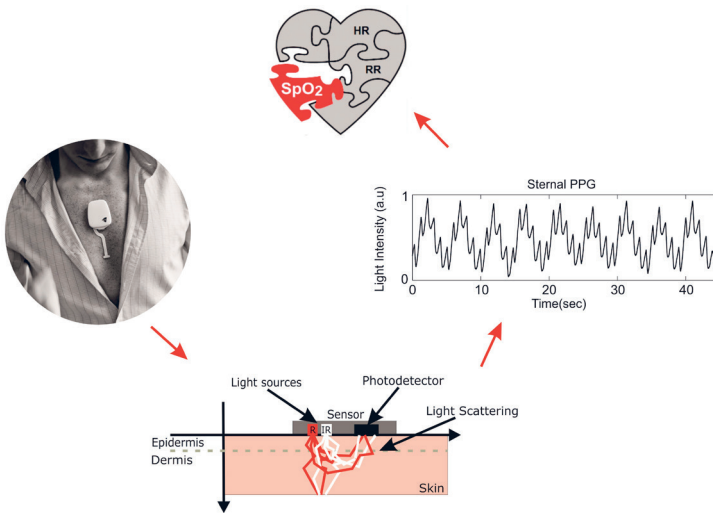

Published by:
DTU Nanotech
Department of Micro- and Nanotechnology
Technical University of Denmark
Ørsteds Plads, building 345C
DK-2800 Kgs. Lyngby